

UNIVERSITÉ DU QUÉBEC

MÉMOIRE PRÉSENTÉ À  
L'UNIVERSITÉ DU QUÉBEC À TROIS-RIVIÈRES

COMME EXIGENCE PARTIELLE  
DE LA MAÎTRISE EN SCIENCES ET GÉNIE DES MATÉRIAUX  
LIGNOCELLULOSIQUES

PAR  
XIAOMAN XU

ÉTUDE DES RELATIONS ENTRE LA DISPERSION DE LA MICRO-NANO  
CELLULOSE FIBRILLÉE (MNFC) ET SON APTITUDE AU COUCHAGE  
RIDEAU

AOÛT 2014

Université du Québec à Trois-Rivières

Service de la bibliothèque

Avertissement

L'auteur de ce mémoire ou de cette thèse a autorisé l'Université du Québec à Trois-Rivières à diffuser, à des fins non lucratives, une copie de son mémoire ou de sa thèse.

Cette diffusion n'entraîne pas une renonciation de la part de l'auteur à ses droits de propriété intellectuelle, incluant le droit d'auteur, sur ce mémoire ou cette thèse. Notamment, la reproduction ou la publication de la totalité ou d'une partie importante de ce mémoire ou de cette thèse requiert son autorisation.

UNIVERSITY OF QUEBEC

DISSERTATION PRESENTED TO  
UNIVERSITY OF QUEBEC IN TROIS-RIVIERES

AS PARTIAL REQUIREMENT OF THE MASTER  
OF SCIENCES AND ENGINEERING OF LIGNOCELLULOSIC MATERIALS

BY  
XIAOMAN XU

STUDY OF THE RELATIONSHIP BETWEEN  
THE DISPERSION OF MICRO-NANO-FIBRILLATED CELLULOSE (MNFC)  
AND THEIR ABILITY IN CURTAIN COATING

AUGUST 2014

## Foreword

Due to excellent mechanical and barrier properties, the Micro-Nano-Fibrillated-Cellulose (MNFC), a renewable fiber-based wood product, is proposed to be a strengthening agent replacing chemical kraft pulp in paper products made of Thermo Mechanical Pulp (TMP). In order to obtain the full potential of the micro and mainly nano fibrillated part of the product, it needs to be well dispersed as agglomerates would not have the micro-nano properties. Consequently, present master's study main objective is to explore the dispersion of Micro-Nano-Fibrillated-Cellulose and applications as a coating agent in a curtain coating process implemented on a paper machine to improve the mechanical and barrier properties of TMP-based papers and boards.

Present report is divided into two parts. First, we discuss laboratory experiments to explore the optimum dispersion effects of Carboxy-Methyl-Cellulose (CMC) on MNFC. The influence of CMC on the flow properties of MNFC suspensions and on the fibril morphology are analyzed, as well as the interactions between MNFC and CMC. This first part demonstrates the dispersion effects of CMC on MNFC suspensions. We also propose a first attempt to understand the mechanisms underlying the dispersion effects. Second, we focus on the application of MNFC as a coating agent in a curtain coating machine, namely the Hydra-Sizer<sup>TM</sup> from GL&V. The runnability conditions in the Hydra-Sizer<sup>TM</sup> and the performance of MNFC suspensions in the Hydra-Sizer<sup>TM</sup> are verified by off paper machine pilot trials. The improved MNFC dispersions and the available curtain performance of MNFC suspension in Hydra-Sizer<sup>TM</sup> are considered essential for the valorization of paper structured with MNFC.

## Acknowledgements

I wish to express my sincere gratitude to Professor Patrice J. Mangin who provided me with the opportunity to study at the University of Quebec in Trois-Rivieres and perform a Master's thesis under his direction. In the course of last two years, Professor Patrice J. Mangin introduced me to Quebec, Canada where people speak French that originally I did not understand at all. Professor Patrice J. Mangin offered me the time and the opportunity to attend French courses and was always so kind to encourage me to learn the new language and culture. For my master program, Professor Patrice J. Mangin introduced me – it was a first for me - to the fascinating world of nanocellulose. Under his direction, I learned much about the topic, performed the research to develop the subject and finally, hopefully successfully, completed it. I feel honored to have entered the world of renewable forest products which is one of the most promising materials in the future and to graduate having worked on a critical topic in the field under his direction.

I also gratefully thank Dr. Fabrice Roussière, post-doctoral fellow in Professor's Mangin research team. As my closest co-supervisor, Dr. Fabrice Roussière has always provided me with patient guidance and with never ending good suggestions and ideas. During the two years of my study, we spent much time together developing the research methods and analyzing often not too obvious and expected results. Indeed, I have learned very much from him. He taught me whatever he knew and introduced me to the amazing way, and unwritten methods, of how to connect results and other things in research. His extra carefulness, patience, and sense of responsibility are quite impressive. Without the help of Dr. Fabrice Roussière, present work and my master study would really not be the same.

I would like to thank Dr. Daniel Matte, presently with Resolute Forest Products (during my thesis both with The International Coating Centre and UQTR), who also acted as my co-supervisor. At the beginning of my project, he introduced me with the curtain coating instrument Hydra-Sizer<sup>TM</sup>, fully explaining its structure and operation in due details.

Although he was part of our research team for about one year, this basic and practical engineering knowledge he taught me laid foundation for the balance of my research.

I am grateful to Dr. Martin Dubé for his support and assistance as he helped me in improving the rheological measurements methods effectively. He was also quite inspiring in the way to explain research results. Thanks to Dr. Martin Dubé I was able to complete difficult rheological measurements successfully. He was always available for help and discussion.

Thanks are also due to Gilles Lenfant, Marion Treguer and Sahila Ouali, internship students from France. We have worked on different parts of the same project and I appreciated their works and camaraderie very much. Their collaborations and presence somehow allowed me to better perform.

Many thanks to my dear friends at the Lignocellulosic Materials Research Centre (CRML), namely Mohamed Ali Charfeddine, Clément Villemont, Ichrak Lakhthar, Gabriel St-Pierre-Lemieux, Filip Sillerström, Jean-Baptiste Petry, and Abdeladim Tibouda. Their selfless help and care make my time studying in CRML an enjoyable experience.

To many other friends, who helped me through the years, and who shared hardships and joys with me, I thank you.

In the end, I should apologize to my mother Shangrong Liu and father Guangming Xu for my absence from home during the last two year study in Canada. Dear parents, I wish to express my deep gratitude for your tremendous understanding, unwavering support, and love.

Finally I would like to thank our partners Omya International AG, GL&V Company, and the Arboranano network, and NSERC for their financial supports and more specifically Omya International AG their inputs for added understanding in the rheological behaviour of MNFC suspensions.

July 2014

## Abstract

As a renewable natural forest product, Micro-Nano-Fibrillated-Cellulose (fibrillated cellulose with fibril diameters of few nanometers or micrometers, simply referred to as MNFC) possesses many excellent properties which make it one of the most promising materials in the future. Due to its good mechanical and barrier properties, MNFC is expected to valorize Thermo Mechanical Pulp (TMP) paper and board products when added in the sheet during papermaking as a structuring layer using notably curtain coating. As the dispersion of MNFC suspensions is critical to achieve the performance related to its micro-nano structure, the objective of present work is first to understand and improve the dispersion of MNFC when in water suspensions. The second objective is to explore the application of MNFC in curtain coating process which is carried out by the Hydra-Sizer<sup>TM</sup>, a curtain coater developed by GL&V that can be installed on-line on a paper machine. In present work, MNFC is produced by Omya International A.G. by grinding bleached kraft Eucalypt pulp with calcium carbonate in order to reduce the energy required for MNFC production.

A study of the literature shows that the polyelectrolyte Carboxy-Methyl-Cellulose (CMC) contributes to the dispersion of cellulosic fibers at the micro level. So CMC has been tested to improve the dispersion of MNFC suspensions, gathering that the same effect would occur at the nano level. First, the influence of CMC on MNFC is studied. Rheological tests are used to evaluate MNFC flow behaviour while optical microscope and transmission electron microscope are used to perform the fibril morphology analysis or state of dispersion. When combined, the flow behaviour and fibril morphology may best represent the dispersion effects of CMC on fibrils in suspension and on individual fibril, respectively. Increasing CMC addition from 0 to 8%, based on the quantity of fibrils, helps to eliminate the fibrils agglomeration formation and homogenize MNFC suspensions. However, a 2% CMC concentration is found to minimize the fibril diameter, hence the dispersion. The difference between the optimal values of CMC concentrations brought us to further investigate the interactions between CMC and MNFC. The understanding of the mechanism was centered around the CMC adsorption

on fibril surface and the CMC free in the suspensions. For CMC adsorption, the surface physical chemistry of fibrils is measured by evaluating the fibrils zeta potential. For the free CMC, obtained after centrifuging MNFC suspension, polyelectrolyte titration is conducted to measure the anionic charge in supernatant. The drying matters in the supernatant are analyzed by scanning electron microscope coupled with elemental analysis. The investigation of the interactions between CMC and MNFC reveals that CMC adsorbs on fibril surface through the formation of CMC+CaCO<sub>3</sub> complexes in MNFC suspensions. At low CMC concentration (0-2%), the adsorbed CMC+CaCO<sub>3</sub> complexes promote the fibrillation thus decreasing the measured fibril diameter. When increasing the CMC concentrations from 4 to 8%, the added CMC appears to expand the complexes dimension which in turn causes the complexes to leave the fibrils surface and become free in the suspensions. The free complexes play a role as bridges between the fibrils and thus eliminate potential fibrils agglomeration. As a result, at the highest CMC concentration (8%), the MNFC suspension presents a homogenous rheological behaviour without reduction in the fibrils mean diameter. Taking into account the effects of CMC on fibrils agglomeration and on fibril morphology, a 4 to 6% CMC addition is supposed to achieve the optimum dispersion of MNFC.

In order to realize the application of MNFC, the ability of MNFC suspensions to flow in curtain coating is explored. First, the runnability of Hydra-Sizer<sup>TM</sup> is evaluated by applying water and rheological modifier CMC in off-line recirculation trials. Then MNFC suspensions with and without CMC is used to investigate the curtain stability and uniformity in the Hydra-Sizer<sup>TM</sup> curtain coating process. Both suspensions present good curtain performance in Hydra-Sizer<sup>TM</sup> without distinguishable differences. In conclusion, the application of MNFC through MNFC suspensions containing 4-6% CMC in curtain coating on a paper machine with a Hydra-Sizer<sup>TM</sup> can be achieved.

July 2014

**Keywords**

Micro-Nano-Fibrillated-Cellulose (MNFC); Carboxy-Methyl-Cellulose (CMC); dispersion; rheology; adsorption; calcium carbonate; curtain coating; Hydra-Sizer<sup>TM</sup>

## Résumé

En tant que matériau renouvelable, la Micro-Nano-Cellulose-Fibrillée (cellulose fibrillée avec des diamètres de fibrilles de quelques nanomètres ou micromètres et des longueurs micrométriques, simplement appelée MNFC) possède des propriétés intrinsèques remarquables qui la rendent propice pour de nombreuses applications. Grâce d'excellentes propriétés mécaniques et barrières, la MNFC permet de valoriser de nombreux papiers tels que les produits à base de pâte thermomécanique (TMP). De précédentes études ont démontré les gains en termes de propriétés mécaniques lorsque les MNFC sont ajoutés en masse, lors de la formation de la feuille, et les gains en termes de propriétés barrières lorsque les MNFC sont ajoutés en surface, par couchage du papier. Le présent mémoire s'intéresse à l'ajout de MNFC dans la partie humide lors de la fabrication du papier, non pas dans la masse mais en tant que couche de structure via un procédé de couchage rideau. Étant donné que la dispersion de MNFC en suspension est essentielle pour atteindre les performances liées à sa structure micro-nano, le premier objectif de ce travail est d'abord de comprendre et d'améliorer la dispersion de MNFC en suspension dans l'eau. Le second objectif est d'étudier l'application de MNFC dans le processus de couchage rideau qui est réalisé par l'Hydra-Sizer<sup>TM</sup>, un appareil développé par GL&V, permettant d'effectuer un couchage rideau en partie humide d'une machine à papier.

Deux sortes de MNFC ont été étudiées : la L-MNFC (micro-nano-cellulose-fibrillée avec un faible degré de fibrillation, L pour « low ») et la H-MNFC (micro-nano-cellulose-fibrillée avec un haut degré de fibrillation, H pour « high »). Cette dernière est produite avec un apport énergétique supérieur afin d'augmenter la proportion d'éléments fins; la demande énergétique supérieure en augmente aussi le prix de production. Les deux suspensions de MNFC sont produites par le broyage de pâte d'eucalyptus blanchie en présence de particules de carbonate de calcium broyées. Les produits finaux contiennent 80% de fibrilles de cellulose et 20% de CaCO<sub>3</sub> en masse. Les échantillons préparés sont MNFC 0,5 wt% (poids en fibrilles) + CMC 0, 1, 2, 4, 6, et 8 % en masse, la concentration de CMC étant basée sur la quantité de MNFC ajoutée à

la feuille. Pour L-MNFC, les suspensions sont appelées simplement L-CMC 0, 1, 2, 4, 6, et 8, et pour H-MNFC, elles sont appelées H-CMC 0, 1, 2, 4, 6, et 8.

La revue de littérature a montré que le poly-électrolyte Carboxy Méthyl Cellulose (CMC), un composé anionique, contribue à la dispersion de fibres cellulosiques au niveau micrométrique. Pour optimiser la dispersion de la MNFC, les influences de la CMC sur la MNFC ont donc été étudiées. Afin de quantifier l'action de la CMC, deux types d'essais ont été réalisés : l'étude rhéologique et l'analyse morphologique des micro-nano fibrilles. La première indique le comportement dynamique entre les fibrilles (agglomérations, fluide non newtonien...) alors que la deuxième informe sur le comportement statique, *i.e.* l'état de dispersion, des fibrilles (séparation entre les fibrilles sans apport mécanique).

Pour la L-MNFC, les essais rhéologiques montrent que l'ajout de CMC diminue la viscosité de la suspension et, à hauts cisaillements, efface des perturbations qui sont probablement causées par la formation de floccs. De plus, pour des additions de L-CMC de 0 à 6%, les mesures de viscosité en fonction de taux de cisaillement ascendants et descendants ont montré la présence d'une boucle d'hystérésis démontrant un comportement non homogène. Toutefois, l'augmentation de la concentration de CMC entraîne une diminution de l'amplitude entre les cisaillements ascendants et descendants, jusqu'à sa disparition pour L-CMC 8. Pour la H-MNFC, le phénomène d'hystérésis existe pour H-CMC 0, 1 et 2, mais l'augmentation de la concentration en CMC au-delà de 2% permet d'en diminuer l'amplitude et le comportement de H-MNFC est homogène quand la concentration de CMC est de 4 à 8%. Ces comportements indiquent que les formations des floccs dans la suspension de MNFC diminuent à mesure que la concentration de CMC augmente.

La mesure de l'influence de la CMC sur la morphologie des fibres a été effectuée par microscopie optique (OM) et microscopie électronique à transmission (TEM) qui permettent de mesurer respectivement les fibrilles de tailles micrométriques et nanométriques. Pour la L-MNFC, les mesures réalisées par OM montrent que l'augmentation de la concentration de CMC de 0 à 2%, permet de diminuer significativement le diamètre moyen des fibrilles. Lorsque la concentration de CMC est

de 4 à 8% le diamètre augmente pour revenir au diamètre initial sans addition de CMC, soit L-CMC 0. Les résultats de mesure par TEM prouvent également que la concentration de CMC 2% permet de diminuer significativement le diamètre moyen des fibrilles de taille nanométrique par rapport à L-CMC 0. Pour la H-MNFC, les fibrilles sont toutes très petites (nanométriques) et ne peuvent être observées que par le TEM. Là encore, il a été montré que le diamètre moyen de H-CMC 2 est significativement plus petit que H-CMC 1.

Les analyses statique et dynamique démontrent quantitativement que la CMC contribue à la dispersion de MNFC au niveau micrométrique ainsi que nanométrique. Les informations de l'écoulement et de la morphologie des fibres peuvent être synthétisées ainsi : l'ajout de la CMC permet d'éliminer la formation des flocs et de diminuer le diamètre des fibrilles. Toutefois, les deux concentrations optimales de CMC sont différentes (8% pour complètement éliminer les flocs et 2% pour diminuer significativement le diamètre); la cause de la différence d'optimum peut être expliquée par les différents mécanismes d'interactions entre la CMC et la MNFC. Pour comprendre les relations entre ces deux éléments, une étude approfondie a été menée.

Les recherches ont porté sur l'adsorption possible de CMC sur les fibrilles de MNFC et sur la dissolution de CMC dans la suspension, *i.e.* la présence de molécules de CMC libres en solution. L'adsorption de CMC sur la MNFC peut être détectée par la modification de la physico-chimie de surface de MNFC, donc par l'évolution du potentiel Zêta. La quantité de la CMC libre est étudiée en séparant les fibrilles de la solution par centrifugation combinée à la mesure des charges anioniques dans le surnageant et complétée par l'analyse de la composition des matières sèches dans le surnageant.

Quand la concentration de CMC passe de 0 à 1%, le potentiel Zêta diminue puis, de 2 à 8%, il augmente au-delà du potentiel de la suspension originale. Ce comportement pourrait s'expliquer par une adsorption de CMC sur la MNFC de 0 à 1% puis de 2 à 8% la mesure du potentiel Zêta augmente probablement « artificiellement » à cause de l'augmentation de la conductivité de la suspension. Pour confirmer les analyses de surface, les mesures de la quantité des charges anioniques dans la solution ont été

effectuées. Pour ce faire, les solutions de  $\text{CaCO}_3 + \text{CMC}$  et le surnageant de MNFC sont dosés par titrage par poly-électrolyte. Premièrement, les résultats démontrent que la CMC peut se lier avec les particules de  $\text{CaCO}_3$ , cette association peut se réaliser par l'intermédiaire d'ions calcium présents dans la solution, par formation de complexes, ou par attraction électrostatique : les particules de  $\text{CaCO}_3$  étant légèrement cationiques. En outre, plus la concentration de CMC augmente dans les suspensions de L-MNFC, plus la quantité de charges anioniques augmente. Pour explorer les matières présentes dans le surnageant, la composition des matières sèches a été analysée par le microscope électronique à balayage (MEB) couplé à une analyse élémentaire (EDX). Ces observations ont montré l'adsorption des cristaux de  $\text{CaCO}_3$  sur la surface des fibrilles pour L-MNFC 0. De plus, le MEB a permis d'observer que l'ajout de CMC entraîne l'agglomération des particules de  $\text{CaCO}_3$  via la CMC.

Le  $\text{CaCO}_3$  semble donc jouer un rôle très important dans les interactions entre CMC et MNFC : le  $\text{CaCO}_3$  peut s'adsorber sur les fibrilles et il peut se lier avec la CMC. Donc la CMC peut s'adsorber sur les fibrilles sous forme de complexes  $\text{CMC} + \text{CaCO}_3$ . Sans la CMC, le  $\text{CaCO}_3$  se trouve individuellement dans la suspension; dès l'ajout de CMC, la CMC et le  $\text{CaCO}_3$  se lient, c'est ce qui crée des complexes de  $\text{CMC} + \text{CaCO}_3$  qui augmentent en taille avec la concentration de CMC. Pour les fibrilles, sans CMC, il n'y a que le  $\text{CaCO}_3$  qui s'adsorbe sur la surface. Lorsque la CMC est ajoutée, elle va venir s'adsorber sur les particules de  $\text{CaCO}_3$  à la surface des fibrilles. Quand la concentration de CMC est augmentée, les complexes grandissent et peuvent ne plus s'adsorber sur les fibrilles pour cause d'encombrement stérique.

Pour relier les données entre les interactions de la CMC sur la MNFC et leur impact sur la dispersion en suspension, une synthèse des résultats a été réalisée. La présence de CMC dans la suspension de MNFC permet de créer des complexes  $\text{CMC} + \text{CaCO}_3$  qui vont empêcher l'enchevêtrement des fibrilles et donc limiter la formation des floccs. À faible dose (1-2%), la CMC s'adsorbe sur les fibrilles et permet dans un premier temps de les éloigner, donc de diminuer le diamètre observé. Au-dessus d'une certaine concentration de CMC (environ 2%), les complexes augmentent en taille et leur adsorption sur la surface des fibrilles n'est plus assurée (encombrement stérique); ce qui

entraîne le rapprochement des fibrilles et donc l'augmentation du diamètre moyen. Quand la CMC s'adsorbe sur les particules de  $\text{CaCO}_3$  présentes sur la surface de MNFC, il éloigne les fibrilles. Quand les complexes CMC +  $\text{CaCO}_3$  augmentent en taille, ils ne sont pas adsorbés de manière irréversible et peuvent former des ponts entre les fibrilles en les empêchant de s'agglomérer. En tenant compte des effets de la CMC sur l'agglomération des fibrilles et sur la morphologie des fibrilles, un ajout de CMC de 4 à 6% est considéré comme la concentration optimale de CMC pour atteindre la meilleure dispersion de MNFC. En effet, à cette concentration, la CMC permet de diminuer le diamètre moyen des fibrilles et d'homogénéiser l'écoulement de la suspension.

Afin de réaliser l'application de MNFC en tant qu'agent de couchage, la capacité d'écoulement (débit) des suspensions MNFC dans le processus de couchage rideau a été explorée. Tout d'abord, les caractéristiques de fonctionnement de Hydra-Sizer<sup>TM</sup> ont été évaluées en utilisant de l'eau et la CMC comme modificateur de rhéologie dans des essais hors machine à papier (hors ligne). Les essais montrent que l'uniformité du rideau le long de l'Hydra-Sizer<sup>TM</sup> peut être améliorée en ajustant avec précision l'écartement des lèvres de l'appareil. Le débit global en masse diminue légèrement mais reste constant pour les différentes viscosités. L'Hydra-Sizer<sup>TM</sup> apparaît donc comme un procédé robuste qui ne sera pas perturbé par la rhéologie des suspensions de MNFC. Après l'ajustement des lèvres, les suspensions de MNFC avec et sans CMC ont ensuite été utilisées pour vérifier la stabilité et l'uniformité de rideau dans Hydra-Sizer<sup>TM</sup>. Les deux suspensions ont montré la formation d'un rideau stable et uniforme sans différence notable entre elles. L'application de MNFC dans le couchage rideau effectuée par l'Hydra-Sizer<sup>TM</sup> est donc aisément réalisable et les essais en ligne permettront de valider le procédé en condition dynamique.

Cette étude de maîtrise a permis d'expliquer l'effet et l'importance de la CMC sur la dispersion des fibrilles. Des études quantitatives ont validé la dispersion et l'homogénéisation des suspensions de MNFC par la CMC. A faible dose (1-2%), le poly-électrolyte permet d'éloigner les fibrilles par répulsion électrostatique et donc d'avoir un diamètre moyen de fibrilles plus faible. D'un autre côté, à forte dose (4-8%) il permet de créer des ponts entre les fibrilles ce qui empêche la formation de flocs. En

termes d'application, l'utilisation de l'Hydra-Sizer™ a pu être validée avec les suspensions de MNFC avec et sans CMC. Des essais en ligne permettront de mesurer les impacts de la CMC sur les propriétés finales du papier structuré par une couche de MNFC.

Juillet 2014

### **Mots-clés**

Micro-Nano-Cellulose-Fibrillée (MNFC); Carboxy Méthyl Cellulose (CMC); dispersion; rhéologique; adsorption; carbonate de calcium; curtain coating; Hydra-Sizer™

## Table of Contents

Foreword .....	iii
Acknowledgements .....	iv
Abstract .....	vi
Keywords .....	viii
Résumé .....	ix
Mots-clés .....	xiv
Table of Contents .....	xv
List of Figures .....	xvii
List of Tables .....	xx
List of Equations .....	xxi
List of Abbreviations .....	xxii
Chapter 1 Introduction .....	1
Chapter 2 Literature review .....	4
2.1 MNFC characteristics .....	4
2.2 MNFC dispersion problematic .....	12
2.3 Hydra-Sizer <sup>TM</sup> .....	18
2.4 Conclusion on the literature review .....	25
Chapter 3 Materials and methods .....	27

3.1	Materials.....	27
3.2	Methods.....	28
Chapter 4	Results and discussions.....	39
4.1	Experimental approach.....	39
4.2	Influence of CMC on MNFC .....	41
4.3	Interactions between CMC and MNFC .....	66
4.4	L-MNFC + CMC process ability in offline Hydra-Sizer™ trials.....	90
Chapter 5	Conclusions.....	98
	Future work .....	99
	List of presentations and posters.....	100
	Presentation.....	100
	Posters .....	100
	References.....	101

## List of Figures

Figure 2.1	Hierarchical structure of cellulose [9] .....	5
Figure 2.2	Scanning electron micrographs of: a (kraft pulp); b (30 passes through the refiner + 2 passes through the homogenizer pulp); c (30 passes through the refiner + 30 passes through the homogenizer pulp). Picture (a) is $\times 500$ magnification; Pictures b, c are at $\times 5000$ magnification. [10] .....	6
Figure 2.3	Diagram showing the ionic concentration and potential difference as a function of distance from the charged surface of a particle suspended in a dispersion medium.....	11
Figure 2.4	Fundamental spatial arrangement difference between dispersion and distribution .....	13
Figure 2.5	Effects of CMC on colloidal MCC dispersions [35] .....	14
Figure 2.6	Phase contrast images of highly beaten fines free fibers without polymer treatment (a), treated with dispersing polymer, CMC (b) [32] .....	15
Figure 2.7	CMC highly promotes the fiber surface fibrillation .....	15
Figure 2.8	Relative viscosity of suspensions of polymer and MNFC ( $\eta_{rel} = \eta_{susp} / \eta_{sol}$ , susp consists of 0.5% polymer + 0.5%MNFC and sol is 0.5% polymer solution) [36] .....	16
Figure 2.9	Tan delta of suspensions of polymer and MFC [36] .....	17
Figure 2.10	Operating window in curtain coating [40] (U: web speed, Vc: curtain speed at impact, Re: Curtain Reynolds number) .....	20
Figure 2.11	Hydra-Sizer™ at CRML (Centre de recherche sur les matériaux lignocellulosiques) running with water .....	21
Figure 2.12	Stationary part of Hydra-Sizer™ .....	22
Figure 2.13	Active part of Hydra-Sizer™ .....	22
Figure 2.14	Stationary part .....	23
Figure 2.15	Active part .....	23
Figure 2.16	Curtain coating application with typical flow pattern and process parameters [39] .....	24
Figure 3.1	Mütek™ SZP-06 System Zeta Potential.....	30
Figure 3.2	Measuring cell of a Mütek™ SZP-06 System Zeta Potential.....	31
Figure 3.3	PCD 03 Particle Charge Detector32	
Figure 3.4	Structure of schematic of Particle Charge Detector [44].....	33
Figure 3.5	JSM-5500 Scanning Electron Microscope .....	35

Figure 3.6	Diagram of the installation of Hydra-Sizer™ for off-line tests.....	36
Figure 3.7	Installation of Hydra-Sizer™ with a recirculation tank. ....	36
Figure 3.8	Method for testing uniformity and mass flow of Hydra-Sizer™ .....	37
Figure 4.1	Experimental approach to study MNFC dispersions.....	40
Figure 4.2	The viscosity-shear rate curve of L-MNFC suspensions in upward sweep (a: L-CMC 0, 1, 2; b: L-CMC 4, 6, 8).....	43
Figure 4.3	Agglomeration of fibrils in rheological test.....	44
Figure 4.4	The viscosity-shear rate curves for L-CMC 0, 1, 2, 4 suspensions in up and down sweep (closed symbol: upward sweep; open symbol: downward sweep. a: L-MNFC 0, 1; b: L-MNFC 2, 4) .....	45
Figure 4.5	The viscosity-shear rate curves of L-CMC 6 and 8 suspensions in up and down sweep (closed symbol: upward sweep; open symbol: downward sweep) .....	46
Figure 4.6	The viscosity-shear rate curve of H-MNFC 0.5% in upward sweep.....	48
Figure 4.7	The viscosity-shear rate curve of H-MNFC suspensions in up and down sweep (closed symbol: upward sweep; open symbol: downward sweep), (a: H-CMC 0, 1, 2; b: H-CMC 4, 6, 8).....	50
Figure 4.8	Distribution of fiber width FQA .....	53
Figure 4.9	Average fiber width vs. length (FQA).....	54
Figure 4.10	OM pictures of L-MNFC 0.5% (a) and L-MNFC 0.5% + CMC 1% (b) .....	55
Figure 4.11	Statistical analysis of L-MNFC 0.5% suspensions (a: fibrils diameters and box charts; b: density distribution of fibrils diameter). .....	55
Figure 4.12	Whisker box structure [47] .....	56
Figure 4.13	TEM pictures of L-MNFC 0.5% at the magnification of 56 000X and 110 000X .....	58
Figure 4.14	TEM picture of L-MNFC 0.5% at the magnification of 28 000X.....	59
Figure 4.15	Statistical analysis of L-MNFC 0.5% suspensions (a: fibrils diameters and box charts; b: density distribution of fibrils diameter). .....	59
Figure 4.16	TEM pictures of H-MNFC 0.5% at the magnification of 28 000X.....	61
Figure 4.17	TEM pictures of H-MNFC 0.5%+CMC 2% at the magnification of 56 000X (a) and of 110 000X (b).....	62
Figure 4.18	Statistical analysis of H-MNFC 0.5% suspensions (a: fibrils diameters and box charts; b: density distribution of fibrils diameter). .....	63

Figure 4.19	Schematic representation of the dispersion and distribution of the fibrils in the L-CMC suspension according to the CMC concentration .....	66
Figure 4.20	Zeta potential of CMC 0.1% with different pH value .....	67
Figure 4.21	Zeta potential and conductivity of L-MNFC 0.5% (a) and H-MNFC 0.5% (b) suspensions with different concentrations of CMC .....	69
Figure 4.22	Calibration line for Poly-DADMAC consumption versus CMC amount .....	71
Figure 4.23	Measured anionic charge quantity of C-CMC solutions .....	74
Figure 4.24	Measured anionic charge quantity of the supernatant of L-MNFC suspensions (centrifugation at 10 000rpm for 1h).....	77
Figure 4.25	SEM pictures of L-CMC 0, L-CMC 1, L-CMC 4 and L-CMC 8.....	79
Figure 4.26	SEM picture of pure CMC 0.04wt% solution after drying (5 000X) .....	80
Figure 4.27	SEM pictures and the corresponding elemental analysis of L-CMC 0, 1, 2, 4, 6, and 8 at 2500X magnification. ....	82
Figure 4.28	SEM picture of L-CMC 0 with fibril (2500X) .....	84
Figure 4.29	SEM picture of L-CMC 1 with fibril (5000X) .....	84
Figure 4.30	Formation of calcium alginate from sodium alginate [53] .....	86
Figure 4.31	Structure of sodium carboxy-methyl cellulose .....	86
Figure 4.32	Fibrils, CMC molecules, and CaCO <sub>3</sub> in the suspensions of L-CMC 0, L-CMC 1 and L-CMC 8 .....	89
Figure 4.33	Mass flow of water with different recirculation rates and the nozzle gap at different positions .....	92
Figure 4.34	Global mass flow and viscosity of CMC .....	93
Figure 4.35	Flow curtains of L-MNFC 0.5% at the flow rate of 50L/min (left) and 70L/min (right) .....	94
Figure 4.36	Mass flow of L-MNFC 0.5% along the outlet of Hydra-Sizer™ .....	94
Figure 4.37	Flow curtain of L-MNFC 0.5% + CMC 6% at the flow rate of 50 L/min (left) and 70 L/min (right) .....	96
Figure 4.38	Mass flow of L-MNFC 0.5% + CMC 6% along the outlet of Hydra-Sizer™ .....	97

## List of Tables

Table 3.1	Characteristics of L-MNFC and H-MNFC .....	27
Table 3.2	Trials of MNFC suspensions in the off-line Hydra-Sizer™ .....	38
Table 4.1	Composition concentration and composition ratio in L-MNFC suspensions .....	41
Table 4.2	Influence of CMC on rheological characteristics of MNFC.....	51
Table 4.3	Significant difference of fibril diameters between L-MNFC 0.5% suspensions (OM) .....	57
Table 4.4	Significant difference of fibril diameter between L-MNFC 0.5% solutions (TEM) .....	60
Table 4.5	Significant difference of fibril diameters between H-MNFC 0.5% suspensions (TEM) .....	63
Table 4.6	Influence of CMC on L-MNFC flow behaviour and fiber morphology .....	64
Table 4.7	Influence of CMC on H-MNFC flow behaviour and fiber morphology.....	65
Table 4.8	The anionic charge quantity per gram of CMC .....	72
Table 4.9	CMC concentration (g CMC/g solution) and the hypothetical CMC charge quantity (eq/g solution) in the CaCO <sub>3</sub> solutions.....	73
Table 4.10	CMC concentration (g CMC/g supernatant) and the hypothetical CMC charge quantity (eq/g supernatant) in the L-MNFC suspensions .....	76
Table 4.11	Interaction between fibrils and CMC+CaCO <sub>3</sub> complexes .....	86
Table 4.12	Dispersion effects of CMC on L-MNFC .....	87
Table 4.13	Water flow tests in off-line Hydra-Sizer™ trials.....	91

## List of Equations

$r = r_0 \sin(\omega t) \Rightarrow r^* = r_0 \cdot e^{i\omega t}$	Equation 2.1..... 16
$\tau = \tau_0 \sin(\omega t + \delta) \Rightarrow \tau^* = \tau_0 \cdot e^{i(\omega t + \delta)}$	Equation 2.2..... 16
$V_c = V_0 + \sqrt{2gx}$	Equation 2.3..... 24
$r = \frac{Vc}{z}$	Equation 2.4..... 24
$Re = \frac{\rho h_c V_c}{\eta}$	Equation 2.5..... 25
$We = \frac{\rho h_c V_c^2}{\sigma}$	Equation 2.6..... 25
$q = \frac{V \times c}{\omega t}$	Equation 3.1..... 33
$q^* = \frac{V \times c}{\omega t^*}$	Equation 3.2..... 34
$Y = 3765.6X - 0.1541$	Equation 4.1..... 71
$q(\text{hypothetical CMC}) = m(\text{CMC}) \times q(\text{CMC})$	Equation 4.2..... 72

## List of Abbreviations

CMC	carboxy-methyl-cellulose
C-PAM	cationic polyacrylamide
CS	cationic starch
DL	double layer
DS	degree of substitution
FQA	Fibre Quality Analyzer (from OpTest)
GL&V	Groupe Laperrière et Verreault
MCC	micro-crystalline cellulose
MFC	micro-fibrillated cellulose
MNFC	Micro-Nano-Fibrillated-Cellulose
L-MNFC	Micro-Nano-Fibrillated-Cellulose, in a low fibrillated state
H-MNFC	Micro-Nano-Fibrillated-Cellulose, in a high fibrillated state
NFC	nano-fibrillated cellulose
NSERC	Natural Sciences and Engineering Research Council of Canada
OM	optical microscope
OTR	oxygen transmission rate
PCD	particle charge detector
PEO	poly-ethylene-oxide
SEM	scanning electron microscope

TEM	transmission electron microscope
TMP	thermo mechanical pulp
WVP	water vapor permeability
WVTR	water vapor transfer rate
ZP	zeta potential

## Chapter 1 Introduction

The Canadian pulp and paper industry is one of the country's most important industries. In 2013, Canada's pulp and paper exports totaled about 23 million tons: about 40% being newsprint, of which Canada has been the world's largest producer for over 50 years. About 37% of exports are wood pulp, for further processing into paper and paperboard and 23% are a wide variety of packaging papers and boards, book and writing papers, tissue and sanitary papers, and building papers and boards. Québec accounts for the largest share of total pulp and paper production, about 35%; Ontario represents about 25%; British Columbia 22%; and the Atlantic and Prairie provinces together represent around 18% [1].

The Thermo Mechanical Pulp (TMP) process is a backbone of the pulping industry [2]. Due to a high yield and a good bulk, TMP is widely used in the production of newspapers and low-end printing paper while that fact that it ages rapidly (yellowing) and moderate mechanical properties limit its application. Nowadays, due to information technologies related to the advent of ubiquitous electronics (smart phones, tablets and portables), the market share of newspaper and low-end printing and publication grade papers is decreasing year after year. As Canada and especially Quebec was and still is a world leader in the production in the declining market of newsprint, novel applications and products to valorize and maintain TMP production facilities has become an immediate and urgent concern.

Fortunately, the emergence of new high-technology cellulose products such as nanocellulose and micro to nanocellulose fibrils, sometimes called “cellulose filaments”, generates new opportunities to valorize TMP as a component of innovative, green paper, *i.e.* without any chemical pulp and/or chemical additives, grades. Nanocellulose is a cellulosic material composed of nano-sized cellulose crystals and/or fibrils (as far as diameter or width is concerned). As cellulose is an abundant organic compound originating from biomass, nanocellulose is also considered to come from renewable forest resources. Being one kind of nanocellulose or “cellulose filaments”, Micro-Nano-Fibrillated-Cellulose (MNFC) presents an interesting potential for

application in papermaking. As it has been shown that micro-fibrillated cellulose (an MNFC of sorts) may well succeed in improving the mechanical and barrier properties of paper [3], the integration of MNFC in paper products attracts more and more interest. Building on such potential, the Arboranano network, whose objective is to develop applications of nano materials, but mainly nanocellulose, in forest products, has been created to support new business opportunities for the Canadian economy by using Canada's renewable forest resources to manufacture new value-added products with superior performance attributes [4]. In present UQTR-Arboranano related project, it is proposed to apply MNFC during papermaking as a structuring layer within a TMP sheet to improve the mechanical and barrier properties of TMP sheet. It can be done commercially through the use of a Hydra-Sizer<sup>TM</sup>, a curtain coating equipment developed by GL&V to be integrated at the wet-end of a paper machine. To retain the specific properties related to the micro-nano structure of cellulose, namely to achieve the improvement of the barrier and mechanical properties, the fibrils should retain their micro-nano dimension: *i.e.* they should not agglomerate and they should then be well dispersed. Consequently, as the dispersion of MNFC has a significant impact on the properties of the final sheet, the objective of this master's research work is to understand and improve the MNFC dispersion in papermaking applications. In parallel, Carboxy Methyl Cellulose (CMC) is widely used as dispersing agent in industry and its effect on the dispersion of fibers at the micro level has been shown in the literature. In this project, CMC is used to improve the MNFC dispersion surmising that the effect found at the micro level would extend to the nano structures. To find the optimum level of CMC addition, the dispersing effects of CMC on MNFC is researched as well as the mechanism of interactions between CMC and MNFC. To complete the application of MNFC, off-line trials are carried out for the evaluation of the performance of MNFC suspensions in the Hydra-Sizer<sup>TM</sup>.

As an introduction to our project, a thorough literature review on MNFC-like material characteristics and on the interactions between CMC and MNFC is summarized. Materials and methods are then presented, followed by results and discussions. In this last part, the effects of CMC on MNFC have been outlined and a potential mechanism of

interaction is proposed and discussed. Conclusions related to the dispersion mechanism focus on the final application.

## Chapter 2 Literature review

Due to the focus placed on the application of MNFC as a structuring layer in paper sheet, the literature review first explores the micro-fibrils and nano-fibrils properties, the effects of CMC on cellulosic fibers, and the interactions between CMC and micro-cellulose. The curtain coating process and, of course, the Hydra-Sizer™ equipment is also presented, to better understand the limitations and potential of the implementation of a curtain coating operation.

### 2.1 MNFC characteristics

Present section introduces MNFC in detail, including cellulose: the source of MNFC, MNFC production, its morphology, and its properties.

#### 2.1.1 Hierarchical structure of cellulose

Cellulose is a linear, stereo-regular polysaccharide built from repeated D-gluco-pyranose units linked by 1,4-glycoside bonds [5]. Presented in Figure 2.1 (bottom left), is the basic chemical structure of cellulose, namely D-gluco-pyranose. It contains three hydroxyl groups which ensure the formation of strong hydrogen bonds and confers upon cellulose its most important properties, such as the multi-scale micro-fibrillated structure with a glass transition temperature higher than its degradation temperature [6]. Typically, approximately 36 individual cellulose molecules are brought together into larger units known as elementary fibrils, which then pack into large units called micro-fibrils [6]. Depending on the origin, the micro-fibril diameters may vary. However, a micro-fibril has generally an about 2-10 nm thick fibrous cellulose structure and a length of several tens of microns [7]. Each micro-fibril can be considered as a flexible hair strand with cellulose crystals linked along the micro-fibril axis by disordered amorphous, *i.e.* non crystalline, domains [8]. The fibrils bundles are formed by regrouping micro-fibrils. A fiber is formed by the association of the fibrils bundles.

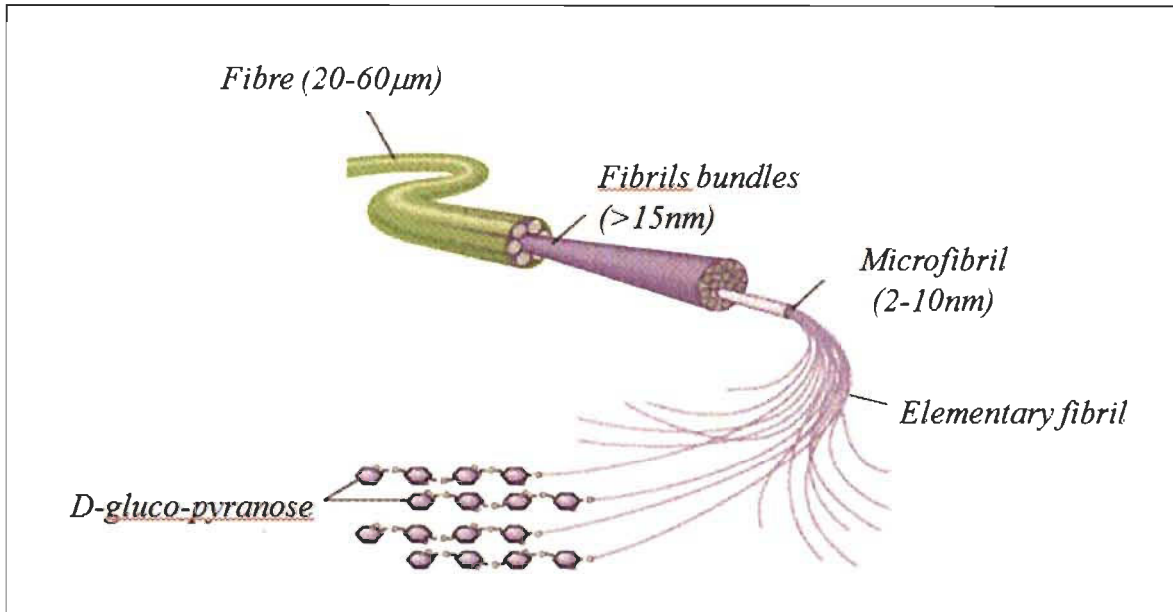


**Figure 2.1 Hierarchical structure of cellulose [9]**

### 2.1.2 MNFC production

Initially obtained by a homogenization process [3], MNFC is currently manufactured from a number of different cellulosic sources, of which wood is still the main raw material. The fibrillation is completed by mechanical treatments through several types of equipment such as homogenizer, micro-fluidizer, and grinder. The various mechanical treatments processes lead to different fibrillation levels or degrees. For instance, Figure 2.2 from Nakagaito *et al.* [10] illustrates an original fiber (a) and the fibrillation of fibers after different mechanical treatments (b and c). Less time was applied in the homogenizer for b than for c, therefore picture c exhibits the highest fibrillation degree. The fibrillation degree is characterized by the fibrils distribution along the fiber and the diameter of individual fibrils. The degree of mechanical treatment determines the degree of fibrillation. For this reason the fibrillation degree cannot be modified after manufacture but the full potential of the fibrillation degree still needs to be obtained through an “as-close-to-perfect” dispersion state.

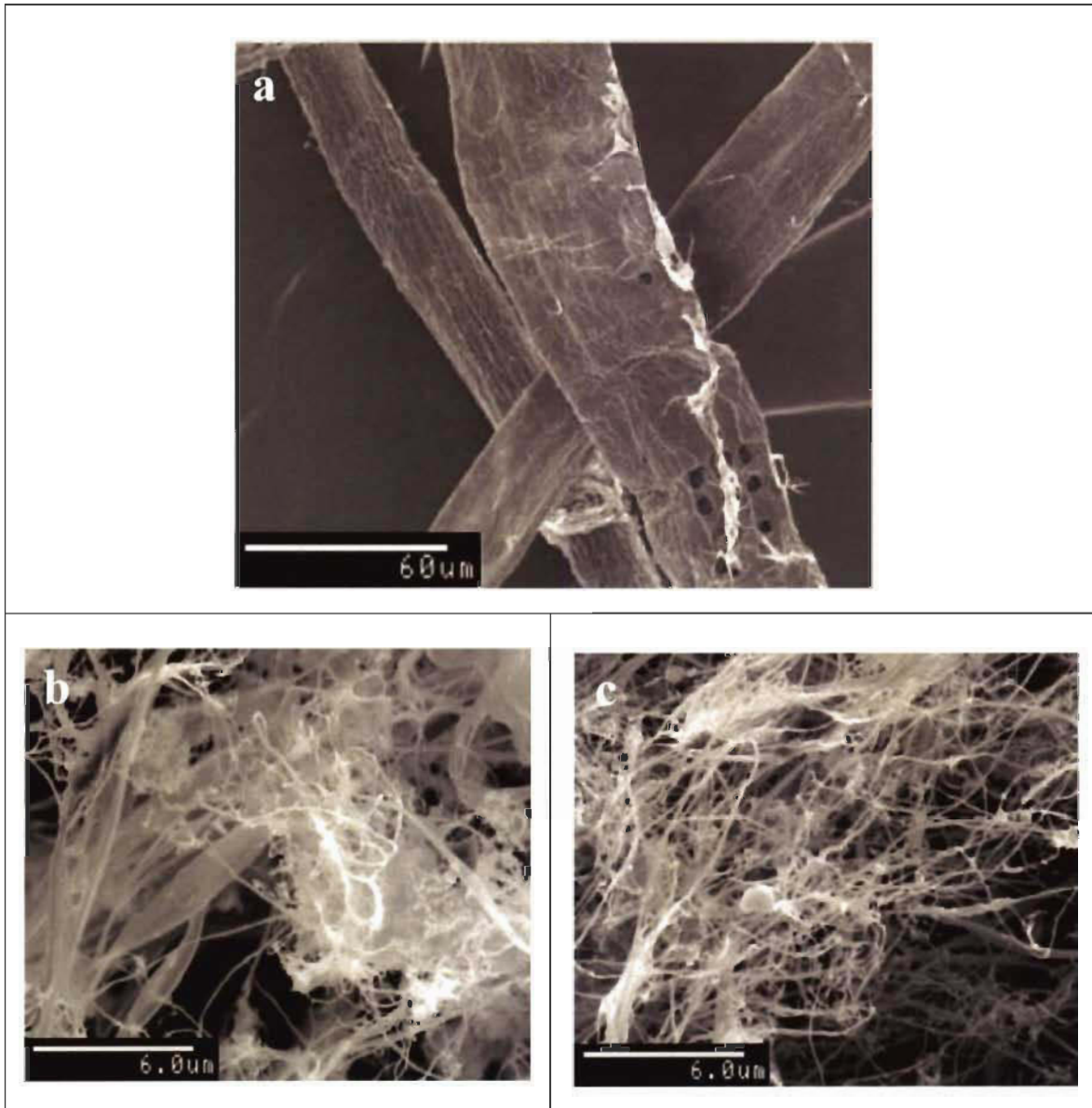


**Figure 2.2 Scanning electron micrographs of: a (kraft pulp); b (30 passes through the refiner + 2 passes through the homogenizer pulp); c (30 passes through the refiner + 30 passes through the homogenizer pulp). Picture (a) is  $\times 500$  magnification; Pictures b, c are at  $\times 5000$  magnification. [10]**

Many companies are investigating the production of MNFC (or “cellulose filaments”) to explore the market. OMYA International AG produces MNFC by a mechanical disintegrated process of wood fibers, and more precisely using the Masuko grinding process known to be the first in the field. OMYA International AG specificity is that fibers are co-processed with ground calcium carbonate thus significantly reducing the

energy input. The calcium carbonate particles remain as a very useful inorganic filler in the resulting MNFC network [11].

Nowadays, more and more pre-treatments and post-treatments are being developed, either to reduce the energy consumption of MNFC production, or to improve the MNFC or even to endow MNFC with specific new properties, from the perspective of new potential applications [7]. Various production methods and diverse raw materials are leading to different fibrillation degrees and result in different MNFC morphology that needs to be further investigated.

### **2.1.3 MNFC morphology**

Due to the application of mechanical treatments, Micro-Nano-Fibrillated-Cellulose (MNFC) can be extracted from cellulose fibers into micro/nano-scale elements of varying micro- and nano- size components. In principle, the thickness of MNFC nano-elements could be as small as 3–10 nm, but, mainly for low fibrillation grades, it is typically in the range of 20–40 nm. Furthermore, the MNFC nano-sized compositions usually consist of aggregates of cellulose nano-fibrils [7]. However, the micro-sized compositions can be considered as fibrils bundles. The fibrillation degree of MNFC determines the distribution of fibril diameters. Moreover, the fibrils length is usually, like many other grades, in the order of tens of micrometers.

In the literature, the terms Micro-Fibrillated Cellulose (MFC) and Nano-Fibrillated Cellulose (NFC) contain both micro and nano sized elements and have often been used without specific size specifications [3, 7], notwithstanding the fact that the micro and nano portions of the fibrils are often mixed. In present work, we coined the term MNFC (Micro-Nano-Fibrillated-Cellulose) to illustrate this fact in preference of the general terms MFC and NFC. The most recent terminology proposed by FP Innovations, “cellulose filaments” may also represent a good “commercial solution (as the term nano is removed) but do not truly apply to describe the product in a scientific perspective.

#### 2.1.4 MNFC properties and application

As a renewable non-toxic forest product [12], MNFC does resemble MFC (the micro part) and like MFC, it possesses several interesting properties. MNFC is composed of expanded high-volume cellulose, moderately degraded. It exhibits a particularly high specific area, flexibility, crystallinity, polymerization degree, and contains a high amount of hydroxyl groups which influence their interactions as a suspension in liquid, or as a film. Furthermore, MFC's high aspect ratio (length/diameter) endows it with a very low percolation threshold. MFC thus has a very good ability to form a rigid network [3]. As it originates from the de-structuring of vegetal fibers, MFC and thus MNFC retain many of the advantageous properties of cellulose fibers, such as the ability to form hydrogen bonds, resulting in strong networks [13]. Indeed, MFC films exhibit remarkable mechanical properties [13] and the mechanical reinforcement property of MNFC in composites has also been shown [14-16].

The many interesting properties of MFC render it attractive for numerous applications such as efficient catalysts, electro optical films, nano-fiber-reinforced composites, microelectronics, gas-barrier films, cosmetics, flame-resistant materials, and other high-tech or high-performance materials [17].

Due to a relatively high crystallinity combined with the ability of the nano-fibers to form a dense network held together by strong inter-fibrillar bonds, it has been hypothesized that MFC, and in our case MNFC, might act as a barrier material [7]. Actually, 100% MFC films exhibit excellent barrier properties in terms of the Water Vapor Transfer Rate (WVTR), Water Vapor Permeability (WVP), and oxygen barrier [3]. As for MFC nano-composites, some papers present interesting barrier properties, notably the addition of MNFC in amylopectin improves oxygen permeability [18] and adding MFC in cellulose nano-composites with a starch matrix also reduces moisture diffusivity [19].

The combination of MFC in papers is relatively recent, some studies indicated that coating MFC on paper results in an improvement of the mechanical and barrier properties [13, 20, 21]. The first studies performed on the Micro-Fibrillated Cellulose

(MFC) actually indicate that the potential exists to combining MFC with paper in fields such as food packaging and printing.

Syverud *et al.* [13] observed that the air permeability decreases drastically with an increase in the weight of the MNFC coating. For 2 g/m<sup>2</sup> the air permeability is about  $3.10^4$  nm.Pa<sup>-1</sup>.s<sup>-1</sup>, while for an 8 g/m<sup>2</sup> of MFC coating, the air permeability dropped to about 360 nm.Pa<sup>-1</sup>.s<sup>-1</sup>, *i.e.* 100 times less. As for the oil barrier, an increase of oil resistance with paper coated with MFC has been observed, probably as a result of the MFC layer reducing the overall sheet porosity [21]. Furthermore, the use of MFC as surface layer (0–8% of total basis weight) on base paper increases the strength of the paper sheets significantly. 8% MFC leads to the improvement of 15% tensile and 30% as fast as the elongation is concerned [13].

In the paper of Hult *et al.* [20], MFC and shellac, a natural resin secreted by the lac insect *Kerria lacca* (with characteristics of hydrophobicity, biodegradability, and renewability making it a good candidate in combination with MFC for commercial use) were used as a coating agent. It was found that both MFC and shellac layers decreased the oxygen transmission rate (OTR), but OTR values still remained too high (about 5,000 cm<sup>3</sup>/m<sup>2</sup>day) to consider that such coated cellulosic materials would provide an efficient oxygen barrier (3 cm<sup>3</sup>/m<sup>2</sup>day). However, this disappointing result was related to the non-homogeneous coating of MFC. The water vapor transmission rate (WVTR) of the coated paper showed no significant improvement compared to the base paper due to the hydrophilic nature of the coating components.

### 2.1.5 Rheology of MNFC

Independently of how the suspension is obtained and its source, MFC in an aqueous environment reveals a pseudo-plasticity (shear thinning) behaviour, *i.e.* when the shear rate increases, the viscosity of the suspension decreases [22, 23]. Regardless of the concentration, in the references from 0.125 to 5.9 wt%, the MFC suspensions display a gel-like behaviour and the values of the storage modulus are rather high. These results show that even at the lowest concentration of 0.125 wt%, MFC suspensions will form a rather strong network [23]. The shear thinning behaviour of MFC suspensions may be

due to a packing aggregation of MFC, which limits the formation of a continuous network. The packing aggregation will result in a decrease in viscosity with increasing shear rate. More recent studies have confirmed such an hypothesis [3].

Iotti *et al.* [24] stated that higher concentrations result in increased yield stress and higher viscosities. Higher concentrations of fibrils facilitate the creation of a network and of structure by the creation of bonds between fibrils. The development of a structure causes an increase in viscosity, *i.e.* resistance to shear. A reduction of viscosity with increasing temperature was also demonstrated in a study by Iotti *et al.* However, the phenomenon was but partly analyzed due to the well-known reduction in viscosity of water with temperature increase. An additional decrease may be related to the ability of cellulose and hemicelluloses to take-up water molecules and swell is an exothermic reaction, the increased temperature leading to a partial de-swelling of the fibers could then bring about an increase in the fibers and fibrils mobility [24].

In conclusion, the rheological analyses presented in the literature so far, are still insufficient to formulate a proper explanation of the peculiar behaviour of MFC, and thus MNFC dispersions, and the high gel forming properties [24]. It seems however quite logical that there must be some relationship between the rheology, the formation of network, and the dispersion of MNFC. The rheological parameters of MNFC dispersions would then represent a very important, if not the most important, index to explore and analyze the dispersions of MNFC. Another measure related to particle mobility, such as the zeta potential, is also here proposed to support the study of the dispersions of MNFC.

### **2.1.6 Zeta potential of MNFC**

Zeta potential is efficient to evaluate the stability of suspensions and the absorption of additives. The zeta potential (ZP) represents the electric charge of a particle with surrounding ions upon dissolution. The Zeta potential is then the electric potential in the interfacial double layer (DL) at the location of the slipping plane versus a point in the bulk fluid away from the interface [25]. (See Figure 2.3)

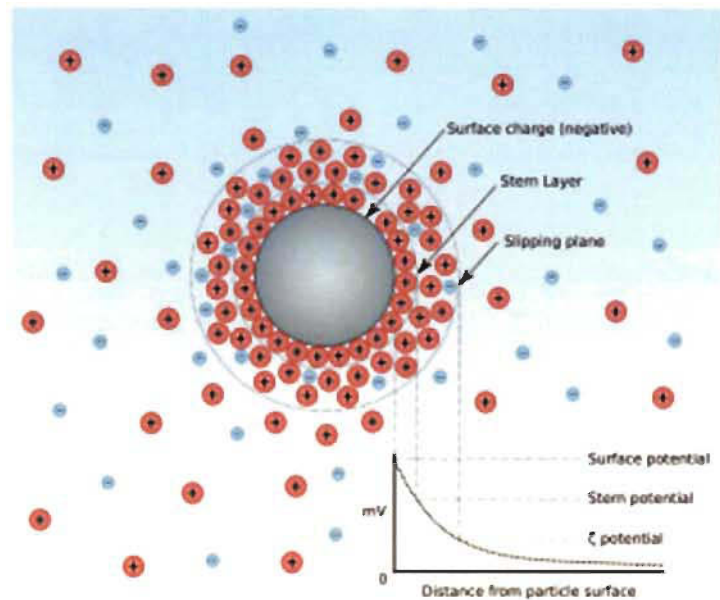


**Figure 2.3** Diagram showing the ionic concentration and potential difference as a function of distance from the charged surface of a particle suspended in a dispersion medium

Generally, ZP is considered as an index that can be used to evaluate the stability of colloidal solutions. A high zeta potential absolute value means a high dispersion of colloidal particles because of high repulsive forces. The zeta potential may also be used to describe adsorption phenomenon. For example Öhman *et al.* used the zeta potential to study the adsorption of aluminum (III) on cellulosic fibers [26].

One should note that the zeta potential depends both on pH and charge density. Zaucha *et al.* show that the zeta potential of polystyrene latex particles decreases as the pH increases [27]. The experiments of Christian demonstrate the influence of concentration of electrolyte on the zeta potential of sulfonated latex particles [28].

The effects of pH on the zeta potential are supposed to be due to the change of charge density in the solution. When adding electrolyte into the solution, more contrary ion would be pushed into the stern layer because of the increasing repulsive force which leads to the compression of the electrical double layer and decreases the charge of the colloidal particles. This will have an influence on the measure of the zeta potential. Therefore the comparison of zeta potential between different MNFC solutions should be analyzed under the same pH and charge density.

Up to now, there are only a few studies about the zeta potential of MNFC solutions. This is partly due to the fact that few apparatus can measure the ZP of particles ranging from micrometer length to nanometer diameter. Nevertheless, Olszewska, *et al.* show that the zeta potential of cationic MNFC decreases as the pH increases and that the net charge is clearly pH dependent [29]. In conclusion, charge density and pH are needed to be taken into account for ZP measurement of MNFC suspension. The ZP value is supposed to evaluate the dispersion and adsorption of MNFC. The combination of ZP measurement, charge density, and rheology analysis could then be applied to explore MNFC suspensions in order to improve the MNFC application.

## **2.2 MNFC dispersion problematic**

Owing to its excellent properties and structural proximity to MNFC, MFC has been reviewed quite recently in terms of application. As only a well dispersed suspension can provide the best micro-related and mainly nano-related properties, the completed understanding of MNFC dispersions is an inevitable milestone for any further commercial application of MNFC that would take a full advantage of the micro-nano-related properties.

### **2.2.1 Definition of fibrils dispersion**

The concepts of fibrillation and dispersion are easily confused. Fibrillation designs the partial delamination of fibers during the mechanical treatment. The level of fibrillation resulting from such mechanical treatment cannot thus be modified after MNFC production. Dispersion is the level of fibrils separation, which is somehow opposite to flocculation or agglomeration. Fibrils separation means fibrils dispersion and fibrils distribution. As shown in Figure 2.4, only when fibrils are well dispersed and distributed, a good dispersion of MNFC suspension is achieved. The state of dispersion could be improved by the addition of a dispersant.

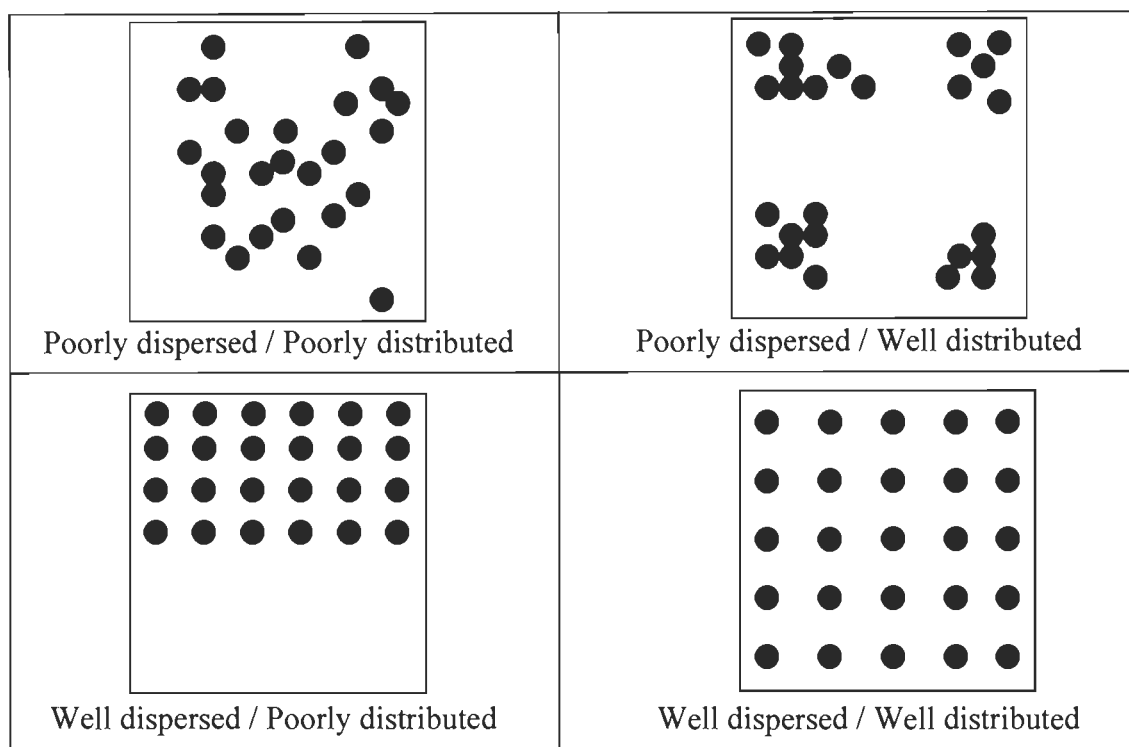


**Figure 2.4 Fundamental spatial arrangement difference between dispersion and distribution**

Cellulose-cellulose adhesion, which has received considerable attention over the past half century, occurs over a practical length scale ranging from the nanometer to the millimeter scale. For nanocellulose, a very high surface area renders the adhesion properties the most important parameter to control for nano-composite applications [30]. It notably appears that the homogeneity of nano-fibrillated cellulose material is more important for the reinforcement potential than the degree of polymerisation [31]. A good dispersion of MNFC suspensions facilitates the formation of strong network and therefore promotes the mechanical and barrier properties of nanocellulose films, nano-composites, and papers coated with MNFC. As the only physical parameter that can be controlled after manufacture, the dispersion of MNFC suspension is then primordial to obtain, and therefore also optimize, the maximum of MNFC excellent mechanical and barrier properties for efficient application in various industrial products.

## 2.2.2 Dispersing agent: Carboxy Methyl Cellulose

It has been seen in the literature that the dispersion of cellulosic fibers could be notably improved by the use of an anionic cellulose derivative such as the Carboxy Methyl Cellulose (CMC) [32-34]. This section presents the effects so far reported and the potential mechanism involved.

### 2.2.2.1 CMC dispersion effect on fiber

The adsorption of CMC on cellulose nano-fibrils has been explored by Ahola et al [34] who show that the adsorption of CMC is reversible on the nano-fibrils film surface and that CMC adsorption results in dispersion effects. The dispersion effects of CMC have also been investigated on Micro Crystalline Cellulose (MCC), see Figure 2.5. CMC is adsorbed on the surface of MCC and the stable 3-dimensional gel network of colloidal MCC dispersions are stabilized by electrostatic repulsion [35]

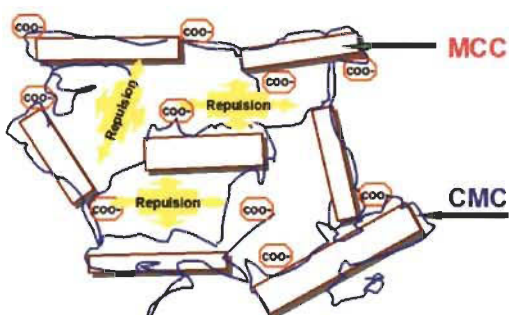


**Figure 2.5** Effects of CMC on colloidal MCC dispersions [35]

Another study conducted by Myllytie *et al.* [32] reveals the effects of CMC on the fiber surface fibrils with the help of optical microscopy to visualize the fibers in water. The optical microscopy images recorded in phase contrast mode of highly beaten fines free fibers without polymer treatment and treated with dispersing polymer, CMC are presented in Figure 2.6.

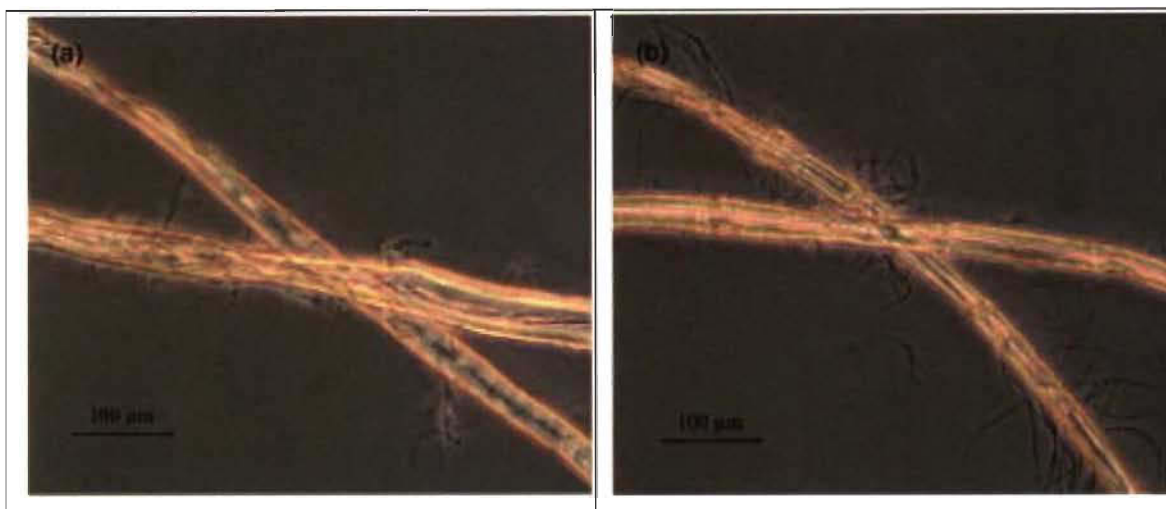


**Figure 2.6** Phase contrast images of highly beaten fines free fibers without polymer treatment (a), treated with dispersing polymer, CMC (b) [32]

The highly beaten fines free fibers in Figure 2.6.a indicate that the fiber surface fibrils are always aggregated to some extent. When treated with CMC the fibrillar structure on the fiber surface becomes quite extended and finely dispersed.

An ineffective mechanical action may lead to the “appearing” agglomerated surface fibrillation. After CMC treatment the fiber surface fibrils are more dispersed and appear as fine webs or thin veils on the fiber surface [32]. As outlined in Figure 2.7, the addition of CMC highly promotes the fiber surface fibrillation.

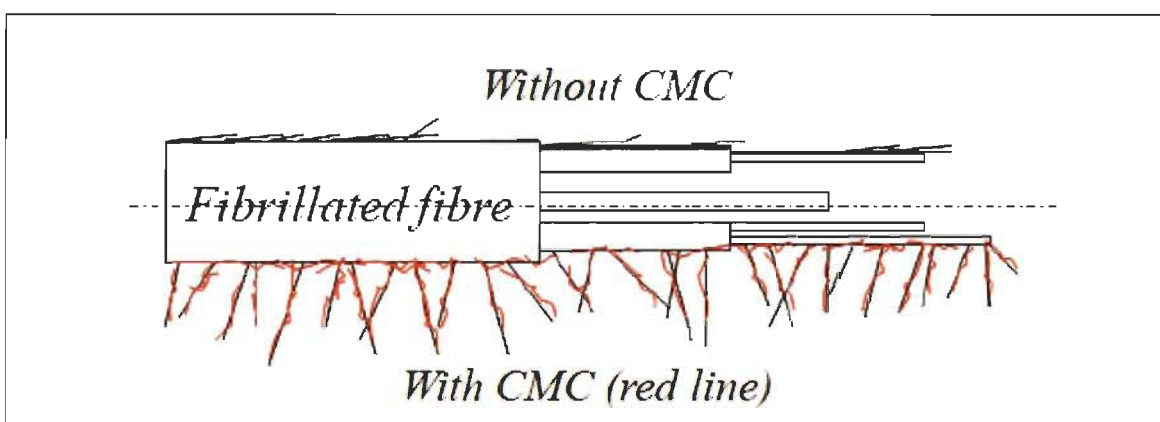


**Figure 2.7** CMC highly promotes the fiber surface fibrillation

### 2.2.2.2 CMC dispersion effect on MNFC rheology

The effects of CMC on MFC rheology have been explored in the study of Vesterinen *et al.* [36]. In the article, relative viscosity values (*i.e.* the ratio between viscosities of the polymer solution and the MFC suspensions) for four different polymers: cationic starch (CS), cationic polyacrylamide (C-PAM), CMC, poly-ethylene-oxide (PEO) are released (see Figure 2.8). For the MFC/CMC solution, the strongly shear thinning behaviour and typical yielding behaviour of MFC disappear. The authors suppose that CMC have a certain dispersing effect in the system, and that it probably decreases the amount of free water in the suspension.

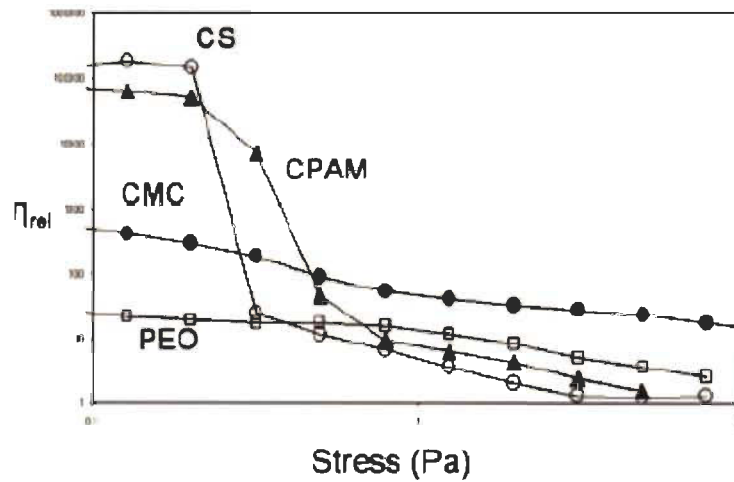


**Figure 2.8** Relative viscosity of suspensions of polymer and MNFC ( $\eta_{rel} = \eta_{susp} / \eta_{sol}$ , susp consists of 0.5% polymer + 0.5% MNFC and sol is 0.5% polymer solution) [36]

The effects of CMC in MFC suspensions was also explored by Vesterinen *et al.* [36] through oscillation tests. In oscillatory rheology, shear rate  $\dot{\gamma}$  and shear stress  $\tau$  are defined by:

$$r = r_0 \sin(\omega t) \Rightarrow r^* = r_0 \cdot e^{i\omega t} \quad \text{Equation 2.1}$$

$$\tau = \tau_0 \sin(\omega t + \delta) \Rightarrow \tau^* = \tau_0 \cdot e^{i(\omega t + \delta)} \quad \text{Equation 2.2}$$

$\delta$  is the phase shift and  $\tan \delta$  (Tan delta) is a value used to determine yielding behaviour. As shown in Figure 2.9, MFC is a strongly yielding material, but when it is mixed with a polymer, the yielding behaviour of the suspension changes dramatically. It is supposed that CMC and PEO modify the forces and the interactions in a system consisting of MFC, water and polymer.

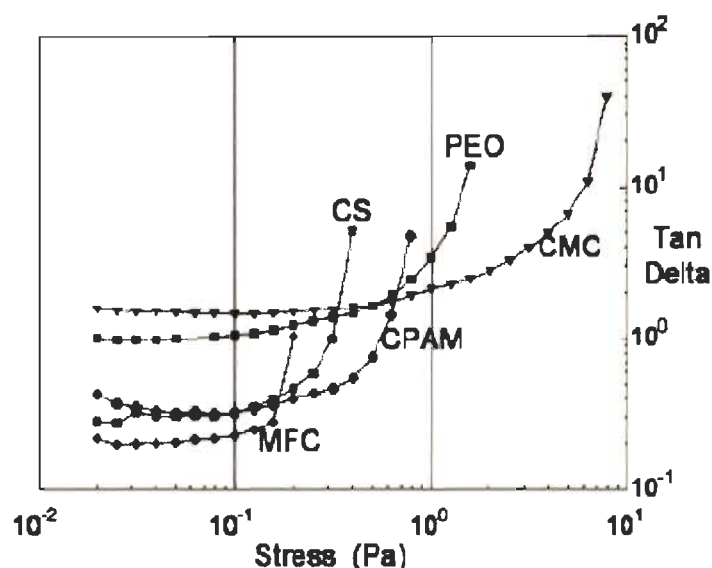


**Figure 2.9 Tan delta of suspensions of polymer and MFC [36]**

The addition of CMC thus contributes favourably to the dispersion of MFC suspensions. To further understand the mechanisms of the dispersion effect, it is then necessary to study the interactions between MNFC and polymer CMC.

### 2.2.2.3 MNFC interaction with polyelectrolyte

The area of polyelectrolyte adsorption onto cellulosic fibers has long been studied in extensive detail. The nature of the interaction between cellulose and polyelectrolytes is strongly affected by the polymer properties, *i.e.* functional groups, charge properties, molecular weight, structure, etc. [37]. The type of interaction affects the properties of the nano-fibril/polymer layer or complex: fiber suspension dispersion, water binding capacity, and mechanical properties [32-34].

CMC has a glucose-glucose attraction with cellulose, but at low electrolyte concentration, the electrostatic repulsion prohibits the adsorption of CMC on MFC or NFC (in our case MNFC) because both CMC and cellulose nano-fibrils are anionic. Therefore CMC is not irreversibly adsorbed onto cellulose nano-fibrils at low electrolyte concentrations. With high electrolyte concentrations and high temperatures, the adsorption of CMC on cellulose (co-crystallization) is irreversible [33].

The state of CMC depends on the electrolyte concentration: in the presence of electrolytes, CMC adsorbs on the fiber surfaces; without the electrolyte, CMC stays in the liquid phase. Both the CMC adsorbed on fiber surfaces and CMC in the liquid phase are able to disperse the fiber suspension due to the ability of CMC to reduce fiber-to-fiber friction in both phases [33].

In present work, CMC is used as a dispersant to improve the dispersion state of MNFC because, as we have seen, an optimum dispersion of MNFC is of high relevance for any application of MNFC as a coating agent on a TMP sheet. Moreover due to a gel-like behaviour, a chemical compatibility with the substrates and an ability to be dispersed in water, MNFC possesses enormous potential as coating agent for paper and paperboard. However, the delamination of coating layer may happen in the general coating process because of a potential deficiency of MNFC's cohesion with paper sheet at the inter-layer surfaces (lack of bonding). To realize the MNFC application, another coating process needs to be used to avoid and/or reduce to a minimum such delamination potential.

### **2.3 Hydra-Sizer™**

The use of Hydra-Sizer™ a curtain coating application that can be integrated on a paper machine, similar to additives for what the equipment was designed, we surmised that MNFC suspensions could impregnate the surface of a TMP sheet during formation on a Fourdrinier table. Indeed, the Hydra-Sizer™ would permit the addition of a thin layer of MNFC in the wet-end section of paper machine while controlling/managing the penetration level. Such a wet-end curtain coating application is then the perfect choice for MNFC application during papermaking.

This section introduces the curtain coating process in general and the Hydra-Sizer™ technology more specifically. For a thorough understanding of the MNFC coating operation in papermaking, the Hydra-Sizer™ structure and curtain coating parameters are also presented.

### 2.3.1 Curtain coating

The curtain coating process consist applying a coating layer to a paper surface from a liquid curtain that emerges out of a narrow slit at a fixed orifice and falls a short distance onto the moving substrate [38]. Curtain coating is a commonly used process to depose a thin liquid film onto a solid moving substrate. It has been used in many industries for many years. Well known examples are chocolate coatings in the food industry, magnetic coatings for audio and video tapes, and the production of photographic papers [39].

For many years papermakers have worked on non-impact coating as it is supposed not to disturb the paper surface: *i.e.* a method to apply a perfectly controlled and uniform layer of coating on the surface without any mechanical impact on the paper. Curtain coating is now opening new possibilities for coated papers. During the late 1990's, it has become a state-of-the-art technique for specialty paper such as carbonless paper (micro-capsules for "coated back"). Today the range of utilizations for curtain coating is being extended for many other applications such as pigmented coatings or barrier coatings [39].The coating applications compared with a laminated system would have the advantages of high flexibility and absence of adhesives [24].

In curtain coating, different phenomena limit a successful coating: the curtain stability, the air entrainment, the heel formation, and the pulled film. All these phenomena define an operating window presented in Figure 2.10. The limits are often drawn according to dimensionless numbers (units not presented here) which govern the flow field in the impingement region.

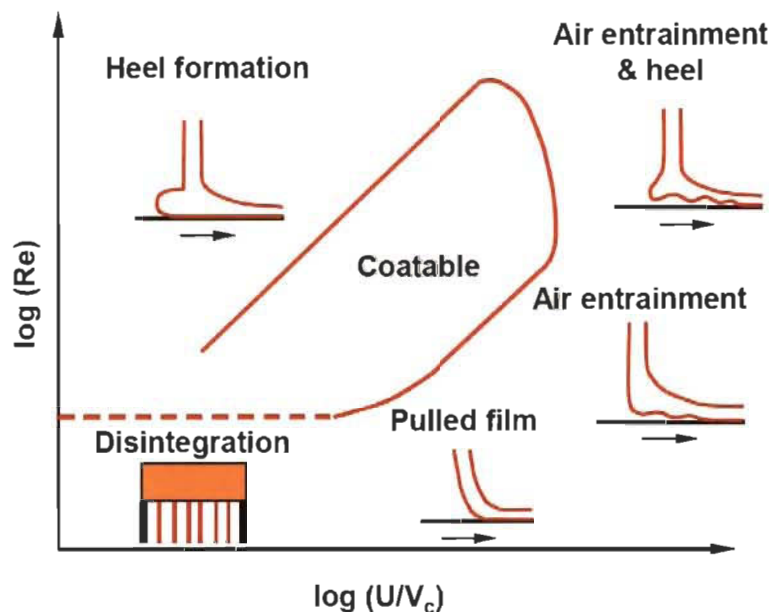


**Figure 2.10** Operating window in curtain coating [40] ( $U$ : web speed,  $V_c$ : curtain speed at impact,  $Re$ : Curtain Reynolds number)

The lower limit of flow is given by the need to maintain a stable curtain, the highest coating speeds are given by the need to avoid air entrainment to keep the coating stable. With increasing flow rates, the coating speeds can be increased while still avoiding air entrainment. At high flow rate, both air entrainment and heel formation occur. The low-speed limit is due to heel formation.

Curtain coating is designed to be achieved by Hydra-Sizer™ equipment in the present project. The details of Hydra-Sizer™ are presented below.

### 2.3.2 Introduction of Hydra-Sizer™

The Hydra-Sizer™ sheet impregnation system, developed by GL&V, is a not-so-recent development (about 15 years old) that uses curtain coating technology to impregnate paper or board with additives such as starch, or other mechanically dispersed particles, applied in the wet-end of the paper machine, practically on the formation table. Trials using Hydra-Sizer™ with starch slurry have shown increases in sheet strength properties such as Scott bond and tensile strength, and significant reductions in porosity [41].

Varying slurry solid concentrations in the Hydra-Sizer™ control the application rate. The applicator and its catwalk assembly can be positioned along the wire to change the consistency at the point of application. The retention mechanism for the process is physical entrapment, so applying the slurry at low sheet consistencies of 2-3% disperses the additives through the thickness of the sheet. Application at higher sheet consistencies, typically 6-8%, applies the additives generally to the sheet surface [40].

GL&V claims that when starch is applied by the Hydra-Sizer™ significant strength improvements is achieved with no loss in drying capacity, making it an ideal retrofit for an existing machine. The firsts installations on industrial paper machine were rather limited but demonstrated an increase in strength properties, allowing the mill to reduce refining and speed-up the machine [40].



**Figure 2.11 Hydra-Sizer™ at CRML (Centre de recherche sur les matériaux lignocellulosiques) running with water**

To ensure the good runnability of Hydra-Sizer™, some key parts of the internal structure of the Hydra-Sizer™ are presented below.

### 2.3.3 Structure of the Hydra-Sizer™

The Hydra-Sizer™ can be divided into two parts. One part that is equipped with the inlet tubes is called stationary part (see Figure 2.12). The part on the opposite side is called the active part (see Figure 2.13) which is accessible to control and adjust the nozzle gap.

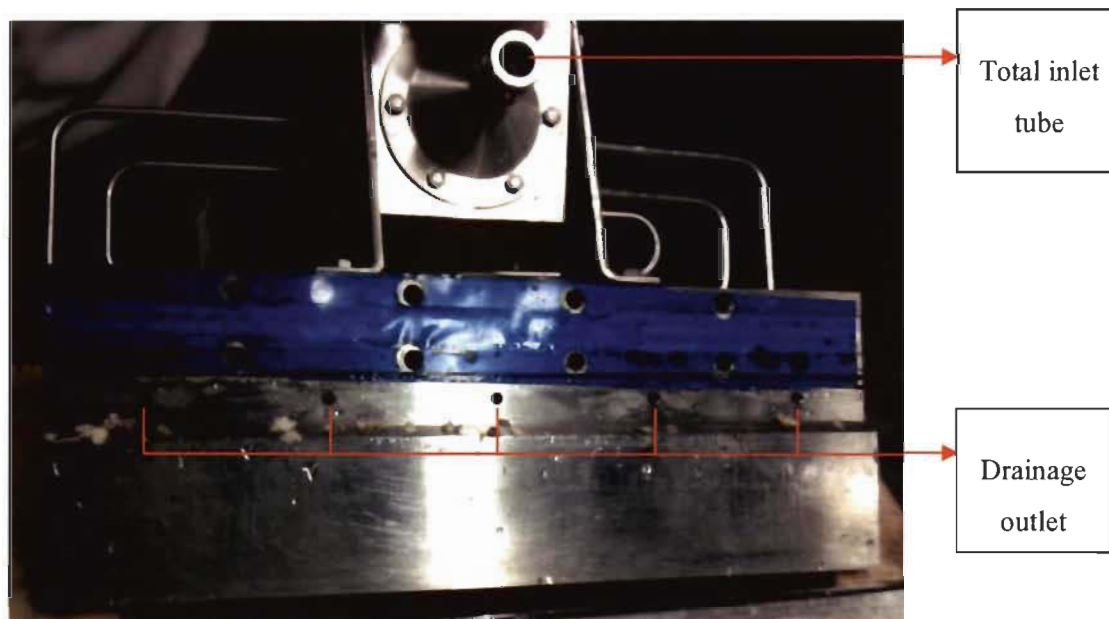


**Figure 2.12** Stationary part of Hydra-Sizer™

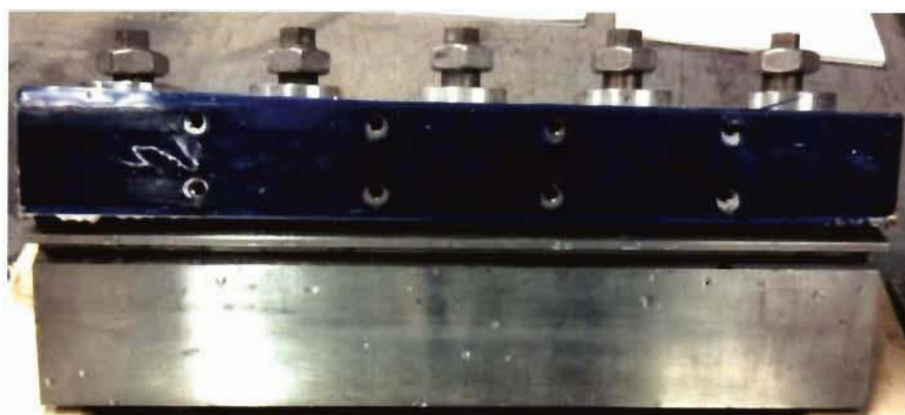


**Figure 2.13** Active part of Hydra-Sizer™

Figure 2.14 and Figure 2.15 are the front views and cross-section outlined of the two parts. The inlet tubes and drainage outlet have been coloured in red, the others circles with horizontal lines represent screws.

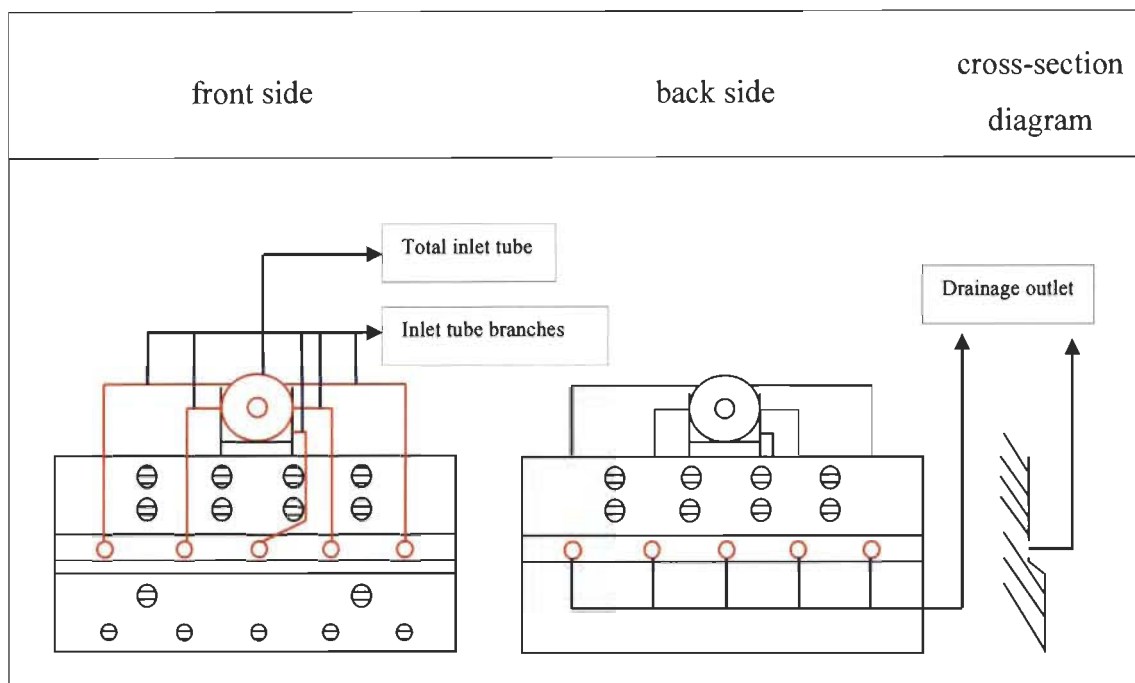


**Figure 2.14** Stationary part

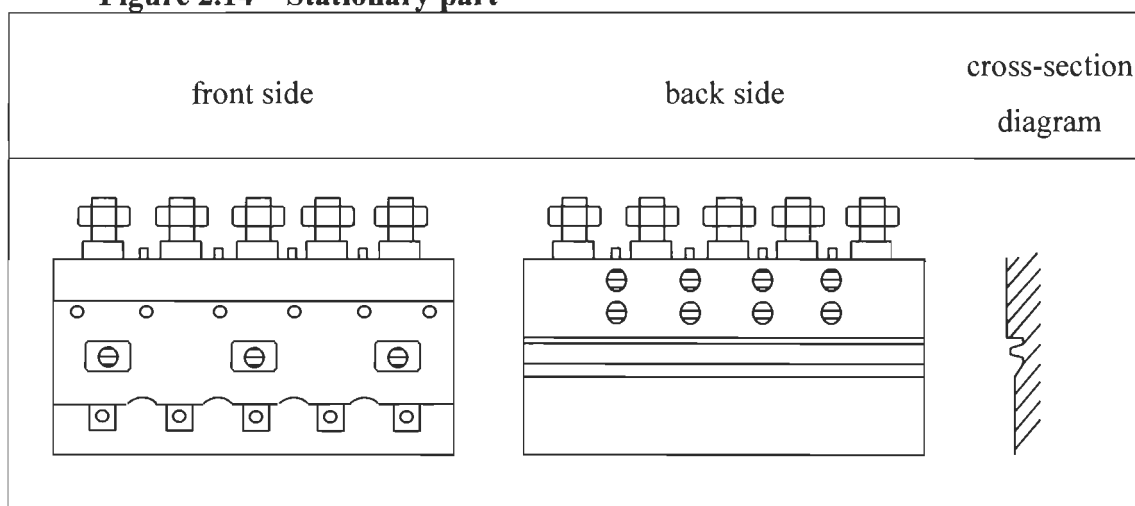


**Figure 2.15** Active part

The target of the adjustment is to make the two parts totally parallel and adjust the nozzle gap to obtain the desired uniform global mass flow.

### 2.3.4 Process parameter

The curtain coating process carried out by Hydra-Sizer™ involves three critical stages: The formation of the liquid curtain in the nozzle, the falling and accelerating of the curtain, and the curtain impingement on the moving web [40].

In order to discuss these important process parameters, the dimensions and flow patterns are shown in Figure 2.16. With a given slot width, the volumetric flow and the resulting exit velocity  $V_0$  of the curtain are the main parameters for this part of the process.

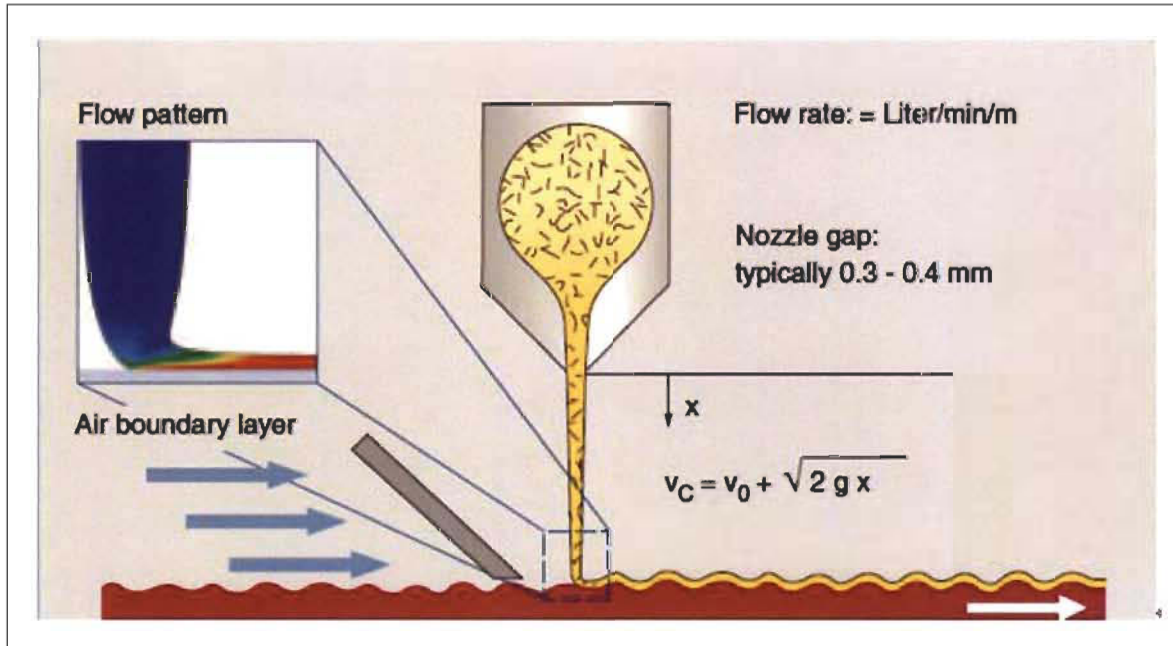


**Figure 2.16** Curtain coating application with typical flow pattern and process parameters [39]

Once the curtain flow exits the nozzle, it starts accelerating and reaches a curtain speed  $V_C$  depending on the distance  $x$ . The curtain velocity is approximated by:

$$V_c = V_0 + \sqrt{2gx} \quad \text{Equation 2.3}$$

with  $g$  being the gravitational constant.

Knowing the nozzle gap  $z$ , the shear rate  $\gamma$  in the nozzle is calculated as:

$$r = \frac{V_c}{z} \quad \text{Equation 2.4}$$

With the density  $\rho$ , viscosity  $\mu$  of the solution, the curtain velocity  $V_C$  and the curtain thickness  $h_c$ , the flow behaviour of the falling curtain is expressed by the Reynolds-number, defined for this case as

$$\text{Re} = \frac{\rho h_c V_c}{\eta} \quad \text{Equation 2.5}$$

As the curtain is falling and accelerating, it becomes thinner and more vulnerable to turbulences of the surrounding air, but one should consider that the danger of curtain break-up is increasing with very thin curtains. To estimate the stability of a thin film the Weber number can be calculated. It represents a measure of the relative importance of the fluid inertia compared to its surface tension:

$$\text{We} = \frac{\rho h_c V_c^2}{\sigma} \quad \text{Equation 2.6}$$

with the surface tension  $\sigma$ , a stable curtain flow can be expected empirically for Weber-numbers above 2.

Considering that in pilot tests  $V_c$  needs to be adjusted according to the running speed of the paper machine,  $V_0$  is a key control parameter according to Equation 2.3. Shear rate  $\gamma$  is the significant parameter to determine the viscosity of the flow. Furthermore the Reynolds-number also depends on the viscosity.

The Hydra-Sizer™ could impregnate MNFC in paper sheet with controlled in-depth (z) penetration. Also not a part of present study, it is obvious that for an optimum curtain coating operation, the Hydra-Sizer™ needs to be well adjusted and the various coating parameters well regulated and controlled.

## 2.4 Conclusion on the literature review

To summarize the literature review, the outstanding mechanical and barrier properties of MFC, and in our case MNFC, make such renewable material an attractive product for papermaking applications. However MNFC must be well dispersed to act as a structuring efficient layer in the paper sheet. CMC is expected to disperse MNFC as it shows dispersion effects on fibers and on MFC rheology. The adsorption of CMC on MFC or MNFC and having the CMC free in suspensions are both feasible. Furthermore,

we conclude that MNFC could well be added to paper products while using the Hydra-Sizer™ as an on-line curtain coating during papermaking.

The literature review is here used to focus our master's research direction. First, the effect of CMC on MNFC needs to be investigated to verify the dispersion effects. Then some analysis (e.g. rheology, zeta potential, charge, ..., and scanning electron microscopy) is required to explore the interaction of CMC and MNFC, and especially the CMC adsorption on fibrils. Finally, Hydra-Sizer™ trials need to be effected to evaluate the performance and potential of MNFC as a papermaking on-line coating agent.

## Chapter 3 Materials and methods

### 3.1 Materials

Two types of Micro-Nano-Fibrillated-Cellulose (MNFC) are used in the experiments, namely Micro-Nano-Fibrillated-Cellulose in a low fibrillated state (L-MNFC) and Micro-Nano-Fibrillated-Cellulose in a high fibrillated state (H-MNFC). Both were produced by OMYA International AG with the Masuko grinding equipment. Bleached kraft (no lignin content) Eucalyptus fibers are co-processed with ground calcium carbonate to improve the fibrillation of the cellulosic fibers. The product numbers of L-MNFC and H-MNFC are VP-215900 NFC383 and VP-0157 NFC RS1, respectively. The characteristics of L-MNFC and H-MNFC are measured and presented in Table 3.1. For both L-MNFC and H-MNFC, the ratio of fibril to calcium carbonate is about 4:1.

**Table 3.1 Characteristics of L-MNFC and H-MNFC**

	Solid content (wt %)	Filler Ratio (wt %)	Fiber Ratio (wt %)
L-MNFC	3.57	0.71	2.86
H-MNFC			

The Carboxy Methyl Cellulose (CMC) used in the experiments as dispersant is the Finifix 10 from CP Kelco. It is a commercial product of minimum 98% purify grade with small amounts of sodium chloride and sodium glycolate. Its degree of substitution (DS) is 0.8, molecular weight is about 60,000g/mol [42, 43].

The calcium carbonate used to prepare the  $\text{CaCO}_3 + \text{CMC}$  solutions are provided by OMYA International AG. It is the same ground calcium carbonate that was used in the grinding process of OMYA International AG to manufacture MNFC. The product number of  $\text{CaCO}_3$  is Hydrocarb 50-GU, it is a dry ground marble powder containing no dispersants.

The suspensions prepared for the experiments are MNFC of 0.5 wt% (percent weight) of fibrils + CMC 0, 1, 2, 4, 6, 8 wt%. The concentrations of CMC are based on the quantity of MNFC. Through conversion, the total concentration of CMC in MNFC suspensions are then  $0, 5 \cdot 10^{-5}, 1 \cdot 10^{-4}, 2 \cdot 10^{-4}, 3 \cdot 10^{-4}, 4 \cdot 10^{-4} \text{ g}_{\text{CMC}}/\text{g}_{\text{suspension}}$ , respectively.

The  $\text{CaCO}_3$  + CMC solutions prepared are  $\text{CaCO}_3$  0.125 wt% + CMC 0, 4, 8, 16, 24, 32 wt%. The concentrations of CMC are here based on the quantity of calcium carbonate and the total concentrations of CMC in  $\text{CaCO}_3$  + CMC solution are the same as in the MNFC suspensions once converted.

## **3.2 Methods**

The methods applied are rheology test, fiber morphology analysis (Fiber Quality Analyzer, Optical Microscopy and Transmission Electron Microscopy), polyelectrolyte titration, microscope observation, and the measurements of uniformity and mass flow in the Hydra-Sizer<sup>TM</sup>.

### **3.2.1 Rheology**

The rheology measurements are performed on a Rheologica rheometer Stresstech from ATS Rheo-System. For all the rheology measurements, parallel plates P20 is used and the gap is set as 1mm. Before each rheology measurement, 0.2ml sample is deposited on the plate by using the syringe and is allowed to rest for 10 minutes. During measurement the temperature is controlled to be constant at 21°C.

For each samples, dynamic viscosity is recorded in both the up and down sweeps of shear rates in order to investigate the shear rate/time dependency properties (hysteresis) and to furthermore investigate the modification of the internal structure of MNFC suspensions as a function of CMC addition.

### **3.2.2 Fiber Quality Analyzer (FQA)**

The fiber morphological analysis is performed to study the size distribution of MNFC. The equipment used is a HiRes Fiber Quality Analyzer from OpTest equipment, Inc.

The FQA gives the frequency of size distribution (length and width) related to the number of the counted elements.

### **3.2.3 Optical microscope (OM) and transmission electron microscope (TEM)**

Optical Microscope (OM) used to measure the fiber dimensions is the model number AXIO Scope A1 from ZEISS. All the optical microscope pictures are taken with the 10x objective.

To measure the MNFC fibrils diameters at nanometer scale, Transmission Electron Microscope (TEM) model number EM208S from PHILIPS is used. To prepare the sample for TEM, one drop of the suspension is deposited on a grid and filter paper is used to soak excess water out. For improving contrast, a drop of uranyl acetate is then deposited on the grid. After 30 seconds, the time required for coloring the fibers, the redundant of solution is absorbed by filter paper. All the TEM photographs are taken at a magnification of 28 000x. Some pictures are also taken at bigger magnification to explore the fibril morphologies in MNFC suspensions.

For each sample observed by OM and TEM, the diameters of 300 fibrils are measured using the image analysis software ImageJ. For each fibril, the diameter is the average value of 3 measurements in 3 different positions. When measuring the fibril diameter in a picture, all fibrils with a distinguishable profile need to be measured. In order to ensure the process randomness, the maximum quantity of fibrils measured in one image is 40.

The software JMP is used for analysing the distribution of fibril diameter by statistical tests and methods to detect the significant differences in fibril diameter between the various MNFC suspensions. The statistical method applied is the Wilcoxon Each Pair.

### **3.2.4 Zeta potential**

The zeta potential of CMC solutions is measured with a Malvern instrument Zetasizer Nano ZS.



**Figure 3.1 Mütek™ SZP-06 System Zeta Potential**

Further, the measurement of zeta potential of MNFC suspensions with different concentrations of CMC is performed with the Mütek™ SZP-06 System Zeta Potential (Figure 3.1). It can measure a streaming current in mV when counter-ions of all colloids and solid particles dissolved in water are separated from or sheared off the particles (see principle in Figure 3.2). The mesh size of the screen electrode of the machine Mütek™ SZP-06 is 40  $\mu\text{m}$ . In order to measure the zeta potential of MNFC, a Millipore filter membrane of 0.4  $\mu\text{m}$  is deposited on the screen electrode to form the fiber plug.

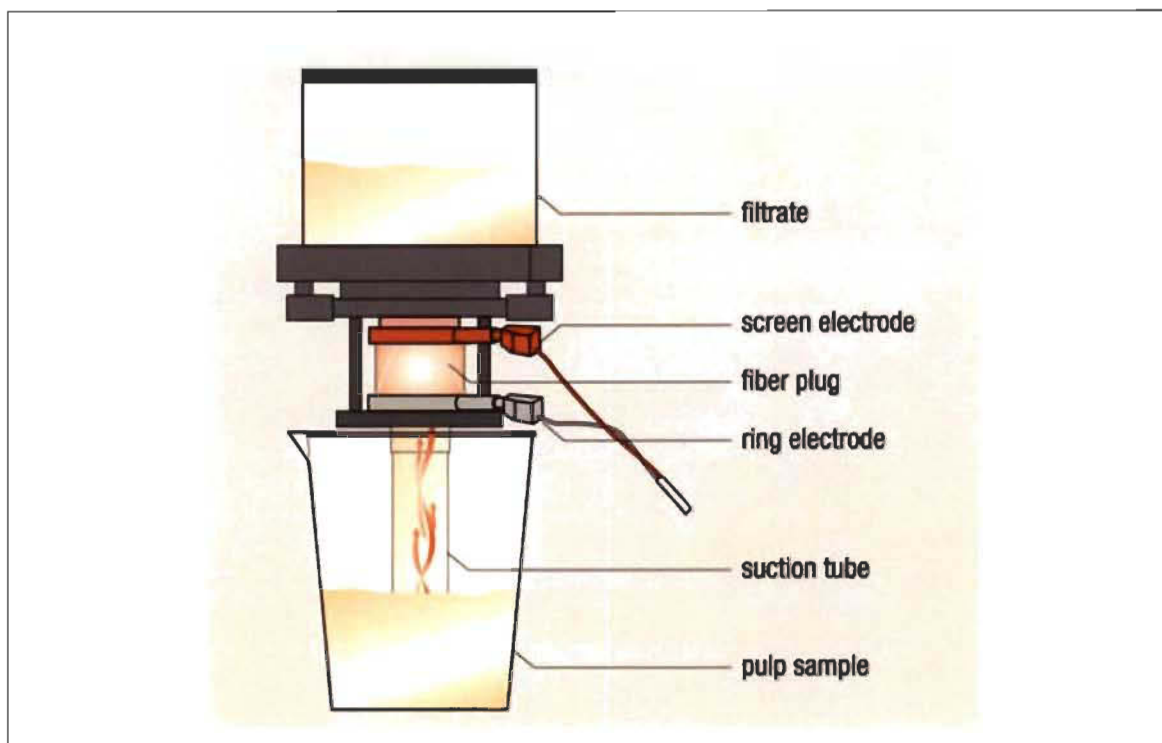


**Figure 3.2** Measuring cell of a Mütek™ SZP-06 System Zeta Potential

For each sample five effective measurements of zeta potential are required in order to get accurate zeta potential values and conductivity values. Moreover, pH is measured by Accumet AB 15/15+ bench-top meter.

### 3.2.5 Polyelectrolyte titration

PCD 03 Particle Charge Detector (Figure 3.3) is used to carry out a polyelectrolyte titration for quantitative charge measurement of the samples.

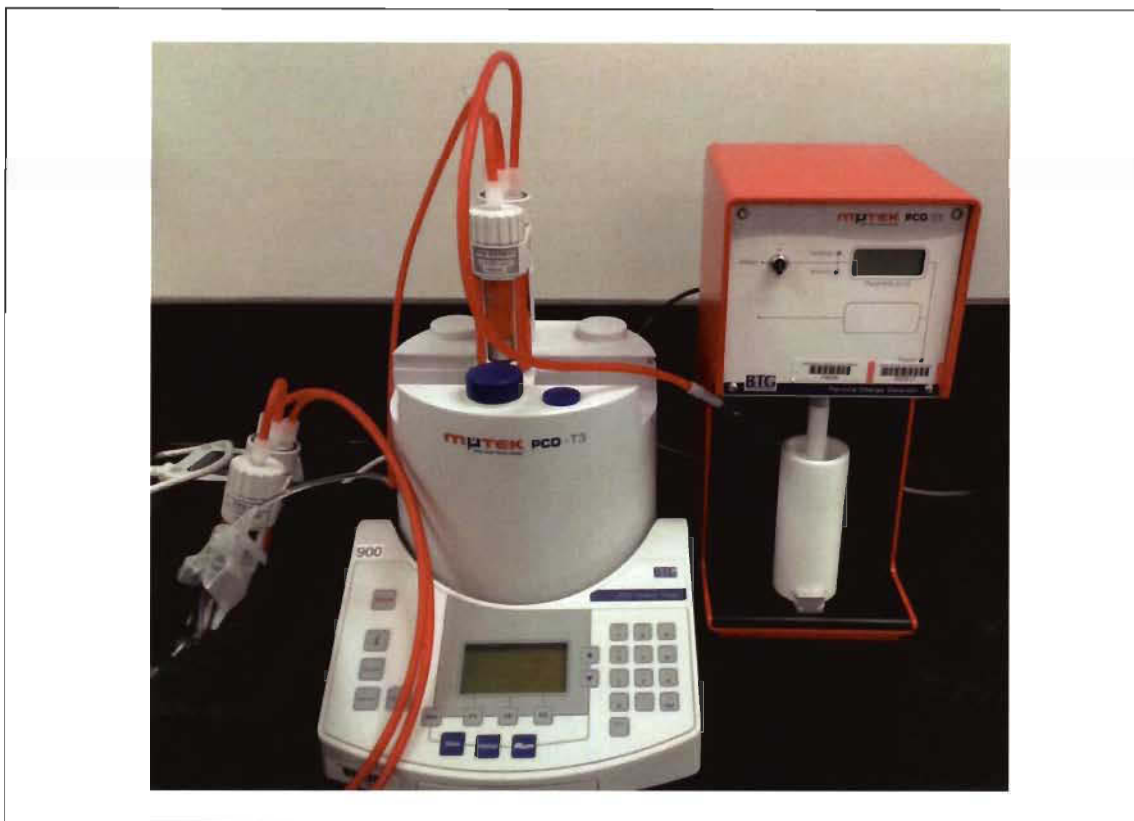


**Figure 3.3 PCD 03 Particle Charge Detector**

Practically all colloidal dissolved substances and solid particles in water carry electric charges. It leads to a concentration of oppositely charged ions, the so-called counter-ions, on the colloid surfaces. If the counter-ions are separated from, or sheared off, the dissociated macromolecule or particle, a streaming current can be measured in mV. A streaming current of zero mV denotes the point of zero charge, *i.e.* all existing charges in the sample are neutralized.

Streaming current measurement with the PCD 03 are based on the principle exhibited in Figure 3.4. When aqueous sample is filled into the measuring cell, colloidal dissolved molecules will adsorb at the plastic surface of the piston and on the cell walls under the action of van der Waals forces. The counter-ions remain comparatively free. Driven by a motor, the piston oscillated in the measuring cell and creates an intensive liquid flow which entrains the free counter-ions, thus separating them from the adsorbed sample material. At the built-in electrodes, the counter-ions induce a current which is shown on the display [44].

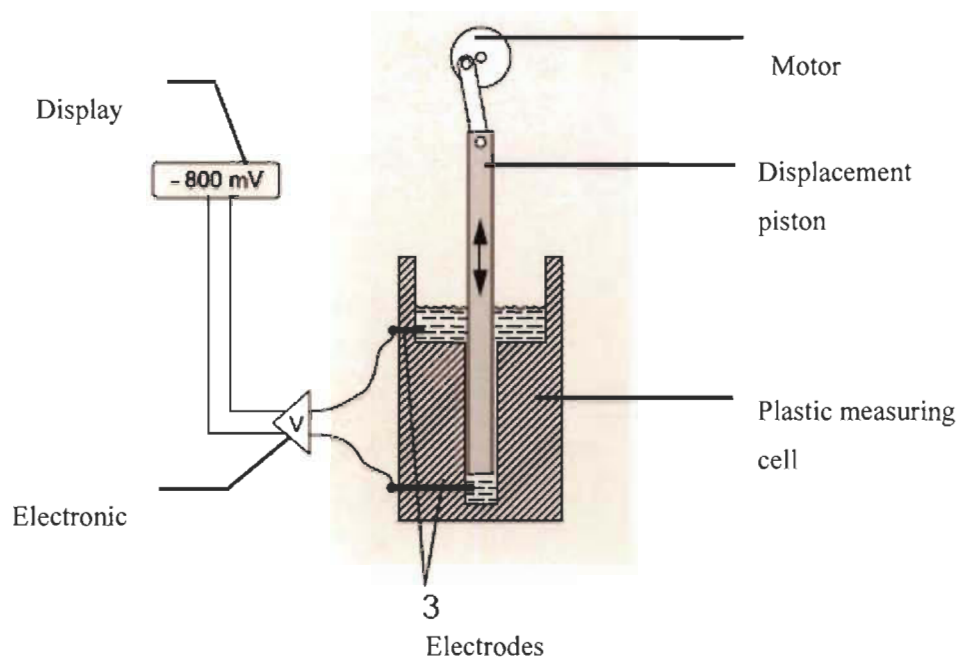


**Figure 3.4 Structure of schematic of Particle Charge Detector [44]**

For quantitative charge measurements of the sample, a polyelectrolyte titration has to be conducted which uses the streaming current to identify the point of zero charge (0 mv). An oppositely charged polyelectrolyte of known charge density is added to the sample as a titrant. The titrant charges neutralize existing charges of the sample. Titration is discontinued as soon as the point of zero charge (0 mv) is reached. Titrant consumption in ml is the actual measured value which forms the basis for the calculation of specific charge quantity. The specific charge quantity  $q$  [eq/g] of the sample is calculated according to the following formula:

$$q = \frac{V \times c}{wt} \quad \text{Equation 3.1}$$

$V$  = consumed titrant volume [l]

$c$  = titrant concentration [eq/l]

$wt$  = solids of the sample or the sample active substance [g]

$q$  = specific charge quantity [eq/g]

When Equation 3.1 is applied to the supernatant of MNFC suspensions, due to the fact that the solids in the supernatant contain various materials whose active substances are not definite, the anionic charge quantity is defined as

$$q^* = \frac{V \times c}{wt^*} \quad \text{Equation 3.2}$$

V = consumed titrant volume [l]

c = titrant concentration [eq/l]

wt\* = supernatant mass [g]

q\* = specific charge quantity [eq/g supernatant]

Equation 3.2 is also applicable to the anionic charge quantity measurement of CaCO<sub>3</sub> + CMC solutions as the active anionic substance is not definite.

Poly-DADMAC, a cationic polyelectrolyte is used as titrant. Calibration line for Poly-DADMAC consumption versus CMC amount is obtained by measuring the Poly-DADMAC consumption to titrate different CMC solutions with known concentrations. This calibration line is used to calculate the anionic charge quantity per gram of CMC according to Equation 3.1.

The samples prepared for the polyelectrolyte titration are the CaCO<sub>3</sub> + CMC solutions and the supernatants of L-MNFC suspensions. All L-MNFC suspensions are centrifuged for 1 hour at 10 000 rpm by Thermo Heraeus multifuge X3FR to obtain the supernatant. The samples are titrated by Poly-DADMAC to measure the anionic charge quantity according to Equation 3.2.

According to the calibration line between the mass of CMC (presented in Results) and the consumption of Poly-DADMAC and Equation 3.1., the anionic charges quantity of pure CMC molecules can be estimated.

### 3.2.5.1 Microscope observation and elemental analysis

A scanning electron microscope (SEM) is a type of electron microscope that produces images by scanning the sample with a focused beam of electrons. The electrons interact with atoms producing various signals (from back scattered electrons) that are detected and that contain information about the sample surface structure and elemental composition [45]. The SEM used is JEOL JSM-5500 (Figure 3.5). The SEM is equipped with an Energy Dispersive X-ray spectroscopy (EDX) probe X-Max from Oxford instrument. This probe enables the elemental analysis of the sample surface.



**Figure 3.5 JSM-5500 Scanning Electron Microscope**

The samples for SEM are dried supernatants of L-MNFC suspensions after centrifugation at 10000 rpm for 1 hour.

These supernatants of L-MNFC suspensions are dried by a compact moisture analyzer METTLER TOLEDO MJ33. The taken solid materials are observed and analyzed by SEM.

### 3.2.6 Application of MNFC with curtain coating

#### 3.2.6.1 Installation of Hydra-Sizer™

Before installing Hydra-Sizer™ in the wet-end of the paper machine, off-line tests are run with a set-up in water closed circuit system presented in Figure 3.6 and Figure 3.7.

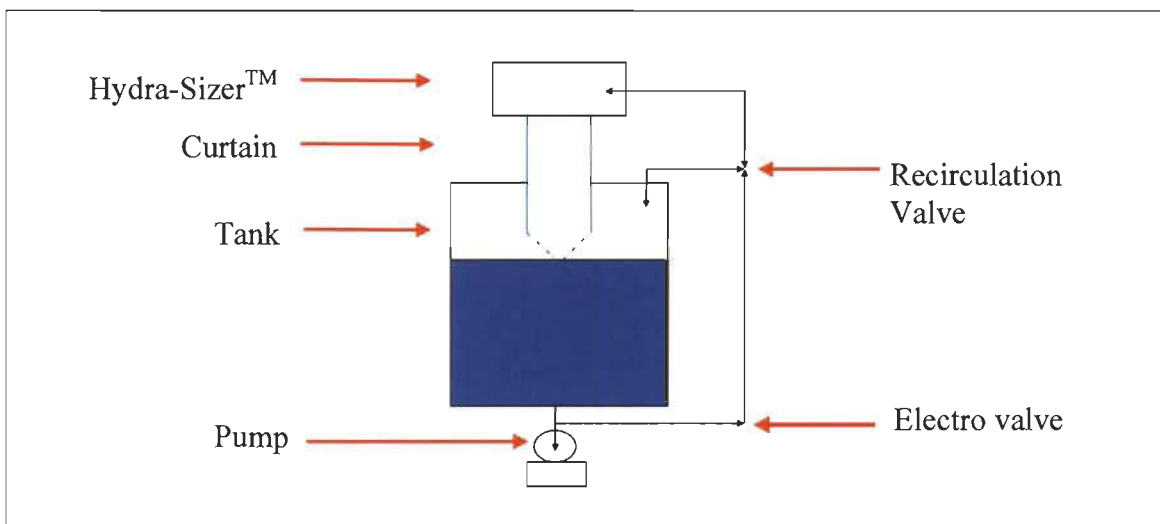


**Figure 3.6** Diagram of the installation of Hydra-Sizer™ for off-line tests



**Figure 3.7** Installation of Hydra-Sizer™ with a recirculation tank.

### 3.2.6.2 The measurement of flow uniformity and mass flow

The measurement of flow uniformity (width) and mass flow is carried out with a recirculation valve which allows the setting of the recirculation ratio.

#### 3.2.6.2.1 Method for uniformity and mass flow measurement

The steps for testing uniformity and mass flow are explained below (see Figure 3.8).

- a) Identification and labelling of 3 positions on the Hydra-Sizer™ length;
- b) Starting of the Hydra-Sizer™;
- c) Setting the recirculation valve;
- d) Using of a container to weight the water in each position within 60 seconds;

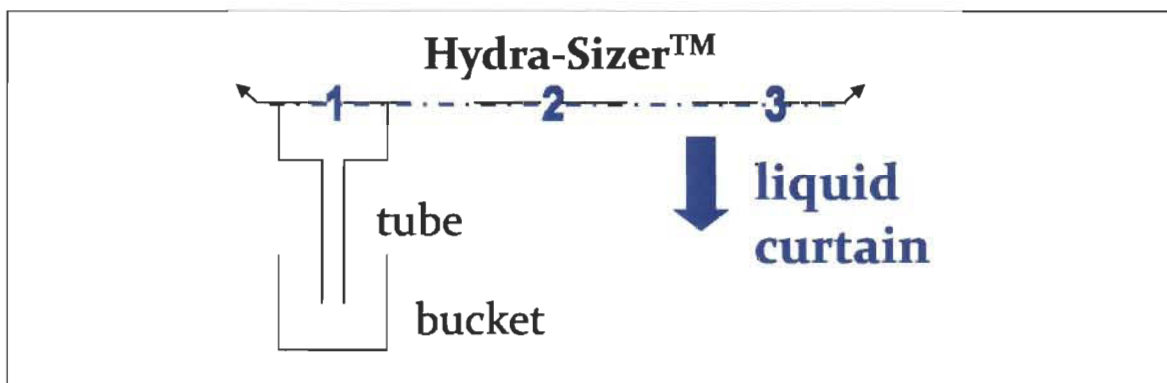


**Figure 3.8 Method for testing uniformity and mass flow of Hydra-Sizer™**

#### 3.2.6.2.2 Uniformity and mass flow measurement

- a) Uniformity and mass flow of water are measured under different recirculation conditions.
- b) The recirculation valve is kept open to maximum possible flow. Initially, the uniformity and mass flow of CMC solutions (CM used as viscosity modifier) are measured. The concentrations of CMC are 1.9, 2.6, 3.4%

### 3.2.6.3 The MNFC performance in offline Hydra-Sizer™

Other than the recirculation valve used in the measurement of uniformity and mass flow, for the off-line tests of MNFC suspensions, an electro-valve is installed to control the pump out-flow.

First, before operating measures, the nozzle gap is adjusted at 1.02 mm along the outlet (width) of the Hydra-Sizer™. Then four trials of different MNFC suspensions at different out-flows (see Table 3.2) are carried out. Pictures of the curtain flow for the performance of MNFC in the Hydra-Sizer™ are taken and the mass flows in the three positions along the outlet of Hydra-Sizer™ (as shown in Figure 3.8) are measured.

**Table 3.2 Trials of MNFC suspensions in the off-line Hydra-Sizer™**

Essay	Suspension	Outflow (L/min)
1	L-MNFC 0.5%	50
2		70
3	L-MNFC 0.5%+CMC 6%	50
4		70

## Chapter 4 Results and discussions

### 4.1 Experimental approach

Present work final aim is to explore the dispersion of MNFC suspensions and their processing abilities in curtain coating. CMC is selected as the dispersing agent for cellulosic fibers. The focus of present study is to understand and improve MNFC dispersions. Hence, the influence of CMC on MNFC is here investigated in terms of fibrils-fibrils interactions in suspension and characterization of individual fibrils which are a direct measure of the dispersion level. The two perspectives provided by optical microscopy and transmission electron microscopy, and to a lesser extent by FQA, represent MNFC dispersions in macro- and micro- views respectively and could be analyzed / understood by compounding information from the flow behaviour (rheology) and fiber morphology (microscopy). Indeed, rheology evaluation is a well-recognized method to evaluate flow behaviour, while fiber morphology may be quantitatively measured by fiber quality analyzer (FQA) and microscopes (OM and TEM). For a better understanding of CMC dispersion effects, the interaction of CMC and MNFC is also investigated. CMC molecules are supposed to be either adsorbed on MNFC surface or free in the suspension. To confirm the adsorption of CMC, the zeta potential (ZP) is measured to detect the surface physical-chemistry changes at different CMC addition levels. To detect the CMC free in suspensions, MNFC suspension are centrifuged, then polyelectrolyte titration is performed to measure the anionic charges in the supernatant and microscope observations are conducted to analyze the drying matters in the supernatants. The experimental approach for the influence of CMC on MNFC and their interaction is illustrated in Figure 4.1.

After the search for the optimum CMC addition to achieve the best MNFC dispersion, the following research is centered on the ability of MNFC suspensions to form a uniform liquid film in curtain coating process. First, the runnability of the Hydra-Sizer<sup>TM</sup> is verified in terms of flow uniformity and the effect of rheological CMC modifications. After some adjustment (some mechanical) to ensure the best runnability of the

Hydra-Sizer™, the curtain stability and the flow uniformity are analyzed to evaluate the performance of MNFC suspensions in the Hydra-Sizer™ curtain coating process. We propose that with a good dispersion and a good processing ability in curtain coating, MNFC suspensions application in papermaking industry will indeed be successfully achieved.

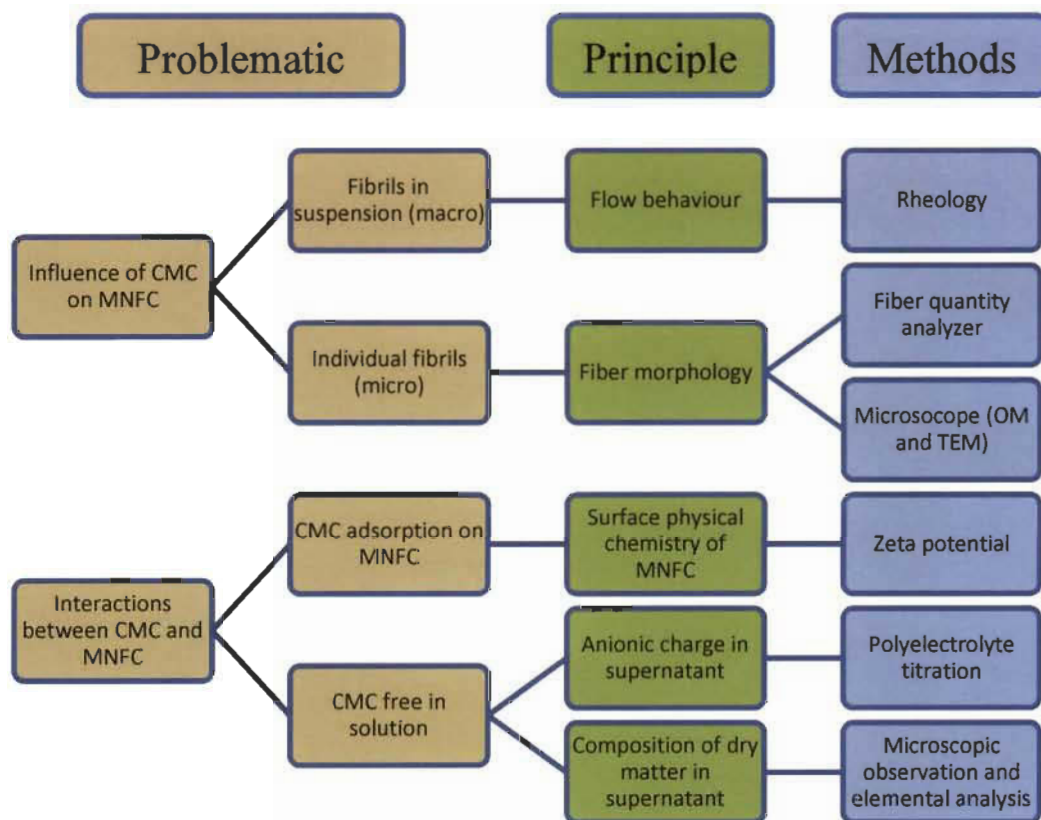


**Figure 4.1 Experimental approach to study MNFC dispersions**

In this chapter, the suspensions L-MNFC 0.5%+CMC0, 1, 2, 4, 6, 8% and H-MNFC 0.5%+CMC 0, 1, 2, 4, 6, 8% are simply referred as L-CMC 0, 1, 2, 4, 6, 8 and H-CMC 0, 1, 2, 4, 6, 8 respectively. Similarly, the  $\text{CaCO}_3$  0.125% + CMC 0, 4, 8, 16, 24, 32% solutions are referred to as C-CMC 0, 4, 8, 16, 24, 32 respectively.

In fact, as the fibril/filler ratio is 4:1 in the original MNFC, the different notations of L-CMC suspensions and C-CMC solutions represent the same calcium carbonate concentration and CMC concentration. As shown in Table 4.1, the  $\text{CaCO}_3$

concentrations, CMC concentrations, and CMC/CaCO<sub>3</sub> ratio in L-CMC series correspond one to one with C-CMC series.

**Table 4.1 Composition concentration and composition ratio in L-MNFC suspensions**

	L-CMC 0	L-CMC 1	L-CMC 2	L-CMC 4	L-CMC 6	L-CMC 8
Fibril concentration (g/g suspension)	0.5%					
CaCO <sub>3</sub> concentration (g/g suspension)	0.125%					
CMC concentration (g/g suspensions)	0	5E-5	1E-4	2E-4	3E-4	4E-4
CMC/CaCO <sub>3</sub> ratio	0	4	8	16	24	32

## 4.2 Influence of CMC on MNFC

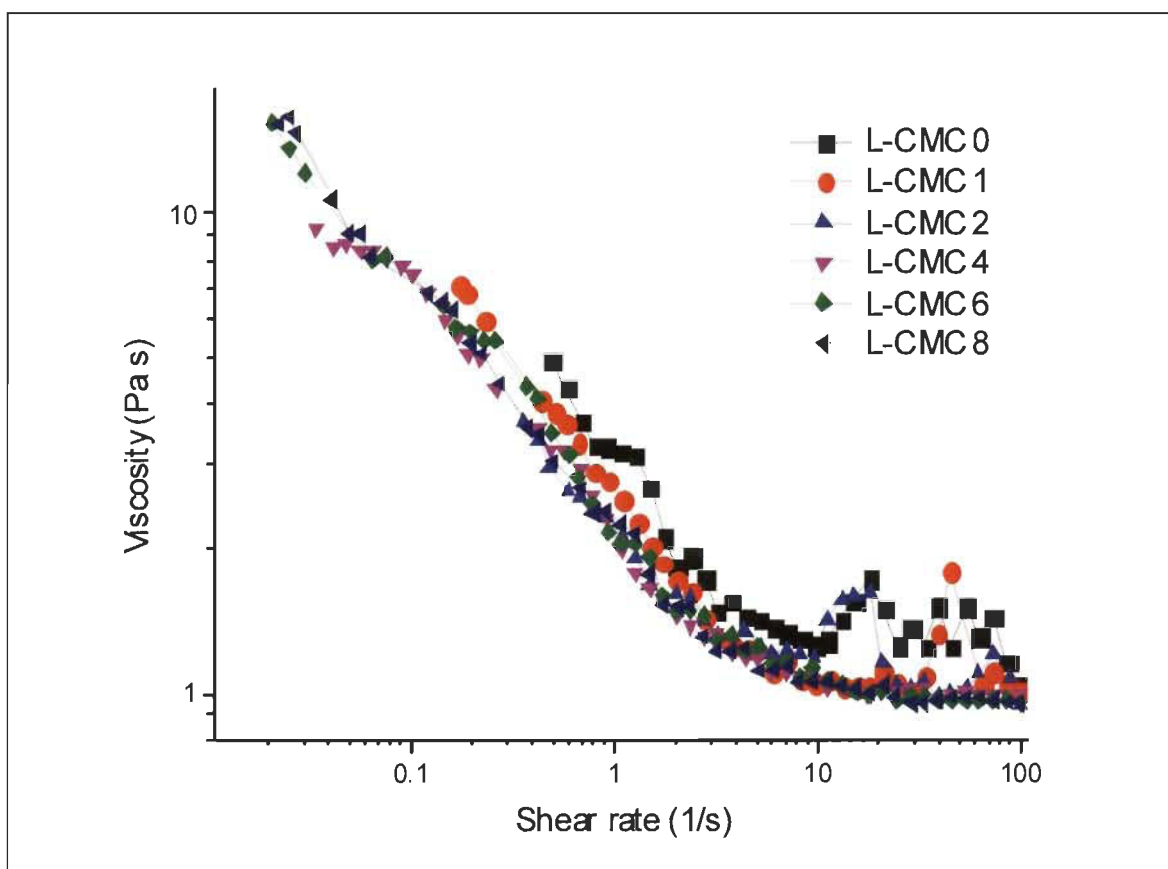
### 4.2.1 Rheology

Rheological tests are here used to explore the influences of CMC on the rheological characteristics and the intern structure of MNFC suspensions as an indication to fibril-fibril interactions. For all the L-MNFC and H-MNFC suspensions, the rheology tests are carried out by measuring the viscosity both in ascending and descending shear rates. Results of viscosity-shear rate curves in upward sweep are first presented to discuss the shear rate dependence of the suspensions and suspension structures. Then the viscosity-shear rate curves in upward and downward sweep are used to investigate the time dependence for both L-MNFC and H-MNFC suspensions: *i.e.* as related to the time for suspension structures to recuperate from shear.

## 4.2.2 L-MNFC 0.5% suspensions

### 4.2.2.1 Ascending shear-rate curves

Figure 4.2 shows the curves of viscosity-shear rate in upward sweep of all L-MNFC 0.5% suspensions (for better observation, the inset “a” exhibits the viscosity-shear rate curve of L-MNFC 0,5%+CMC 0, 1, 2% and “b” shows the L-MNFC 0.5%+CMC 4, 6, 8%).



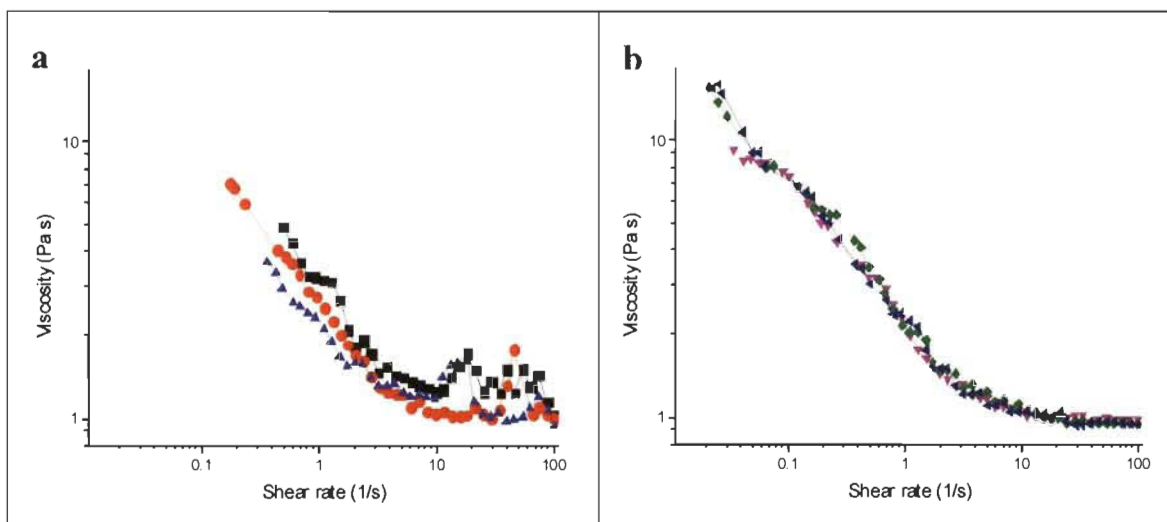


**Figure 4.2** The viscosity-shear rate curve of L-MNFC suspensions in upward sweep (a: L-CMC 0, 1, 2; b: L-CMC 4, 6, 8)

All the L-MNFC 0.5% suspensions present shear thinning behaviour (viscosity decreases as shear rate increases). Without CMC, L-MNFC suspension presents the highest viscosity value and intensive disturbances at high shear rate (between 10 and 100  $\text{s}^{-1}$ ). As the addition of CMC is from 1 to 2%, the increased proportion of CMC contributes to the decrease of the low shear rate viscosity but the instabilities (peaks) at high shear rate still remain. When the CMC addition is increased at 4% to 8%, the viscosity almost remains the same as for CMC 2, however at high shear rate the disturbances peaks disappear.

The shear thinning behaviour of all L-MNFC suspensions may be explained by the fact that upon shearing, the fibers and fibrils of L-MNFC align in the direction of the flow; thus fiber-fiber interaction is reduced because they are separated physically by shear [46]. The reduced fiber-fiber interaction results in decreasing viscosity.

The disturbances at high shear rate do not only represent a change of viscosity value, but the transformation of internal structure of L-MNFC suspensions [24, 46]. Based on the experimental observations, the internal structure is supposed to be the agglomeration of fibrils (see Figure 4.3). The agglomerations of fibrils result in wall-slipping during measurement causing the appearance of abrupt peaks (up and down). The creation of agglomeration could increase the viscosity as it is more difficult to shear the

agglomerations, but then the resulted wall slip occurs which leads to viscosity falls back down. When the CMC addition increases from 1% to 8%, the peaks progressively disappear indicating that CMC most probably prevents the agglomeration of fibrils in the L-MNFC suspensions.



**Figure 4.3 Agglomeration of fibrils in rheological test**

#### **4.2.2.2 Ascending and descending shear rate curves**

Figure 4.4 presents the viscosity-shear rate curves in up and down sweep of L-CMC 0, 1, 2, 4 suspensions. To detect the difference between the four suspensions in detail, graph a in Figure 4.4 exhibits the L-CMC 0 and 1 while graph b shows the L-CMC 2 and 4. The viscosity-shear rate curves in up and down sweep of L-CMC 6 and 8 are presented in Figure 4.5. In both Figure 4.4 and Figure 4.5, the closed symbols represent the upward sweep and the open symbols indicate the downward sweep.

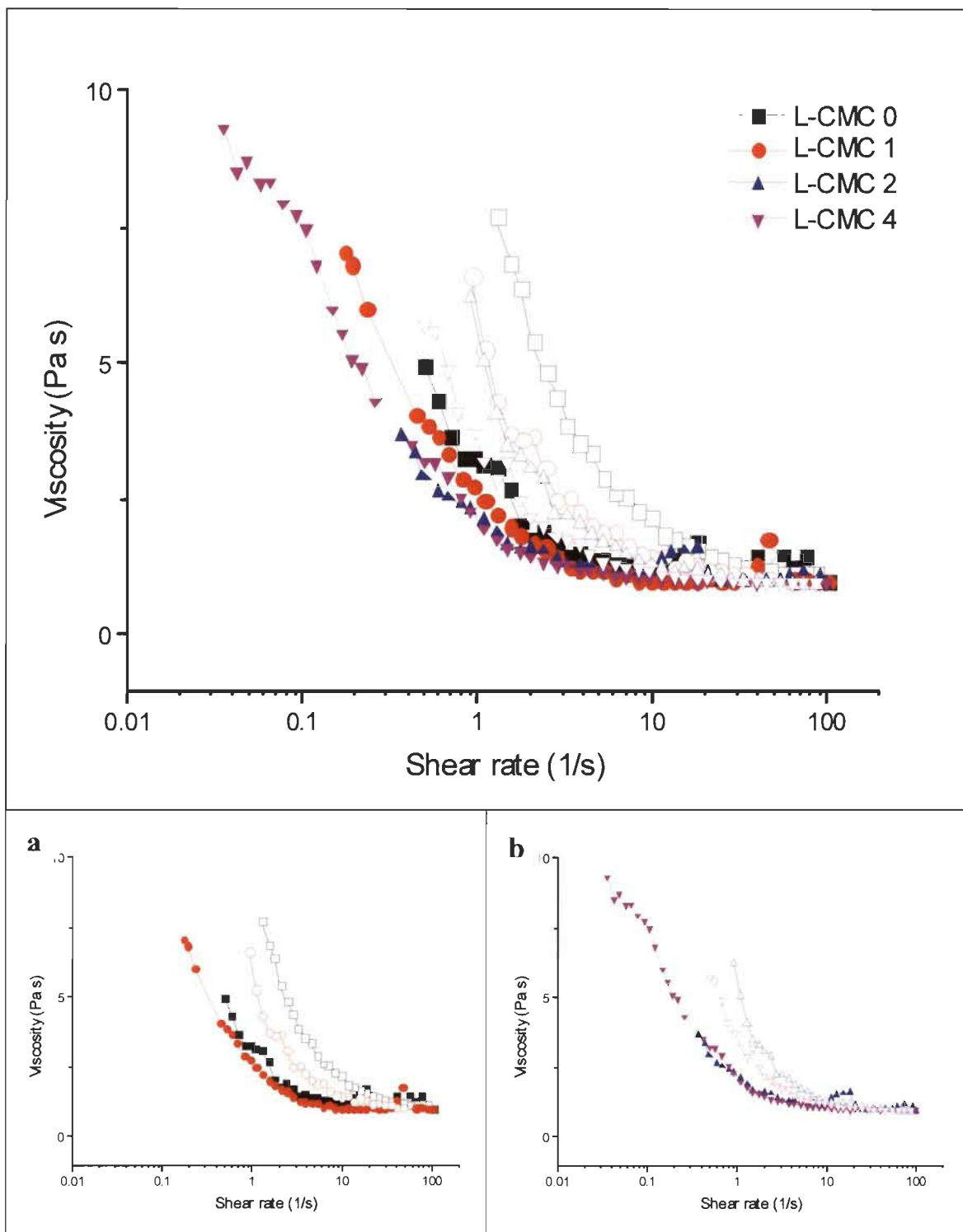


**Figure 4.4** The viscosity-shear rate curves for L-CMC 0, 1, 2, 4 suspensions in up and down sweep (closed symbol: upward sweep; open symbol: downward sweep. a: L-MNFC 0, 1; b: L-MNFC 2, 4)

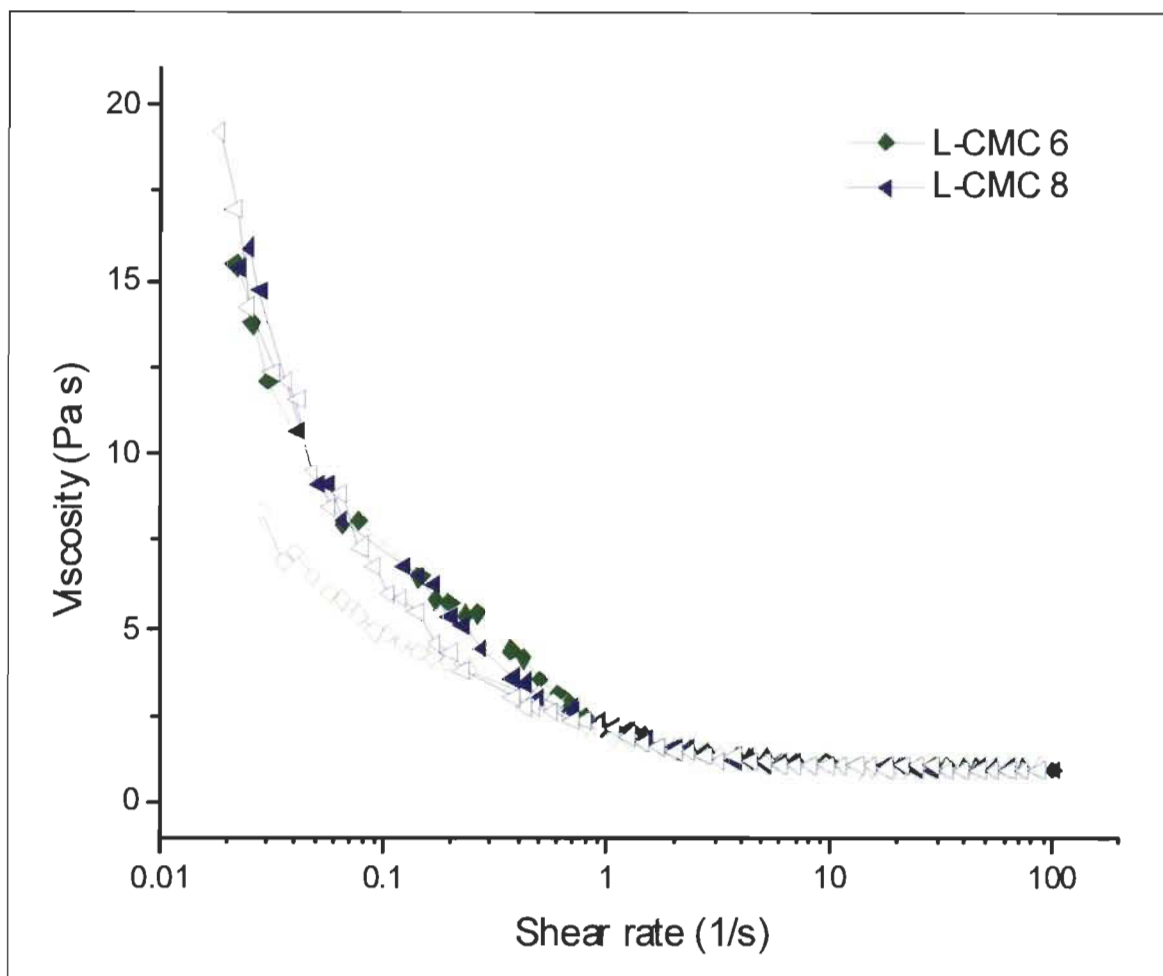


**Figure 4.5** The viscosity-shear rate curves of L-CMC 6 and 8 suspensions in up and down sweep (closed symbol: upward sweep; open symbol: downward sweep)

Without CMC, L-MNFC suspensions present hysteresis behaviour between the upward and downward sweep of shear rates. The increasing addition of CMC gradually decreases the amplitude of the hysteresis loop until it fully eliminates hysteresis at 8%.

The presence of hysteresis demonstrated that L-MNFC suspensions are time dependent materials because the changes of viscosity which indicate a change of internal structure happen with a measurable delay [46]. In Figure 4.4 the four curves of L-CMC 0, 1, 2 and 4, the viscosity in downwards sweep is higher than that in upwards sweep. It is supposed to be caused by the aggregation of fibrils at high shear rate which increases the resistance to flow in downward sweep. For L-CMC 0, 1, 2, 4, these suspensions present weak static structure. The application of shear has for first effect to “thin” the

agglomerated fibrils (small remaining amount of material from the low level of static structure), and then creates ordering of the high aspect ratio materials and/or phase separation of the components as the agglomerated fibrils would dissociate upon higher shear. When returning under reducing shear rate, a hysteresis with increased viscosity is displayed, illustrating that the induced structure/phase separation is retained for a considerable timescale. From L-CMC 0 to L-CMC 4, the increasing CMC addition retains the static structure and prevents phase separation during shearing. Therefore a reduced hysteresis loop is presented in the returning upward sweep from L-CMC 0 to L-CMC 4.

In Figure 4.5 L-CMC 6 also presents the hysteresis loop, but the viscosity in downward sweep is smaller than the upward sweep. It is supposed that compared to L-CMC 4 L-CMC 6 suspension has smaller and less agglomerations of fibrils at high shear rate which facilitate it to flow in downward sweep, however the rebuilt of structure is slower than the rate of reduction of shear rate. At medium-high CMC dose, L-CMC 6 shows a relatively strong static structure which can be shear thinned without phase separation at high shear rate. A much stronger elastic static structure is expected to occur when CMC further disperses the L-MNFC and eliminates the fibrils agglomerations.

As for L-CMC 8, the disappearance of hysteresis loop indicates that the addition amount of CMC is enough to prevent the aggregation of L-MNFC fibrils. At that highest CMC addition, the static structure is very strong and its structure rebuild very fast after shearing.

For L-MNFC, the addition of CMC benefits to reduce the friction between fibrils, therefore the viscosity at low shear rate decreases, the aggregations of fibrils at higher shear rate are restrained and the static structure is strengthened.

### **4.2.3 H-MNFC 0.5% suspensions**

#### **4.2.3.1 Ascending shear rate curves**

Figure 4.6 presents the viscosity of H-MNFC 0.5% suspensions according to the shear rate (upward sweep) with different concentrations of CMC.

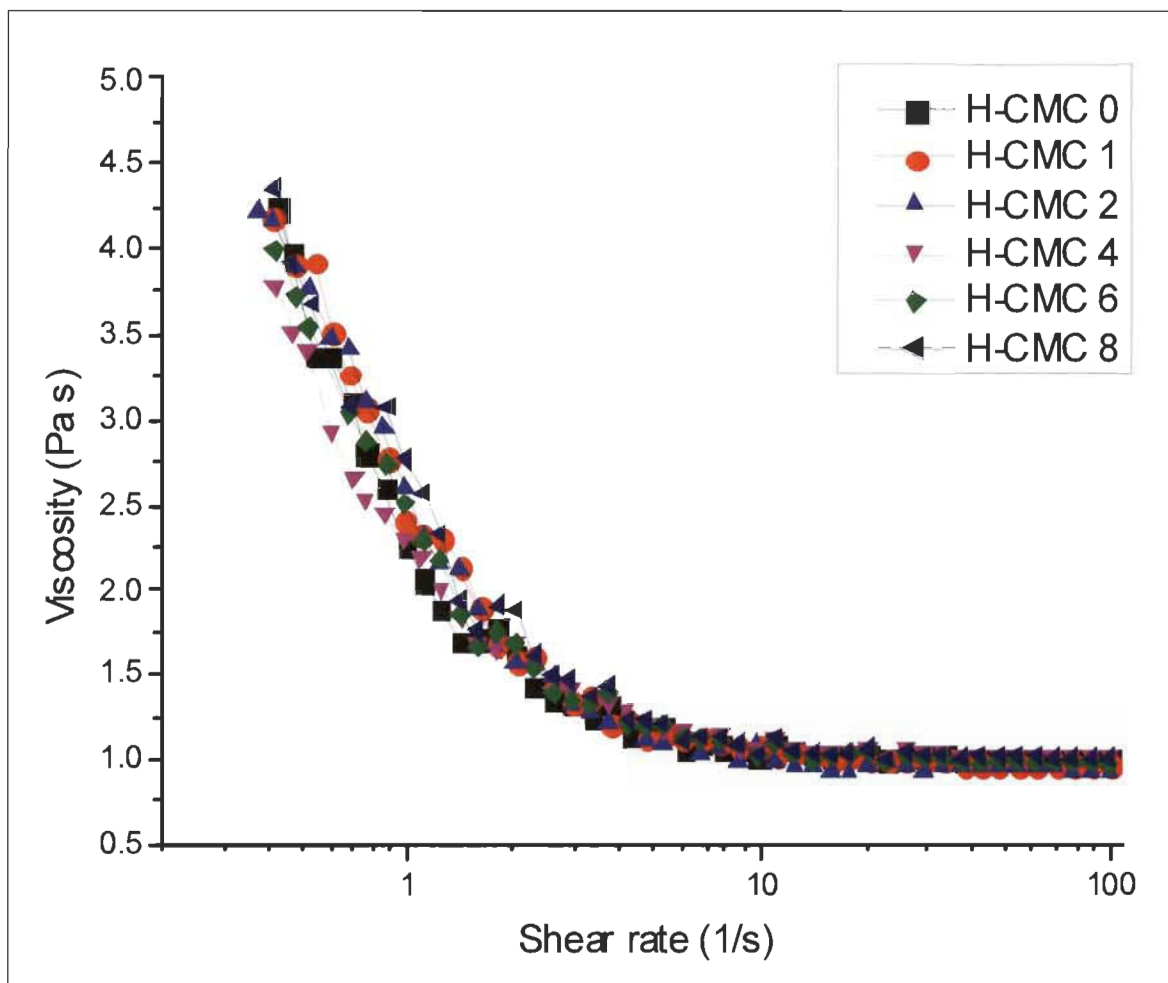


**Figure 4.6** The viscosity-shear rate curve of H-MNFC 0.5% in upward sweep

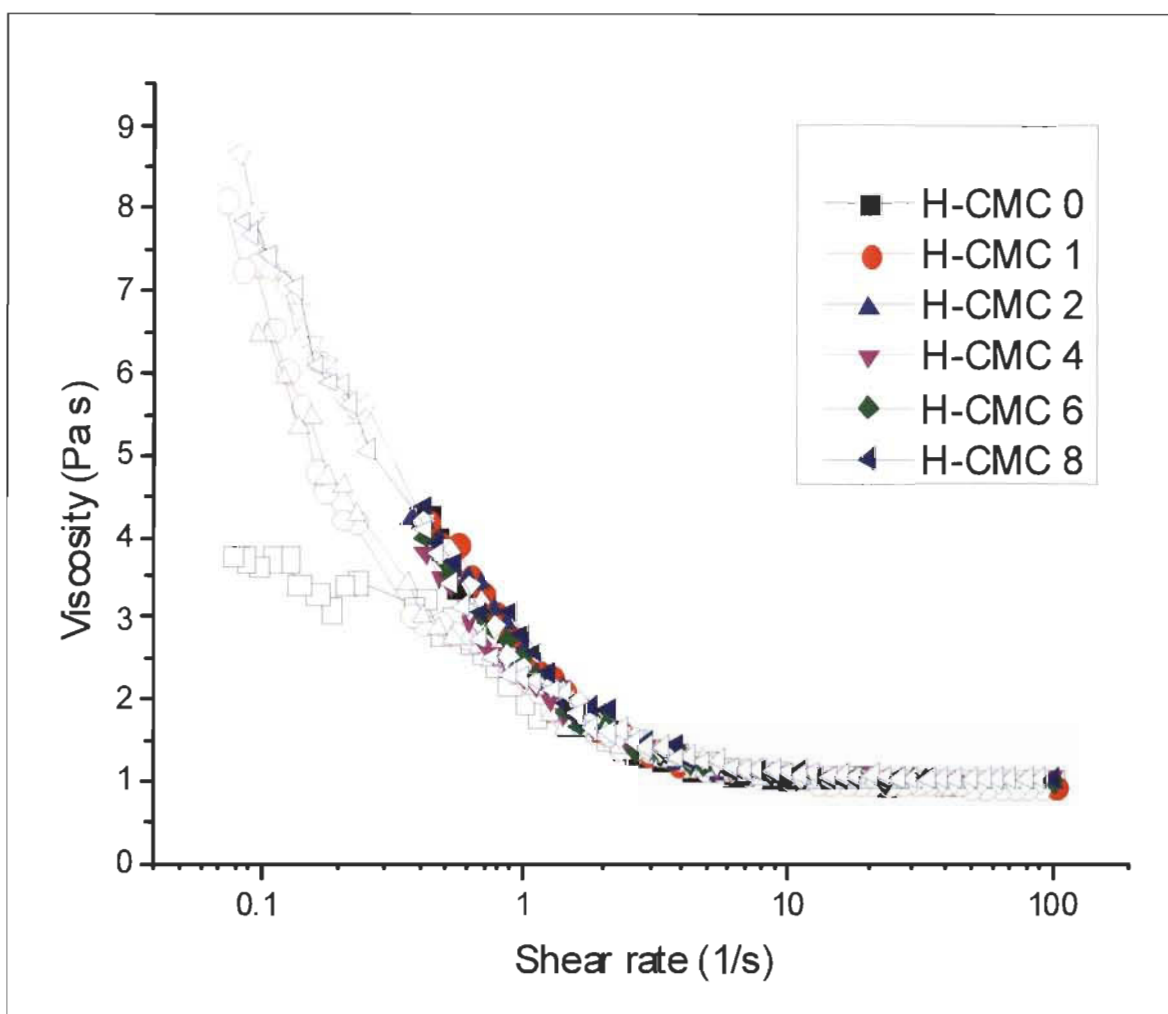
All H-MNFC suspensions present shear-thinning behaviour. The addition of CMC does not influence significantly the viscosity of H-MNFC suspensions.

As for L-MNFC suspensions, the shear-thinning behaviour is due to the reduced fiber-fiber interaction upon shearing. Being the Micro-Nano-Fibrillated-Cellulose with high fibrillated states, H-MNFC undergoes a higher and prolonged shear force than L-MNFC during the production process. This makes H-MNFC put up with higher shear rate and contains more independent and smaller fibrils than L-MNFC. On the one hand, these independent and small fibrils may be less prone to form agglomerates of a certain large dimension (less coarse fibers), on the other hand although the agglomeration is formed; it may be too small to be detected through the rheological measurement. The

good dispersion state and great tolerance for high shear rate of H-MNFC lead to the same resistance to flow regardless of the addition amount of CMC.

#### 4.2.3.2 Ascending and descending shear rate curves

Figure 4.7 shows the viscosity-shear rate curve in both up and down sweep of all H-MNFC 0.5% suspensions. For the better observation of the difference in upward and downward sweep, graph “a” presents the viscosity-shear rate curves of H-CMC 0, 1, 2 and graph “b” exhibits the H-CMC 4, 6, 8. The closed symbols stand for the upward sweep while the open symbols are for the downward sweep.



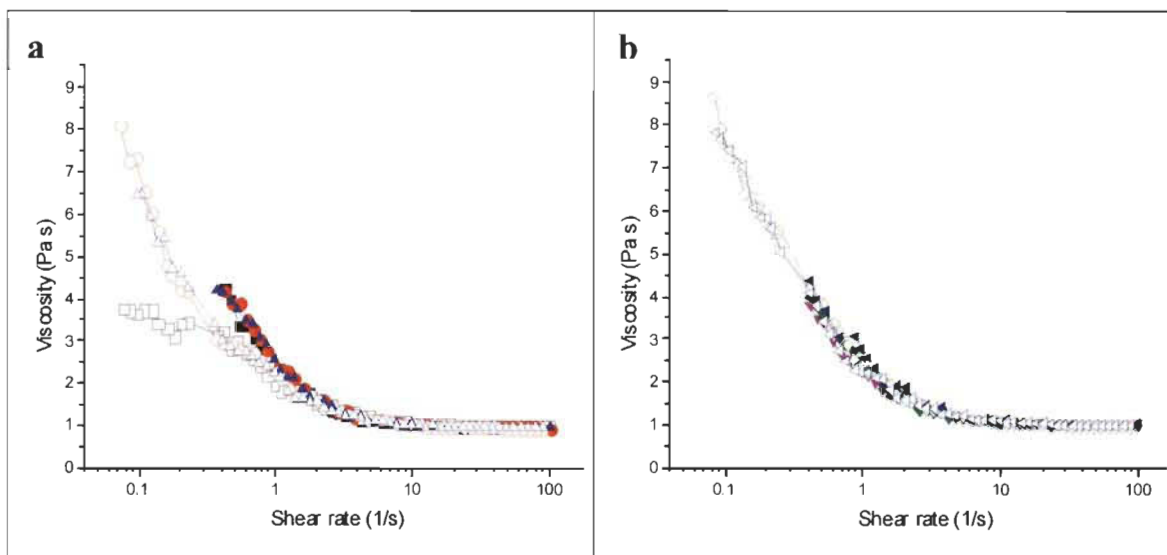


**Figure 4.7** The viscosity-shear rate curve of H-MNFC suspensions in up and down sweep (closed symbol: upward sweep; open symbol: downward sweep), (a: H-CMC 0, 1, 2; b: H-CMC 4, 6, 8)

As for L-MNFC, the viscosity of H-MNFC suspensions in downward sweep varies with the addition of CMC. H-CMC 0, H-CMC 1 and H-CMC 2 present thixotropy behaviour while other samples show no difference of viscosity between upward and downward sweep. Among these samples, H-CMC 0 shows the most apparent thixotropy behaviour.

For thixotropic materials, the viscosity for the downwards sweep is lower than the upwards sweep. This happens because the material has been sheared more and it cannot rebuild the internal structure as fast as the shear rate decreases. Usually the viscosity decreases rapidly, while the rebuilding of the structure would take considerably more time [46]. Without CMC, H-MNFC fibrils assemble to form small fibrils agglomerations at high shear rate, which impede the rebuilding of the structure when shear rate decreases, consequently decreasing the viscosity in downward sweep. As H-MNFC is a highly fibrillated material the aggregates/flocs formed at high shear rate for CMC 0, and 2% are probably quite small and do not induce detectable wall-slipping as for L-MNFC. Upon CMC addition, CMC molecules may create a bridge between H-MNFC fibrils, thus preventing the fibrils to assemble or reducing the fibrils agglomerations when the shear rate increases. It benefits the rebuilding of the structure of H-MNFC in downward sweep that has the same resistance to flow than in upward sweep. The increasing CMC

addition contributes to transform the H-MNFC relatively static structure to very strong elastic static structure.

#### 4.2.4 Conclusion on the influence of CMC on the MNFC flow behaviour

To sum-up the rheological characteristics of L-MNFC and H-MNFC suspensions as a function of CMC addition, we propose in Table 4.2 a schematic of the effects of CMC on the formation of fibrils agglomerations and structure transformation of MNFC suspensions.

**Table 4.2 Influence of CMC on rheological characteristics of MNFC**

CMC addition (%)		0	1	2	4	6	8	
Disturbance at high shear rate	L-MNFC	√	√	√	×	×	×	
	H-MNFC	×	×	×	×	×	×	
Flow behaviour	L-MNFC	Hysteresis ↓					Homogeneous	
	H-MNFC	Hysteresis ↓			Homogeneous			
Agglomeration of fibrils	L-MNFC							
	H-MNFC							
Structure (Static Structure)	L-MNFC	Weak	→	Relatively strong		→	Very strong	
	H-MNFC	Relatively strong		→	Very strong			

As the CMC addition increases from 0 to 8%, for both L-MNFC and H-MNFC the hysteresis loop progressively fades away, indicating that the time to rebuild the structure after shearing decreases. On one hand it is explained by the bridging effect of CMC, preventing the fibrils agglomeration; on the other hand, the increasing CMC addition leads to the enhancement of MNFC static structure. Comparing H-MNFC with L-MNFC, H-MNFC could withstand higher shear forces and form smaller fibrils agglomerations than L-MNFC, due to a higher fibrillated state. The CMC addition at 0-8% eliminates the fibrils agglomeration formation and enforces a stable resilient static structure.

Rheological tests allowed us to explore the effect of CMC on MNFC dispersion in a macro perspective. To study the influence of CMC on dispersion, one needs to measure the state of fibrillation: *i.e.* individual fibril; consequently fiber morphological analyses are carried out.

#### **4.2.5 Fiber morphological analyses**

Fiber morphological analyses quantify the dispersions effects of CMC on MNFC suspensions. These analyses are done by three methods: fiber quality analyzer, optical microscope, and transmission electron microscope.

##### **4.2.5.1 Fiber Quality Analyzer (FQA)**

FQA is common equipment used by paper manufacturers to measure fiber length, width, coarseness and curl index. Fiber length in the range from 0.07 to 10 mm can be measured while for fiber width the limit is above 7  $\mu\text{m}$  but lower than 50  $\mu\text{m}$ . The Fiber Quality Analyzer could be carried out for L-MNFC suspensions, while for H-MNFC the fibrils are too small to be detected.

Figure 4.8 present the distributions of fiber width of L-MNFC 0.5%+CMC0, 1, 2, 4, 6, and 8 % through FQA. The abscissa represents the fiber dimension interval, for example, 7.5 stands for fiber diameter between (6, 7.5], and 9 indicates the (7.5, 9] range.

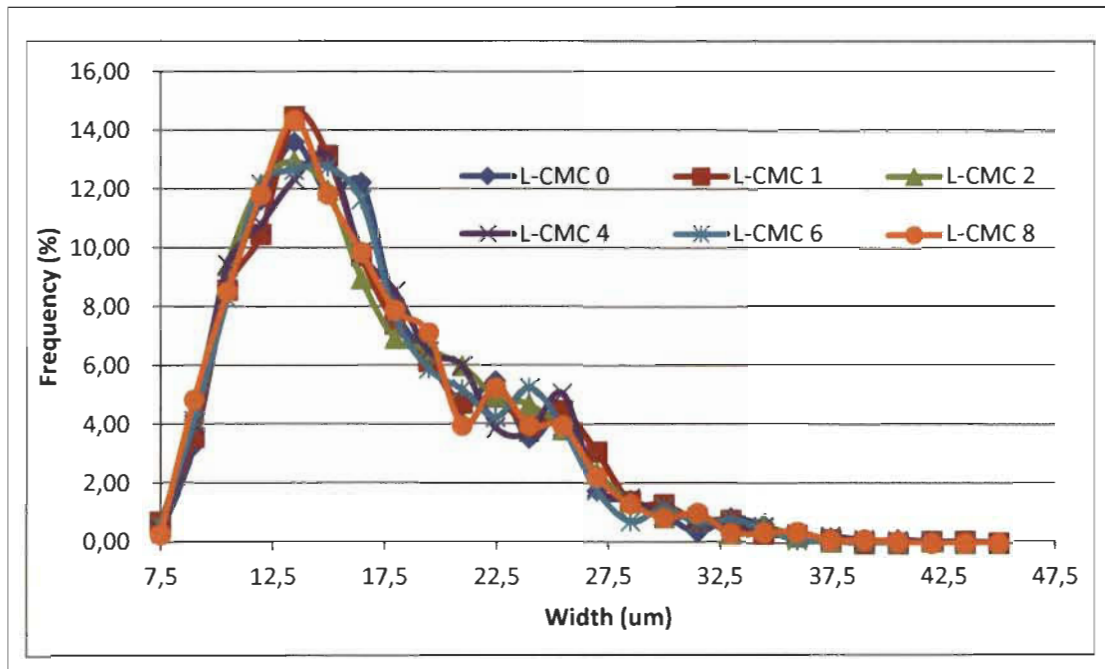


**Figure 4.8 Distribution of fiber width FQA**

The fibers width measured by the FQA ranges from 7.5  $\mu\text{m}$  to 37.5  $\mu\text{m}$ . For the largest ones, it is most presumably fibrils aggregates than single fibril. Most of the fiber widths are located between 10.5 and 22.5  $\mu\text{m}$ . No significant difference between the 6 samples can be detected by such measurements.

The average fiber width according to average fiber length is shown in Figure 4.9. The abscissa represents the fiber length interval, for example 0.6 is (0.5, 0.6]. The measured length by the FQA goes from 0.5 to 3.8 mm. Again the longest fibers are probably fibril aggregates.

Interestingly, L-CMC 0 has apparent longer and thicker fibers than other samples, of which the length spread from 1.3 mm to 4 mm and the width is between 23 and 42  $\mu\text{m}$ . However L-CMC 1 shows few fibrils agglomerations and there are almost no fibrils agglomerations for the other samples as the addition of CMC increases from 2% to 8%.

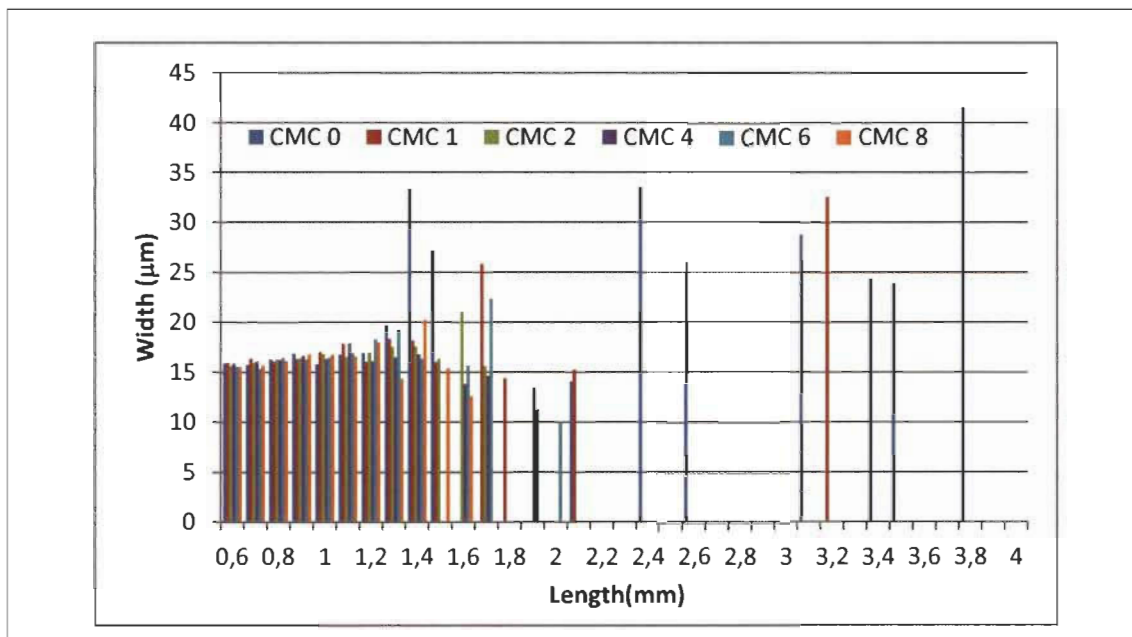


**Figure 4.9 Average fiber width vs. length (FQA)**

FQA results indicate that in the 6 samples of L-MNFC suspensions most of the fibers have diameters between 10.5 and 22.5  $\mu\text{m}$  and the addition of CMC contributes to reduce the number of longer and thicker fibers in L-MNFC 0.5% suspensions. FQA thus shows that CMC helps to reduce the fiber agglomerations in L-MNFC suspensions through what could be considered as a “sketchy fiber morphology analysis”. To have a more precise microscopic fiber distribution for micro and nano elements, optical microscope and transmission electron microscope need to be performed.

#### 4.2.5.2 Optical Microscope (OM) measurements

As the H-MNFC fibrils are obviously too thin to be observed through optical microscopy (our attempt failed to provide any meaningful result), only L-MNFC suspensions are investigated by the OM. The goal is to evaluate if the CMC helps to separate the fibrils and so if the fibrils diameter decreases, as should be expected from rheological measurements, with CMC addition.

Optical microscope pictures of L-MNFC 0.5% + CMC0, 1% are shown in Figure 4.10 to provide an example of the fibril morphology. There is no specific apparent difference between the photographs of all L-MNFC 0.5% samples.

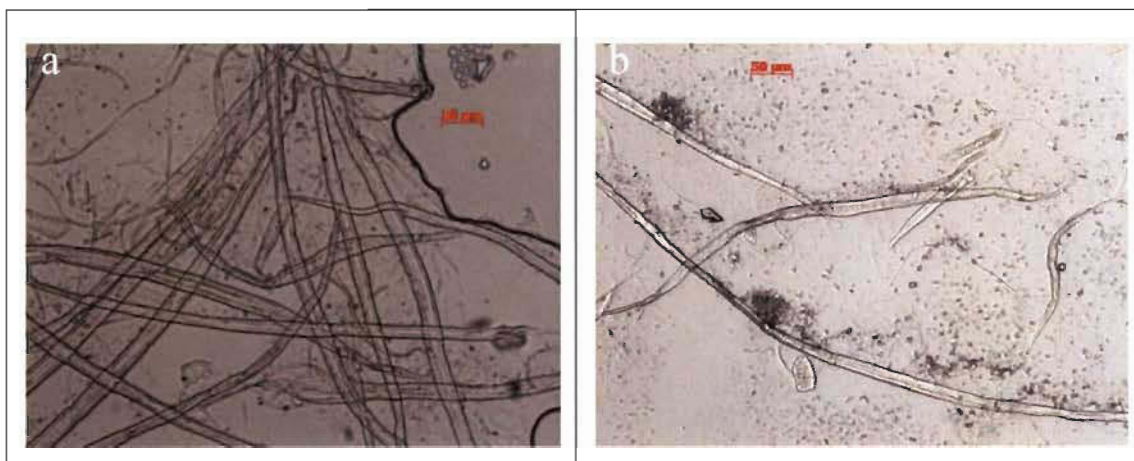


**Figure 4.10** OM pictures of L-MNFC 0.5% (a) and L-MNFC 0.5% + CMC 1% (b)

However, Figure 4.11 is drawn based on the statistical results of fibrils diameters measurements of L-MNFC 0.5% + CMC 0, 1, 2, 4, 6, 8% suspensions (presented simply as 0, 1, 2, 4, 6, 8 CMC concentrations on Figure 4.11 b) by optical microscope.

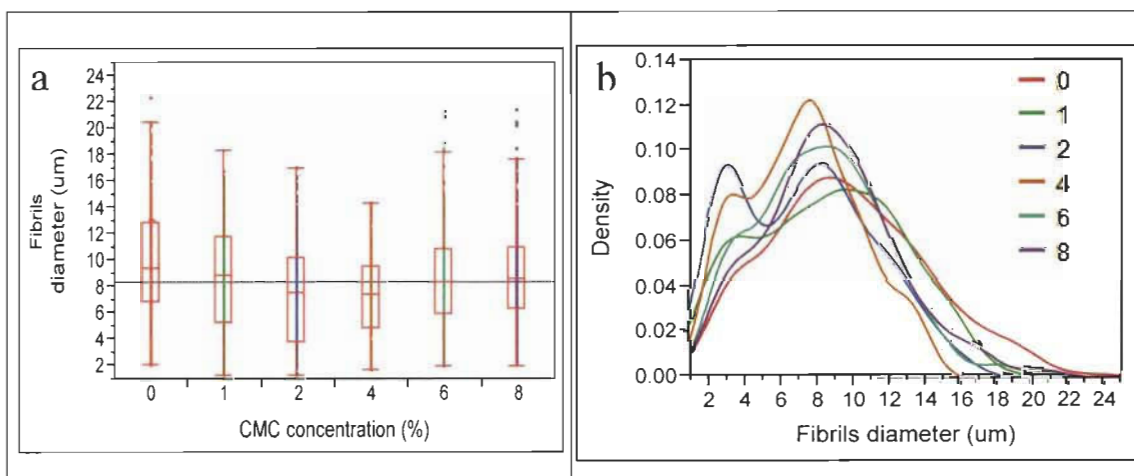


**Figure 4.11** Statistical analysis of L-MNFC 0.5% suspensions (a: fibrils diameters and box charts; b: density distribution of fibrils diameter).

In Figure 4.11.a, every point represents a fibril diameter measurement according to the CMC concentration. As a reminder, a representing whisker box structure is illustrated in Figure 4.12

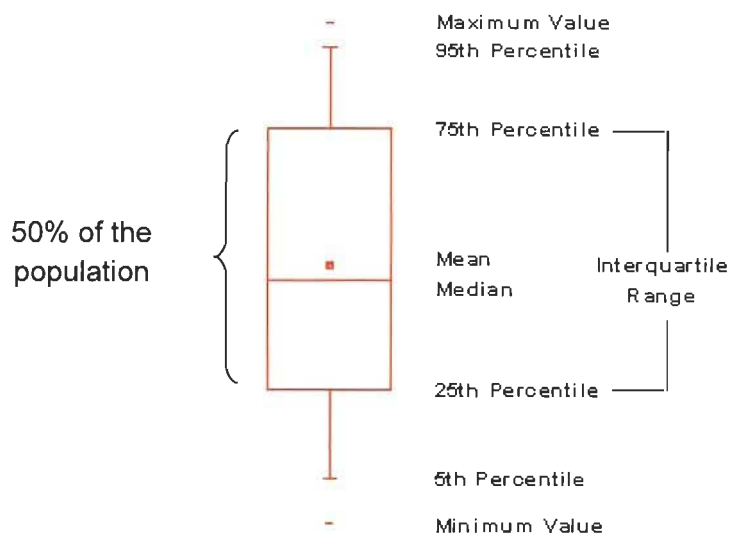


**Figure 4.12 Whisker box structure [47]**

For each CMC concentration, the box charts present the half fibrils in the middle of the fibrils diameter distribution, the red line inside the box stands for the median and the black horizontal line at  $8.4 \mu\text{m}$  represents the global average fibril diameter of all the 6 samples.

From the Figure 4.11, it is observed that the diameters of most fibrils are located between  $6\text{-}12 \mu\text{m}$  and for sample 2 and 4, half of the fibrils diameters are smaller than the global fibril diameter mean at  $8.40 \mu\text{m}$ .

The Figure 4.11.b exhibits the precise density distribution of fibrils diameter. It is notable that there are two groups of fibrils in these L-MNFC suspensions: fibrils population around  $3 \mu\text{m}$  and  $9 \mu\text{m}$ . For samples L-CMC 0, 6 and 8 only one peak at  $9 \mu\text{m}$  appears, while for samples L-CMC 1, 2 and 4, there are two peaks that correspond to the two groups of fibrils. It might also be noted that for sample L-CMC 2 the peak of density at  $3 \mu\text{m}$  is higher than at  $9 \mu\text{m}$  which demonstrate the existence of more thin fibrils in this sample. CMC seems to disperse the fibrils agglomerations of  $9 \mu\text{m}$  width to a large number of thin fibrils.

The distributions of fibrils have been analyzed by JMP to see whether there is a statistical difference between the diameter averages for each CMC concentration. As the

fibrils diameters do not follow a normal distribution, it is suggested to use “Nonparametric Multiple Comparisons”. The statistical method “Wilcoxon Each Pair” has been chosen and applied. The results are presented in Table 4.3. The average level in the right columns of Table 4.3 represents the statistical significance level of fibril diameter with 95% level of confidence. The three letters A, B, C stand for the statistically different populations which indicate the significant difference of mean fibril diameters among samples (A: the biggest fibril diameter; C: the smallest fibril diameter).

**Table 4.3 Significant difference of fibril diameters between L-MNFC 0.5% suspensions (OM)**

CMC (%)	Average diameter ( $\mu\text{m}$ )	Standard deviation ( $\mu\text{m}$ )	Average level		
0	9.82	4.39	A		
1	8.68	4.08		B	
2	7.43	3.77			C
4	7.30	3.15			C
6	8.40	3.67		B	
8	8.79	3.72		B	

When the CMC addition increases from 1% to 4%, the fibril diameter decreases while increasing CMC addition from 4% to 8% leads to the increase in fibrils diameter. The smallest fibril diameter is found around L-CMC 2 and 4 with significant difference compared to the other samples (letter C versus letters A and B). It thus indicates that the addition of CMC in an appropriate amount leads to the decrease of fibrils diameter: *i.e.* an improved dispersion. We may then surmise that on the micro-scale, the appropriate concentration of CMC contributes to the dispersion of L-MNFC fibrils and separates the fibrils agglomerates into thin fibrils. However L-CMC 6 and L-CMC 8 result in the disappearance of dispersion effects, then the fibril diameters seems to regress from the previous state of dispersion.

One key conclusion is that, although not at the nano level, the fibrils diameter measurement realized by Optical Microscope enables the quantification of dispersion

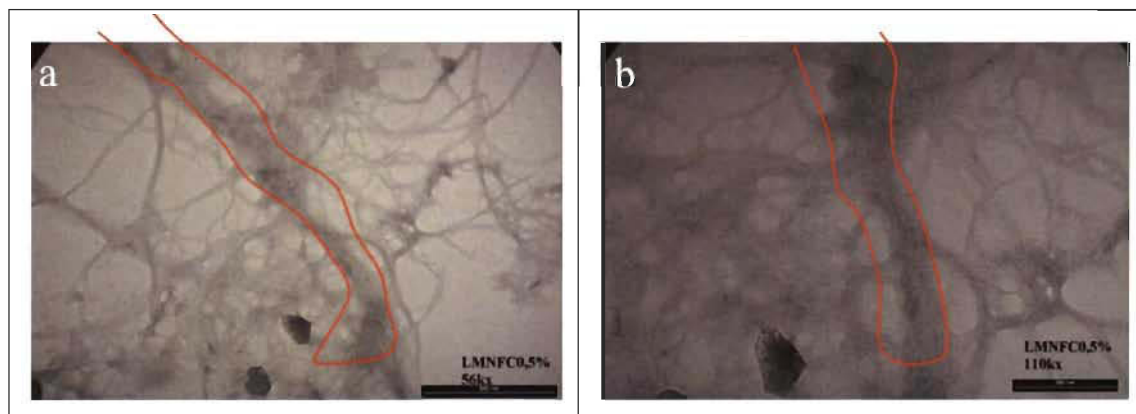
effects of CMC on L-MNFC micro elements. Likewise the dispersion effects of CMC on MNFC nano elements needs to be evaluated quantitatively by Transmission Electron Microscope.

#### 4.2.5.3 Transmission Electron Microscope (TEM) measurements

Through Transmission Electron Microscope the thinnest fibrils in both L-MNFC and H-MNFC suspensions are visible, which permits to analyze the distribution of nano-scale fibril diameter of L-MNFC and H-MNFC.

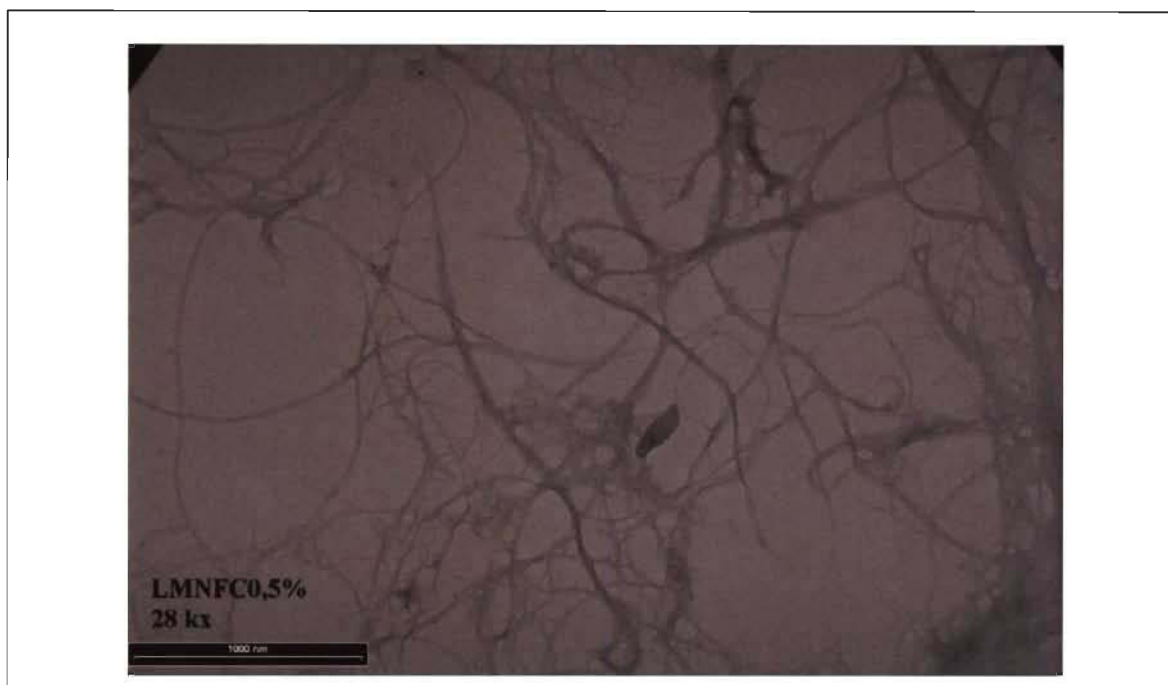
##### 4.2.5.3.1 L-MNFC 0.5% suspensions

Figure 4.13 shows the same fibril agglomerate (circled in red) of L-MNFC 0.5% suspension at magnification of 56 000X and 110 000X. The elementary fibrils can be distinguished more clearly in Figure 4.13.a than in Figure 4.13.b, but the contrast is too low for the measurement of diameter in both pictures.



**Figure 4.13 TEM pictures of L-MNFC 0.5% at the magnification of 56 000X and 110 000X**

Another picture of L-MNFC 0.5% at 28000X magnification (Figure 4.14) shows distinct fibers which diameters that can be measured by image analysis.



**Figure 4.14 TEM picture of L-MNFC 0.5% at the magnification of 28 000X**

Although pictures at the highest magnification of 110 000X allow to see more thin fibrils, it is somehow more difficult to measure diameters. The suitable magnification to measure the diameter is then selected at 28 000X for all L-MNFC 0.5% suspensions. The distribution of fibril diameters of L-MNFC 0.5% is presented in Figure 4.15.

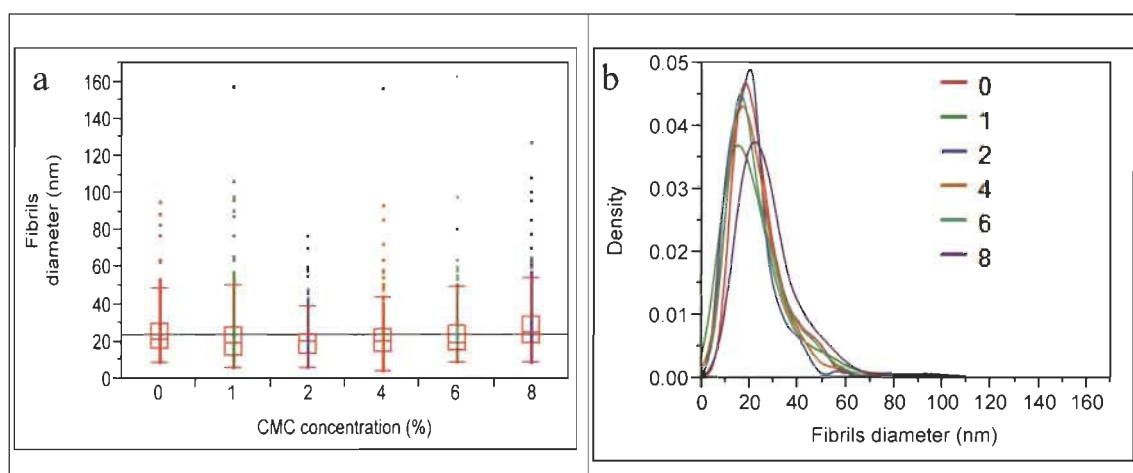


**Figure 4.15 Statistical analysis of L-MNFC 0.5% suspensions (a: fibrils diameters and box charts; b: density distribution of fibrils diameter).**

The global fibril diameter average for L-MNFC is 23.8 nm. Except for L-CMC 8, the diameters of half of the fibrils involved in the fibril diameter measurements are lower than the global fibril diameter mean. Notably, L-CMC 2 has 75% of its fibril diameters thinner than the global average level.

Figure 4.15 b represents the density distribution of fibrils diameters of L-MNFC 0.5% suspensions with different CMC concentrations (0, 1, 2, 4, 6, 8 stand for L-CMC 0, 1, 2, 4, 6, 8, respectively). All the samples present unimodal distribution (as compared to the optical microscopy) and the fibril diameters are distributed mainly between 10 and 40 nm.

The same statistical method that has been applied for the distribution of fibril diameter through optical microscope has been used to compare the fibril diameter of MNFC suspensions through transmission electron microscope. The results are shown in Table 4.4.

**Table 4.4 Significant difference of fibril diameter between L-MNFC 0.5% solutions (TEM)**

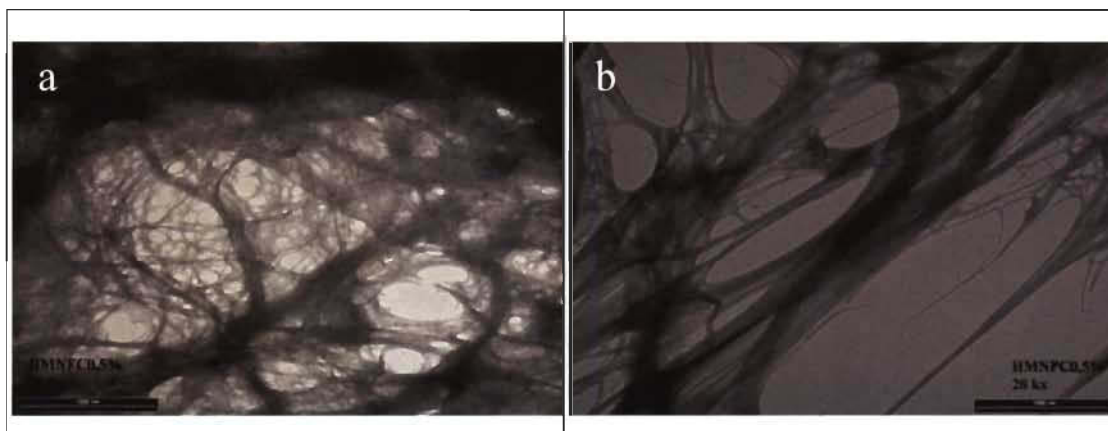
CMC (%)	Average	Standard deviation	Average level		
0	24.55	12.49		B	
1	23.22	17.44			C
2	20.36	10.19			C
4	22.65	14.19			C
6	23.70	18.75			C
8	28.75	15.61	A		

Table 4.4 exhibits the significant difference of average fibril diameter of all the samples. It first shows that L-CMC 1 to 6% have the smallest fibril diameters, which are significantly different from L-CMC 0 and 8. Increasing the concentration of CMC from 0 to 1%, the fibril diameter decreases; from 1% to 6%, the fiber diameter mean does not change statistically significantly; and from 6% to 8%, the fibril diameter increases, even higher than the initial state. Among these samples, L-CMC 2 has the lowest average of

fibril diameter. Compared to the optical microscopy, it looks like the dispersing effect of CMC at the nano level is similar that what occurs at the micro level, with a low level that seems to extend (from statistical evaluation) from 1 to 6 with an increase back at 8 CMC concentration.

#### 4.2.5.3.2 H-MNFC 0.5% suspensions

The fibrils of H-MNFC 0.5% taken by TEM at the magnification of 28 000x are presented in Figure 4.16. Figure 4.16 a shows the entanglement of the fibrils and the formation of the fibrils network. In Figure 4.16 b, some fibrils have been stretched because of the drying shrinking. The measurement of independent fibrils is here not feasible (would be quite difficult and prone to judgement errors).



**Figure 4.16** TEM pictures of H-MNFC 0.5% at the magnification of 28 000X

Pictures of H-MNFC 0.5% + CMC 2% are taken at the same position at two magnifications: 56 000X (Figure 4.17 a) and 180 000X (Figure 4.17 b). The same fiber bundle (circled in red) in the two pictures is constituted by the finest fibrils. Although more fibrils could be observed with 180 000X magnification, the measurement of these fibrils with high magnification is not very efficient.

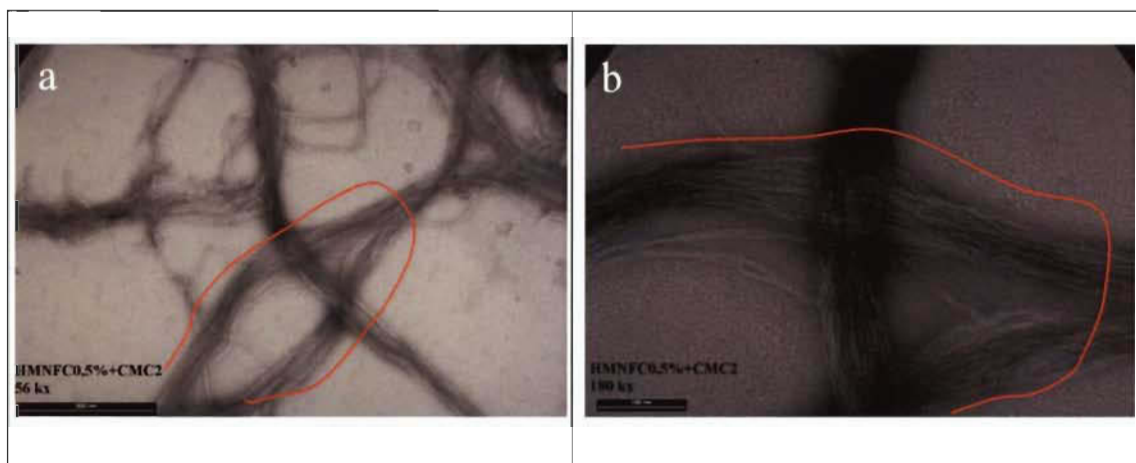


**Figure 4.17 TEM pictures of H-MNFC 0.5%+CMC 2% at the magnification of 56 000X (a) and of 110 000X (b).**

Comparing the TEM photographs of H-MNFC without CMC (Figure 4.16) and with CMC (Figure 4.17), the measurement of diameter is only possible for H-MNFC 0.5% with CMC. TEM photographs of H-MNFC 0.5% +CMC 1, 2, 4, 6, 8% have been taken at the magnification of 28 000X to investigate the distribution of fibrils diameter.

Figure 4.18.a displays the fibrils diameters of H-MNFC 0.5% suspensions with different CMC concentrations. The global fibril diameter is 21.0 nm and the median of all the samples are inferior to the global average. It is noteworthy that for H-CMC 2, the diameter of more than 75% fibrils are lower than the global average which presents the highest proportion of thin fibrils. Figure 4.18.b exhibits the density distribution of fibrils diameter of H-MNFC 0.5% suspensions with different CMC concentrations (1, 2, 4, 6, 8 represent for H-CMC 1, 2, 4, 6, 8 respectively). All the samples have unimodal distribution around 18 nm while the skewness of the peak changes greatly along with the CMC concentration. Among these samples, H-CMC 2 possesses the highest peak, indicating that it has the most important quantity of fibrils with the diameter around 18 nm.

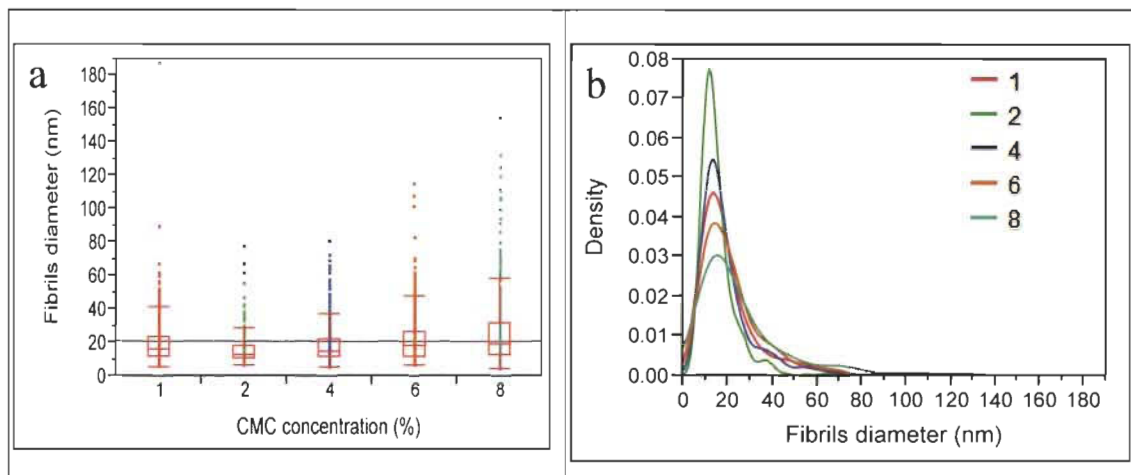


**Figure 4.18** Statistical analysis of H-MNFC 0.5% suspensions (a: fibrils diameters and box charts; b: density distribution of fibrils diameter).

To evaluate the significant difference of fibrils diameter average among the H-MNFC suspensions with CMC, the same statistical method employed for the L-MNFC suspensions is used. The statistic results are shown in Table 4.5.

**Table 4.5** Significant difference of fibril diameters between H-MNFC 0.5% suspensions (TEM)

CMC (%)	Average	Standard deviation	Average level		
1	19.89	15.58		B	
2	15.68	9.07			C
4	19.33	12.54		B	
6	22.78	16.29	A		
8	27.21	23.71	A		

As H-MNFC 0.5% suspension without CMC shows the entanglement of fibrils, no initial state could be measured, but CMC contributes to the dispersion of H-MNFC which enable to measure fibril diameter. In Table 4.5, the fibril diameter of H-CMC 1 is significantly higher than H-CMC 2, and lower than H-CMC 6, 8. The prominent influences of CMC on the fibril diameter are demonstrated in Table 4.5: with the addition of CMC at low dose, H-MNFC fibrils have been dispersed and then with CMC concentration above 2% they aggregated which leads to the change of fibrils diameter.

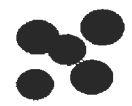
H-CMC 2 has the best dispersion state with the minimum fibril diameter at 15.7 nm which is significantly different from all the other samples.

#### 4.2.6 Discussion on the influence of CMC on MNFC dispersion

Analysis of MNFC with FQA has shown the first indications that CMC helps to reduce the fibrils agglomerations in MNFC suspensions. OM and TEM proved that the reduction of fibrils diameter of MNFC happens at an appropriate CMC concentration. The main conclusion is that CMC disperses the MNFC fibrils both at the nano and micro-scale.

Reviewing the rheology tests and fiber morphology analysis of MNFC suspensions, Table 4.6 and Table 4.7 schematically illustrates the influence of CMC on the flow behaviour, fibrils diameter of L-MNFC, and H-MNFC suspensions, respectively.

**Table 4.6 Influence of CMC on L-MNFC flow behaviour and fiber morphology**

	L-CMC 0	L-CMC 1	L-CMC 2	L-CMC 4	L-CMC 6	L-CMC 8
<b>Flow behaviour</b>	Hysteresis ↓					Homogeneous
<b>Agglomeration of fibrils</b> 						
<b>Diameter (μm)</b> 	A	B	C	C	B	B
<b>Diameter (nm)</b> 	B	C	C	C	C	A

For L-MNFC, the addition of CMC eliminates the formation of fibrils agglomeration with a homogeneous behaviour at 8% while the smallest fibrils mean diameter (both

micro elements and nano elements) occurs at concentration around 2-4%. The two optimum concentrations are different.

**Table 4.7 Influence of CMC on H-MNFC flow behaviour and fiber morphology**

	H-CMC 0	H-CMC 1	H-CMC 2	H-CMC 4	H-CMC 6	H-CMC 8
<b>Flow behaviour</b>	Hysteresis ↓			Homogeneous		
<b>Agglomeration of fibrils</b> ●						
<b>Diameter (nm)</b>		B	C	B	A	A

For H-MNFC, H-CMC 4 begins to show no hysteresis loop, illustrating the non-existence of fibrils agglomeration. However H-CMC 2 is found to have the smallest fibrils diameter. The optimum concentrations for H-MNFC are also different but the difference is smaller than for L-MNFC.

The flow behaviour investigates the fibril-fibril interaction in suspension while fiber morphology analyzes the fibrils individually, *i.e.* it provides a direct evaluation of the “true” dispersion effects. The optimum concentrations in rheology test and in fiber morphology evaluate the dispersion in different perspectives: the former means the most homogeneous suspension with minimum agglomerations; the latter means the individual thinnest fibrils. Figure 4.19 represents the schematic organization in the suspension at different CMC concentrations. Without CMC fibrils aggregates together to form “flocs”; at low CMC addition level, fibrils spread and the fibrils diameter mean decreases with low modification of aggregates (flocs) formation; while at higher addition level of CMC, fibrils do not spread but separate from each other.

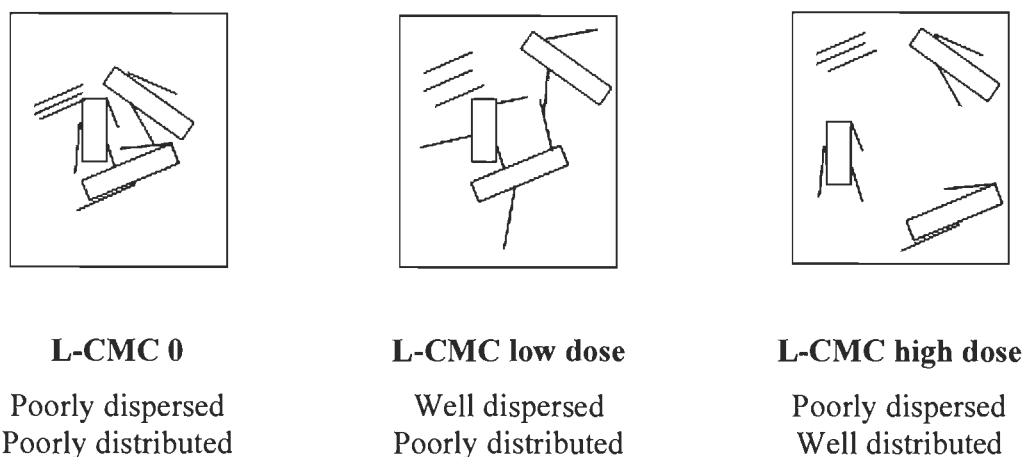


**Figure 4.19 Schematic representation of the dispersion and distribution of the fibrils in the L-CMC suspension according to the CMC concentration**

Therefore the difference between the two optimum concentrations may be due to different interaction mechanisms between CMC and MNFC as a function of CMC addition. Considering that L-MNFC reveals the largest difference between the two optimum concentrations than H-MNFC, a more in-depth investigation on the interactions between CMC and MNFC are carried out for L-MNFC. Referring to the literature review, the interaction mechanism research will focus on the CMC adsorption on MNFC and the CMC free in suspension. Surface physical-chemistry study, polyelectrolyte titration, and composition analysis will be applied for L-MNFC suspensions to fulfill the investigation objective. The surface physical-chemistry analysis has nevertheless been carried out for H-MNFC, as a comparison to the results of L-MNFC.

### 4.3 Interactions between CMC and MNFC

To investigate the adsorption of CMC on MNFC surface, the surface physical-chemistry is evaluated first by a measure the zeta potential of MNFC suspensions as a function of CMC addition. Zeta potential is the common scientific term for electro kinetic potential in colloidal systems [25]. Electro kinetic measurements play an important role in the characterization of surface properties of fibers and in papermaking industries to investigate the relationships between zeta-potential and uptake of additives [48]. In

MNFC suspensions, zeta potential indicates the potential on slipping plane (see Figure 2.3) of anionic fiber. If CMC adsorbs on MNFC surface the surface physical-chemistry properties of fibers should evolve and the zeta potential should then change. To detect the CMC free in suspension, the anionic charges in the supernatant of MNFC suspension has been quantitatively measured by polyelectrolyte titration. Microscope observation and elementary analysis are then applied to the drying matters of the supernatant to inspect the potential existence of CMC free.

### 4.3.1 Surface physical-chemistry

#### 4.3.1.1 Zeta potential of CMC solutions

The pH of the MNFC suspensions is 9 and the pH of CMC solution is 7, mixing MNFC and CMC do slightly modify the pH of the CMC solutions. Therefore the zeta potential of CMC with different pH has been measured by Zetasizer Nano ZS (see Figure 4.20).

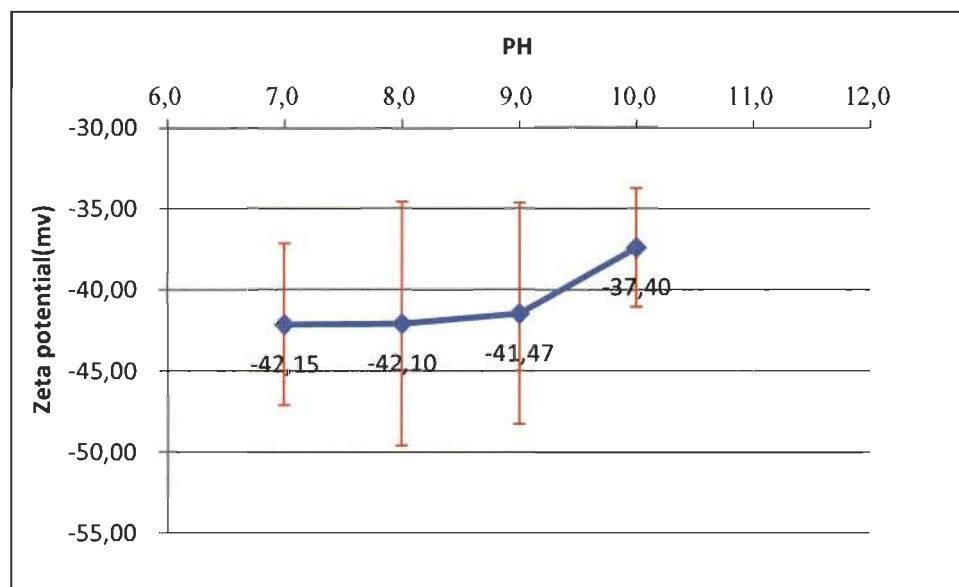
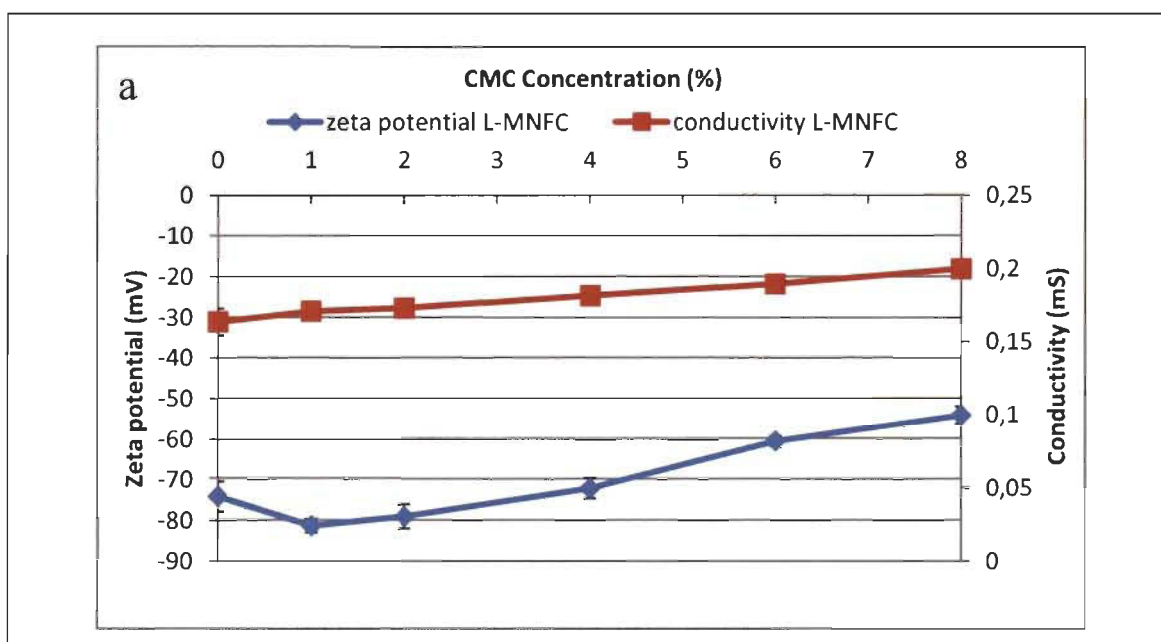


**Figure 4.20 Zeta potential of CMC 0.1% with different pH value**

The standard deviation is quite important but it can be seen that between 7 and 9 the pH does not influence strongly the CMC zeta potential. The average zeta potential of CMC 0.1% between pH 7 and 9 is about -42 mV.

### 4.3.1.2 Zeta potential of MNFC fibrils

Usually, to measure zeta potential, conductivity needs to be adjusted with electrolytes (KCl for instance) to be constant for each and every sample. In this case, it is known that electrolytes may interact with the fibrils dispersion (screening effect) and will modify the surface physical chemistry of the fibrils. Therefore, we decided to measure the ZP without adjusting the conductivity. The zeta potential of L-MNFC/H-MNFC with different concentrations of CMC is presented in Figure 4.21.a and Figure 4.21.b. During the experiments, pH values of each L-MNFC and H-MNFC solutions have been measured and are similar (pH 9).



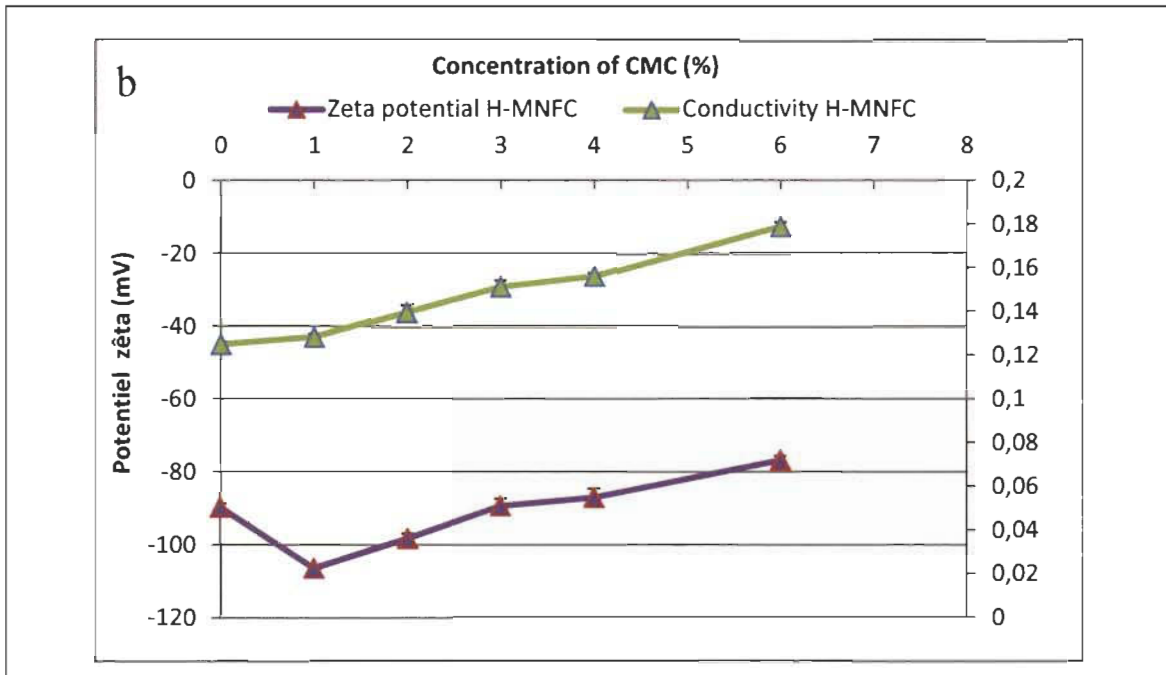


**Figure 4.21 Zeta potential and conductivity of L-MNFC 0.5% (a) and H-MNFC 0.5% (b) suspensions with different concentrations of CMC**

Figure 4.21 shows that CMC first leads to a significant decrease in ZP as the addition of CMC is from 0 to 1% and then when CMC concentration increase, ZP increases for both L-MNFC and H-MNFC. The concentration of CMC which brings about the most important impact is 1-2%.

When low amount of CMC (below 2%) is added to MNFC suspensions, the zeta potential of MNFC particles decreases - or increases in absolute value. It means that the surface charges of the fibrils have changed. The change may be due to the adsorption of CMC on the surface of MNFC. While more CMC is added, zeta potential increases. On the one hand, the increase may be due to the saturation of CMC on the surface of MNFC, on the other hand, the CMC brings electrolyte such as sodium salts into the suspensions and leads to an increase in conductivity which results in an increase of the zeta potential.

Nevertheless the surface area of H-MNFC is much higher than that of L-MNFC, so if the change in ZP is due to surface saturation, the minimum in ZP should occur at a higher CMC concentration for H-MNFC (in other terms more CMC would be needed to

saturate the surface). It appears that the modification of the zeta potential is not related to the surface of MNFC fibrils. Furthermore, one should note that a common characteristic of H-MNFC and L-MNFC is the ratio cellulose/calcium carbonate (around 80/20). As it is known that electrolyte presence is necessary for adsorption of CMC on cellulose surface, the calcium carbonate in the suspension may play a significant role in the CMC adsorption and so in the MNFC dispersion.

Another point is worth mentioning. The measurement of zeta potential does not take into account the permeability of the MNFC plug formed in the Müttek™ SZP-06 instrument. It is known that the lower permeability of plug decreases the absolute value of zeta potential (lower flow of counter ions inducing lower streaming current). If CMC really adsorbs on fibril surface and helps to disperse MNFC at the concentration of 0-2%, the lower permeability of MNFC plug should decrease the absolute value of ZP. Therefore the increase in absolute value of zeta potential at 2% CMC addition is another clue that demonstrates the adsorption of CMC on fibril surface.

The zeta potential measurements have shown that CMC most probably adsorbs on the surface of both L-MNFC and H-MNFC. As the zeta potential indicates the repulsion between the fibrils, it is surmised that the addition of CMC at 1-2% which leads to the lowest zeta potential value may promote the dispersion of MNFC suspensions. Nevertheless, the CMC behaviour at higher addition levels needs to be further investigated to confirm that the CMC above 2% is either free in the suspension or adsorbs on the fibrils surface.

#### **4.3.2 CMC dosage by polyelectrolyte titration**

To explore the state of CMC molecule in MNFC suspensions, the suspensions have been centrifuged and the supernatants of MNFC suspensions are evaluated. Polyelectrolyte titration is carried out to measure the quantity of CMC dissolved in liquid phase. First, the anionic charges of pure CMC are determined by the calibration line of pure CMC. Then the anionic charges quantity of CaCO<sub>3</sub> + CMC solution is measured to investigate the influence of CaCO<sub>3</sub> on CMC. Finally polyelectrolyte titration is applied to the

MNFC supernatant to explore the evolution of anionic charges quantity with CMC addition.

#### 4.3.2.1 Calibration line (anionic charges of CMC)

First, the anionic charges of pure CMC solutions have been measured. The calibration line for Poly-DADMAC consumption versus CMC amount is shown in Figure 4.22.

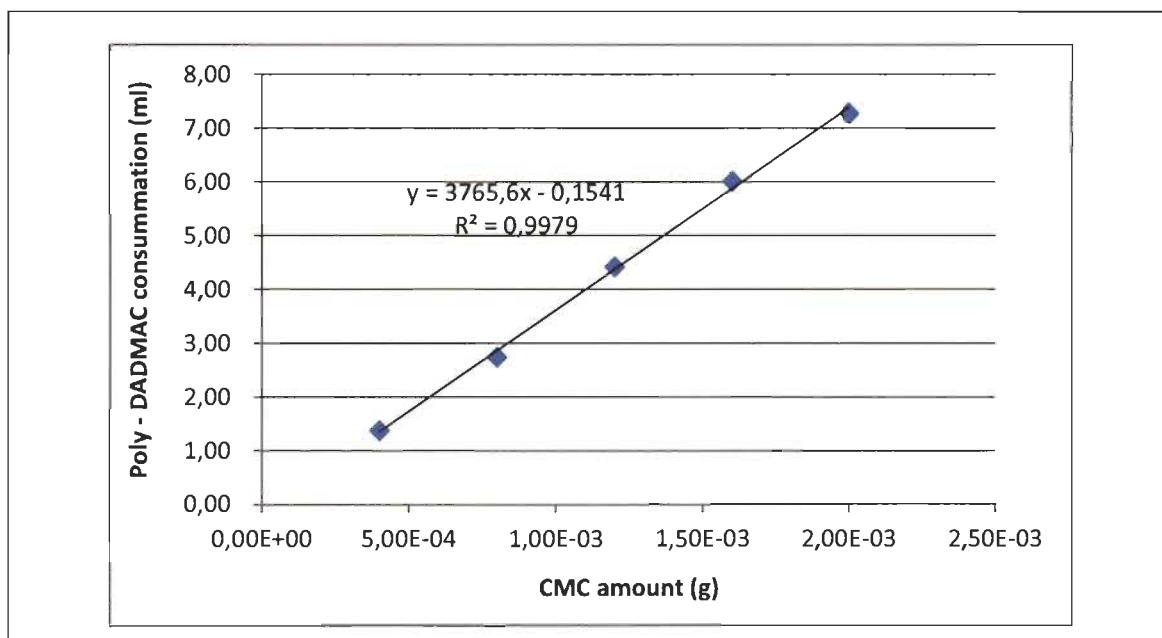


**Figure 4.22 Calibration line for Poly-DADMAC consumption versus CMC amount**

Equation 4.1 presents the linear fitting of the calibration line (determination coefficient  $R^2 > 0.99$ ).

$$Y = 3765.6X - 0.1541 \quad \text{Equation 4.1}$$

X = CMC amount (g)

Y = Poly-DADMAC consumption (ml)

According to the CMC amount and the corresponding Poly-DADMAC consumption in Figure 4.22, the anionic charge quantity per gram of CMC is calculated through Equation 3.1 and results presented in Table 4.8.

**Table 4.8 The anionic charge quantity per gram of CMC**

	CMC amount (g)	Poly-DADMAC consumption (ml)	Anionic charge quantity (eq/g CMC)	Average of anionic charge of CMC (eq/g CMC)
1	0.0004	1.380	3.45E-03	3.59E-03 (Standard deviation: 1.46E-04)
2	0.0008	2.740	3.42E-03	
3	0.0012	4.416	3.68E-03	
4	0.0016	6.011	3.76E-03	
5	0.002	7.276	3.64E-03	

The anionic charge quantity of CMC is 0.00359 eq/g with a standard deviation of 0.000146 (about 4%).

For the latter measurement, the anionic charges measurement in  $\text{CaCO}_3$  solution and L-MNFC suspensions are compared considering the null hypothesis. The statement of the null hypothesis is: CMC is the only anionic charge source. So the anionic charge quantity of the solution (suspension) should be the same as the anionic charge quantity of the CMC molecules. In this case, the anionic charge quantity of the solution (suspension) is called “hypothetical” CMC charge quantity. With known CMC concentration, the hypothetical CMC charge quantity may be calculated according to Equation 4.2.

$$q(\text{hypothetical CMC}) = m(\text{CMC}) \times q(\text{CMC}) \quad \text{Equation 4.2}$$

$m(\text{CMC})$  = CMC concentration (g CMC/g solution or g CMC/g suspension)

$q(\text{CMC})$  = Anionic charge quantity of CMC (eq/g CMC)

$q(\text{hypothetical CMC})$  = CMC total anionic charge quantity (eq/g solution or eq/g suspension)

### 4.3.2.2 Anionic charge measurement of CaCO<sub>3</sub> solutions

As electrolyte presence is essential for adsorption of CMC, there may be some interaction between the calcium carbonate and CMC. The anionic charges quantity of CaCO<sub>3</sub> solutions is measured to investigate the influence of CaCO<sub>3</sub> on CMC.

The CaCO<sub>3</sub> used is a little cationic and the cationic charge quantity of CaCO<sub>3</sub> is  $5.01 \times 10^{-8}$  eq/g CaCO<sub>3</sub>, measured by polyelectrolyte titration. Compared with the anionic charge quantity of CMC (0.00359 eq/g), the cationic charge of CaCO<sub>3</sub> is then negligible. Thus in C-CMC solutions, CMC molecules are the only source of anionic charge. For C-CMC solutions, the CMC concentration and the hypothetical CMC charge quantity is presented in Table 4.9. The standard deviation of the hypothetical anionic charge quantity is presented in brackets.

**Table 4.9 CMC concentration (g CMC/g solution) and the hypothetical CMC charge quantity (eq/g solution) in the CaCO<sub>3</sub> solutions**

	C-CMC 0	C-CMC 1	C-CMC 2	C-CMC 4	C-CMC 6	C-CMC 8
CMC concentration (g CMC / g solution)	0	5E-5	1E-4	2E-4	3E-4	4E-4
Hypothetical CMC charge quantity (eq/g supernatant)	0 (0)	1.80E-07 (7.29E-09)	3.59E-07 (1.46E-08)	7.18E-07 (2.91E-08)	1.08E-06 (4.37E-08)	1.44E-06 (5.83E-8)
The measured anionic charge quantity of C-CMC solution is shown in Figure 4.23, in comparison with the hypothetical CMC charge quantity.						

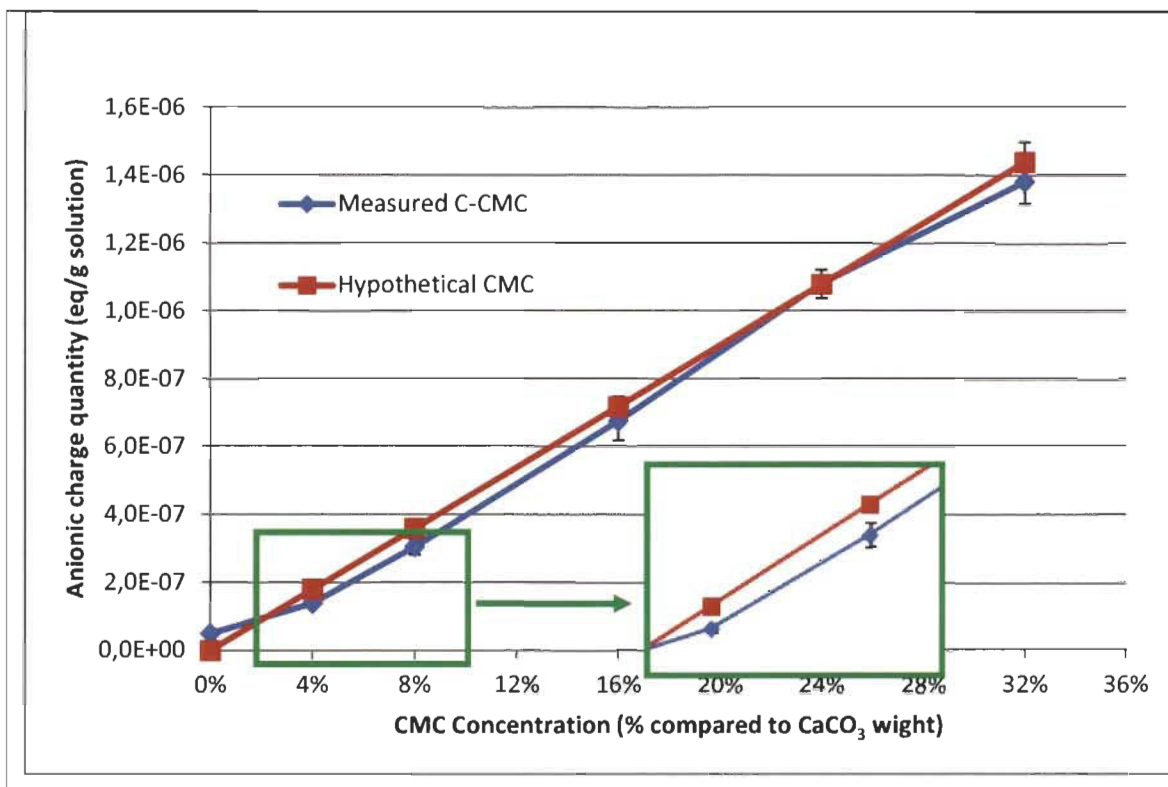


**Figure 4.23 Measured anionic charge quantity of C-CMC solutions**

For the CaCO<sub>3</sub> solutions with CMC addition, C-CMC 4 and C-CMC 8 (which present the same CaCO<sub>3</sub> concentrations and CMC concentrations as in L-CMC 1, L-CMC 2) reveal a slight but significant difference between the measured charge quantity and the hypothetical charge quantity. The inferior measured charge quantity indicates that some interaction exists between CaCO<sub>3</sub> and CMC. Considering the negatively charged CMC and the positively charge calcium carbonate, electrostatic interaction is the most relevant mechanism. At CMC 1 and 2, a part of the CMC will interact with CaCO<sub>3</sub> and the agglomerations should be considered as neutral particles decreasing the anionic charge measured when compared to the hypothetical ones.

However, increasing the CMC concentration from 16 to 32%, the measured charge quantity stays at the same level as the hypothetical. We propose two potential explanations. First, as the quantity of CMC increases, the small amount of CMC neutralized by CaCO<sub>3</sub> is negligible when compared to the CMC anionic charges. Therefore, the difference is obliterated by the measurement uncertainties. Second, as reported in the literature, the CMC adsorption on cellulose is influenced by the

electrolytes presence and especially the calcium ions [49]. It is then quite possible that an optimum ratio  $CMC/Ca^{2+}$  is obtained at C-CMC 1 and 2 to promote the CMC and  $Ca^{2+}$  interactions. Above this ratio, the CMC may change its behaviour and not interact anymore with  $Ca^{2+}$ . The sodium salts contained in the CMC solution may play a role in this shift.

The interaction between CMC and  $CaCO_3$  is proved to exist by the anionic charge quantity measurement of C-CMC solutions. Similarly, the anionic charge quantity of L-CMC supernatant is studied to further explore the interaction between the CMC and L-MNFC.

#### **4.3.2.3 Anionic charges measurement in L-MNFC supernatant**

L-MNFC suspensions contain fibrils,  $CaCO_3$  and CMC. Among the three components, fibrils and CMC are anionic. To detect the CMC free in suspension, L-MNFC suspensions are centrifuged to separate fibrils. Therefore, the appropriate centrifugation speed should be identified for a separation of fibrils. After fibril sedimentation, the anionic charge quantity of the supernatant is measured. The inspection of CMC free has been achieved by comparing the measured anionic charge quantity with the hypothetical anionic charge quantity.

In the supernatant, the only two possible anionic charges particles are CMC (if CMC is free in solution) and fibrils (if some fibrils remain/stay in the supernatant). As the anionic charges sources are not certain, a null hypothesis is made: no fibrils are in the supernatant and all CMC molecules are free in the solution. In such a case, the CMC concentration in the supernatant is the same as in L-CMC suspensions and CMC is the only anionic particles. The anionic charge quantity under this assumption is called hypothetical CMC charge quantity. Table 4.10 presents the CMC concentration and hypothetical charge quantity in the suspensions. The standard deviation of the hypothetical anionic charge quantity is presented into brackets.

**Table 4.10 CMC concentration (g CMC/g supernatant) and the hypothetical CMC charge quantity (eq/g supernatant) in the L-MNFC suspensions**

	C-CMC 0	C-CMC 1	C-CMC 2	C-CMC 4	C-CMC 6	C-CMC 8
CMC concentration (g CMC / g supernatant)	0	5E-5	1E-4	2E-4	3E-4	4E-4
Hypothetical CMC charge quantity (eq/g supernatant)	0 (0)	1.80E-07 (7.29E-09)	3.59E-07 (1.46E-08)	7.18E-07 (2.91E-08)	1.08E-06 (4.37E-08)	1.44E-06 (5.83E-8)

The centrifugation speed applied to the separation of nanocellulose varies substantially within the literatures, from 4 000 rpm to 10 000 rpm [50, 51]. As no fibrils in the supernatant is under the assumption, in present work, 10 000 rpm is applied for the maximum separation of L-MNFC fibrils and water.

The L-MNFC suspensions are centrifuged at 10 000 rpm for 1 hour. Poly-DADMAC titrates the supernatants to measure the anionic charge quantity. The measured values are referred as measured L-CMC as compared with the hypothetical CMC charge quantity. Figure 4.24 presents the measured anionic charge quantity of L-MNFC supernatants as the blue line and the hypothetical line in red.

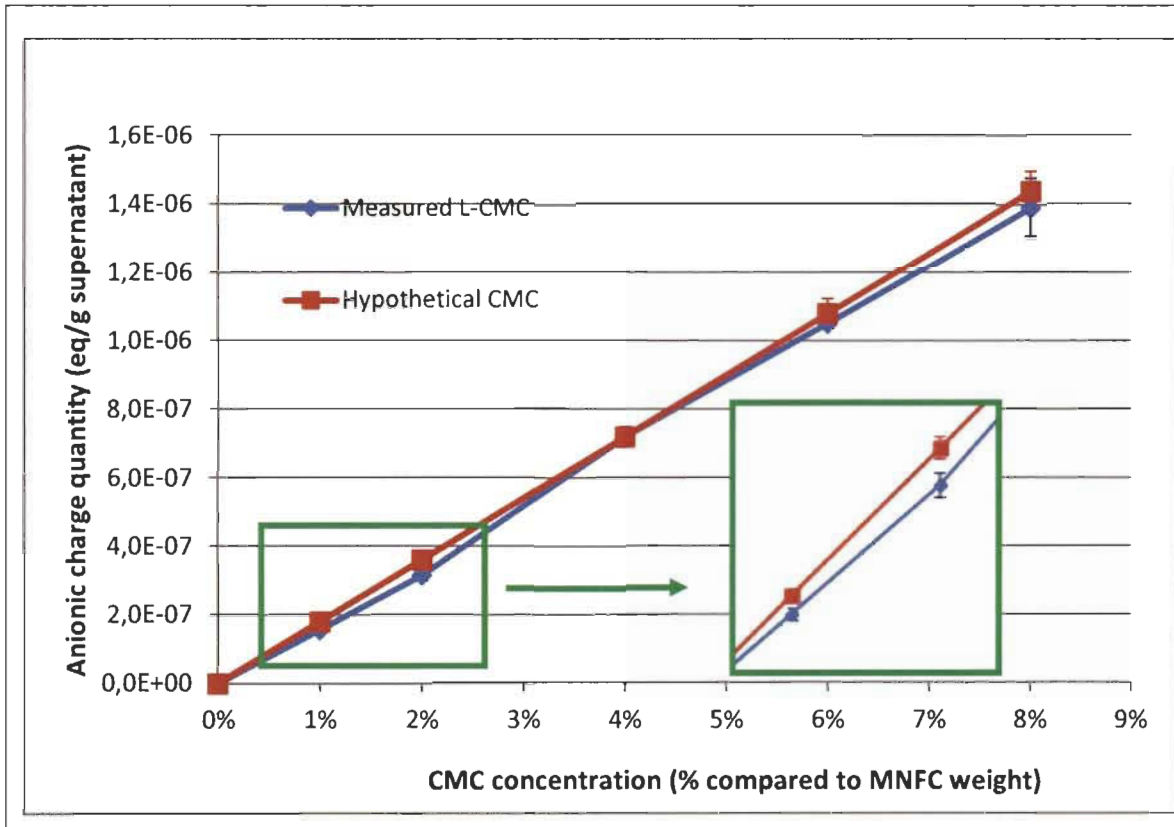


**Figure 4.24** Measured anionic charge quantity of the supernatant of L-MNFC suspensions (centrifugation at 10 000rpm for 1h)

The measured anionic charge quantity of L-CMC 0 is almost the same as deionized water, illustrating that the supernatant of L-CMC 0 is as neutral as deionized water. Comparing the measured and hypothetical values, L-CMC 1 and L-CMC 2 present hypothetical anionic charge quantity higher than the measured values with a significant difference (see error bars). For other samples, no significant difference is found. The difference at CMC 1 and 2 may be due to the adsorption of CMC on the surface of fibrils at low CMC concentration (1-2%). However increasing CMC addition from 4 to 8%, CMC molecules are free in the suspension. Another interpretation may be the interaction between CMC and  $\text{CaCO}_3$  that was shown in Figure 4.23. As L-CMC 1 and C-CMC 4, L-CMC 2 and C-CMC 8 have the same calcium carbonate concentration and CMC/  $\text{CaCO}_3$  ratio, the interaction between CMC and  $\text{CaCO}_3$  found in C-CMC 4, C-CMC 8 could occur in L-CMC 1 and L-CMC 2.

For the samples with CMC addition, the measured anionic charge quantity increases with the CMC concentration in the suspension. It may demonstrate that there are more CMC molecules free when increasing CMC addition from 0-8%.

The reason for this distinct behaviour is still not fully understood as the adsorption of CMC on fibrils inferred from PCD (particle charge detector) corresponds to the zeta potential analysis. To identify the anionic charge particles in L-MNFC suspensions and verify the interaction between CMC and  $\text{CaCO}_3$ , microscopic observation and elemental analysis are applied.

### **4.3.3 Identification of the supernatant composition**

To identify the supernatant composition, first the supernatants have been dried by a humidity analyzer. After drying, the remaining solids of each sample are observed with SEM and analyzed by the elemental analysis at different magnification from 250X to 5000X. The minimum magnification 250X is used to compare the samples on the whole. The identifications of several materials such as the calcium carbonate, the fibrils are explored at higher magnification.

All the supernatants to be dried and then analyzed by scanning electron microscope originate from centrifugation at 10 000 rpm for 1 hour. The supernatants of samples L-MNFC 0.5% + CMC0, 1, 2, 4, 6, and 8 % are simply referred to as L-CMC 0, 1, 2, 4, 6 and 8, respectively.

### **4.3.4 General observation**

Figure 4.25 presents large areas for samples L-CMC 0, 1, 4, and 8 at the same magnification.

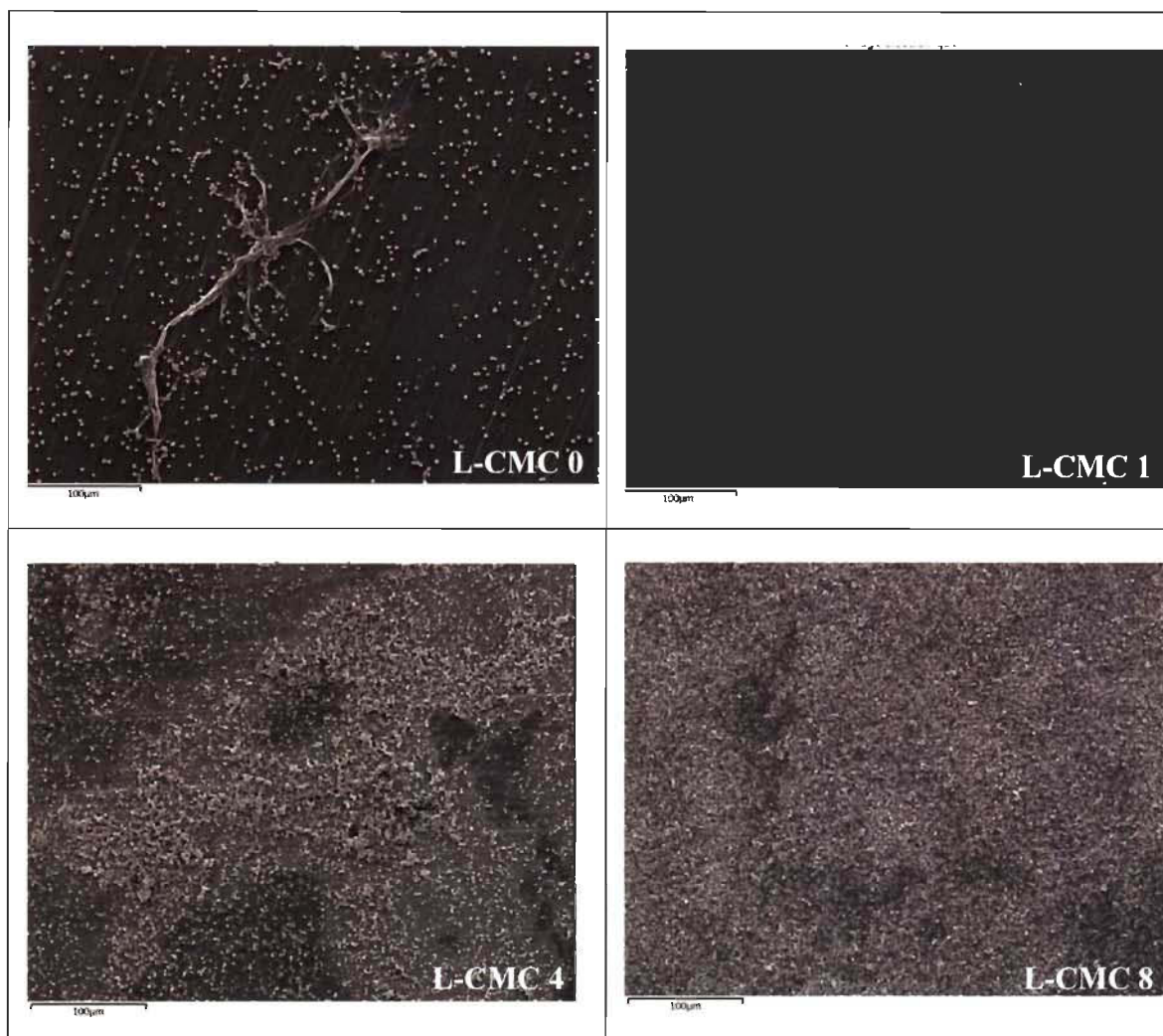


**Figure 4.25 SEM pictures of L-CMC 0, L-CMC 1, L-CMC 4 and L-CMC 8.**

Although in L-CMC 0, a fibril with an approximate diameter of  $5\mu\text{m}$  is found, it still is a rare event. All sample surfaces appear to be covered with small white particles (probably calcium carbonate crystals, with or without CMC). In L-CMC 0 and 1, the small white particles may be observed individually, while from L-CMC 2 to L-CMC 8 agglomerates appear. White particles agglomerate upon increasing CMC addition from 0 to 8%.

Figure 4.26 presents a pure CMC solution after drying in the same conditions as the supernatant. For this material, no agglomeration or aggregate is observed on the entire surface. This indicates that the aggregates seen on the L-CMC 2-8 cannot be solely related to CMC alone.

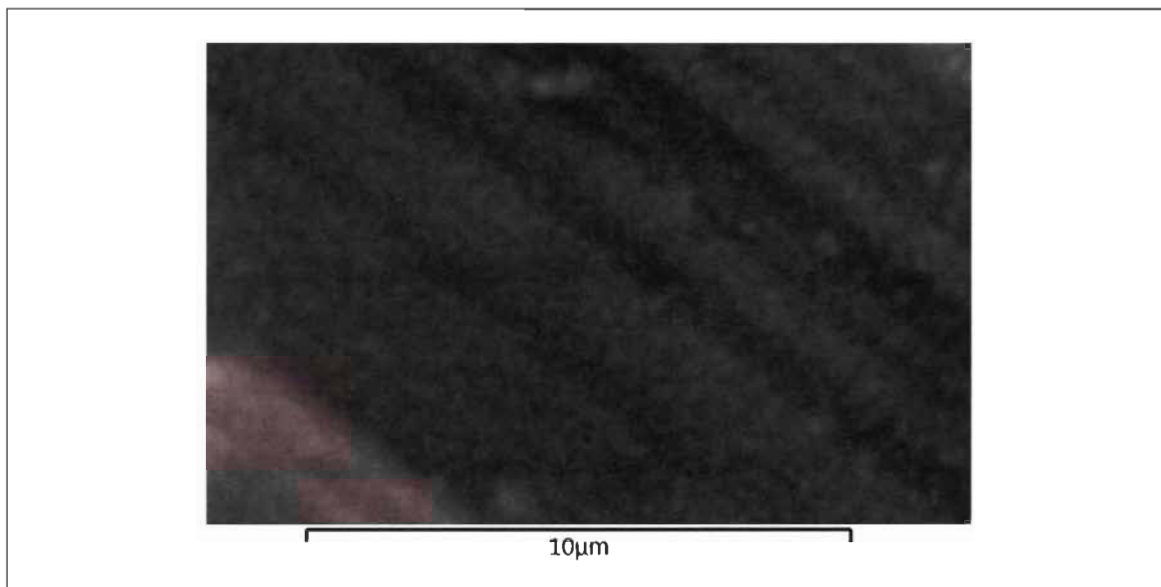
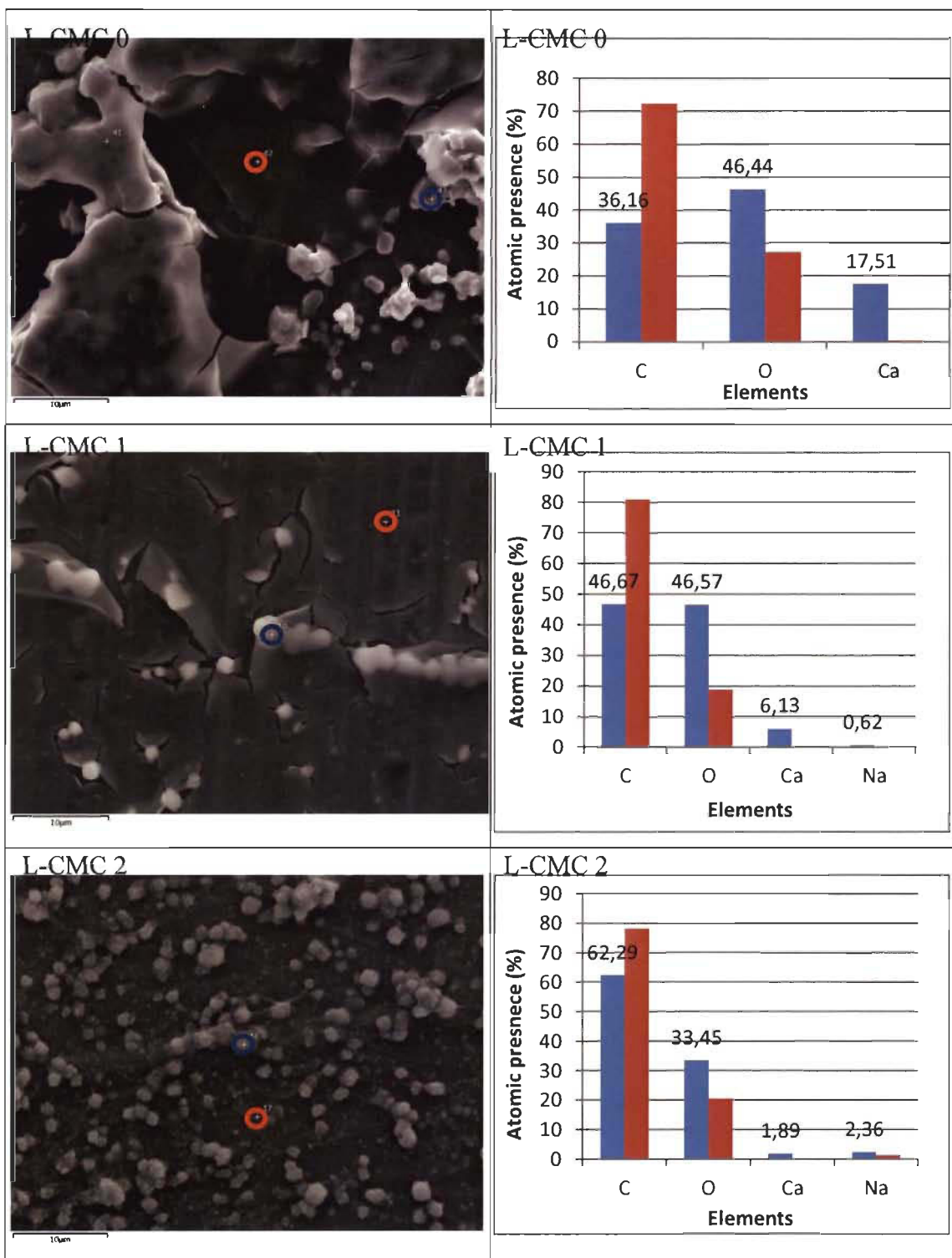


**Figure 4.26 SEM picture of pure CMC 0.04wt% solution after drying (5 000X)**

To identify the materials in the supernatant, SEM pictures at high magnification have been taken and analyzed along with elemental analysis.

#### **4.3.5 Calcium carbonate identification**

The solids of all the samples of L-MNFC have been analysed by SEM at the 2500X magnification and the elemental analyzes have been effected on various picture spots for material nature and/or composition identification. In Figure 4.27 the left column presents SEM pictures of L-CMC 0, 1, 2, 4, 6, and 8 at 2500X magnification. In each photograph, elemental analyses are applied and presented for two zones: a “particle” zone and an amorphous zone (respectively presented as blue and red circles) and the atomic percentages are presented in the right columns.



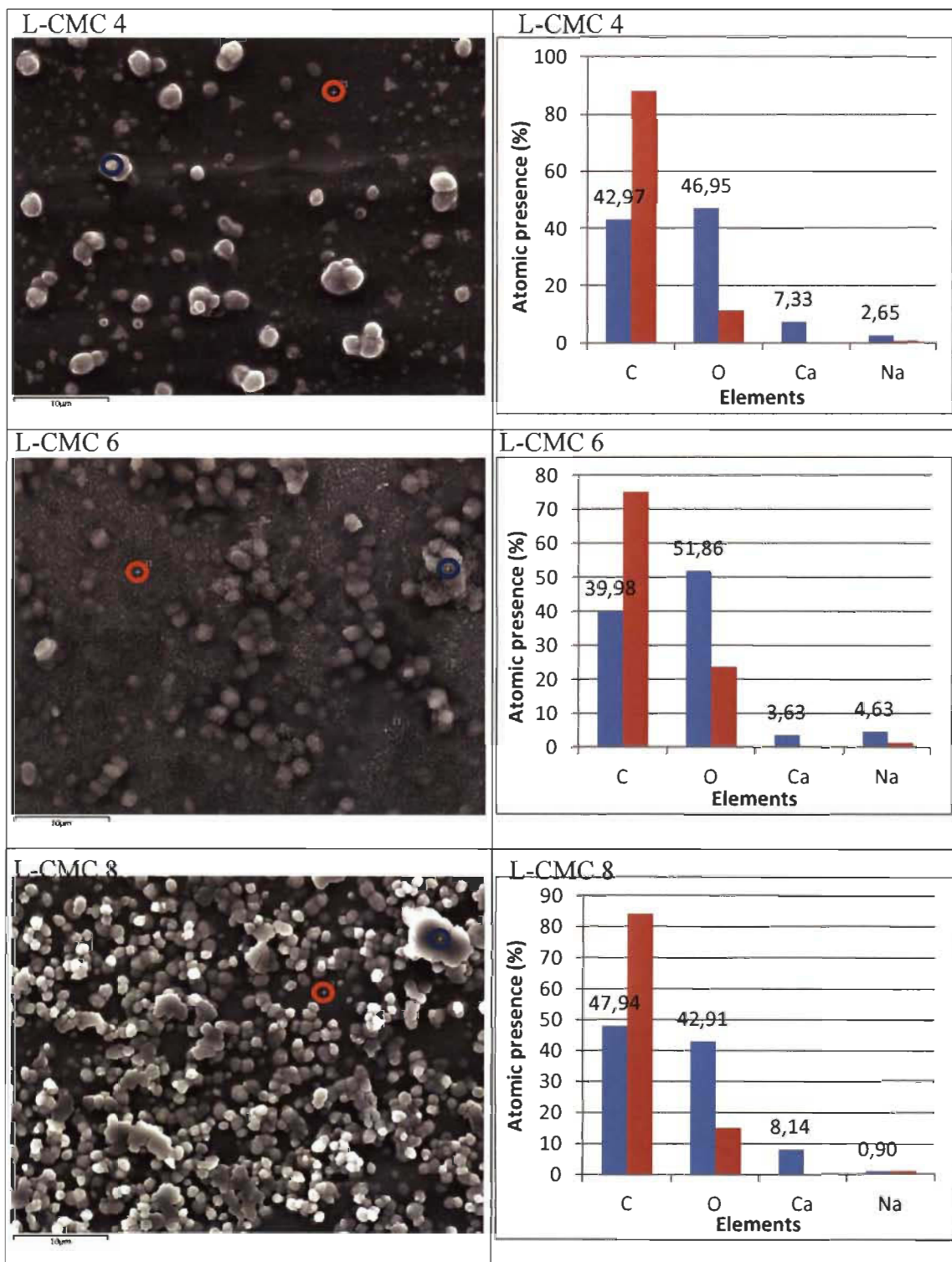


**Figure 4.27 SEM pictures and the corresponding elemental analysis of L-CMC 0, 1, 2, 4, 6, and 8 at 2500X magnification.**

To summarise, concerning the elements in the dry mass of supernatant, Carbon and Oxygen could come from the fibrils, the CMC molecules, or the calcium carbonate;

Calcium exclusively originates from calcium carbonate and Sodium from CMC molecule (as the  $\text{CaCO}_3$  used here does not contain Na).

As shown in Figure 4.27, for each sample, and as expected, the particle zone presents remarkable more Ca than the amorphous zone, illustrating that the particles are calcium carbonate. Interestingly, for L-CMC 1, 2, 4, 6, the zone which contains more Ca also reveals more Na. It might indicate that  $\text{CaCO}_3$  and CMC are bound. Without CMC addition,  $\text{CaCO}_3$  is found in the dry mass alone. Increasing the CMC addition probably leads to the formation of CMC +  $\text{CaCO}_3$  complexes. The low Na present in the particle zone at L-CMC 8 somehow indicates that  $\text{CaCO}_3$  is, in such spots, rather pure crystal of  $\text{CaCO}_3$  which is not bound with CMC.

Following the calcium carbonate identification, the fiber/fibril identification is carried out by the same SEM observations and elemental analyzes at different magnification.

#### **4.3.6 Fiber identification**

A few micrometric fibrils are found in the solids of the supernatant of L-CMC 0, one is shown in Figure 4.28. Only one micrometric fibril has been discovered in L-CMC 1 (Figure 4.29) and for other samples, no fibril was ever found.

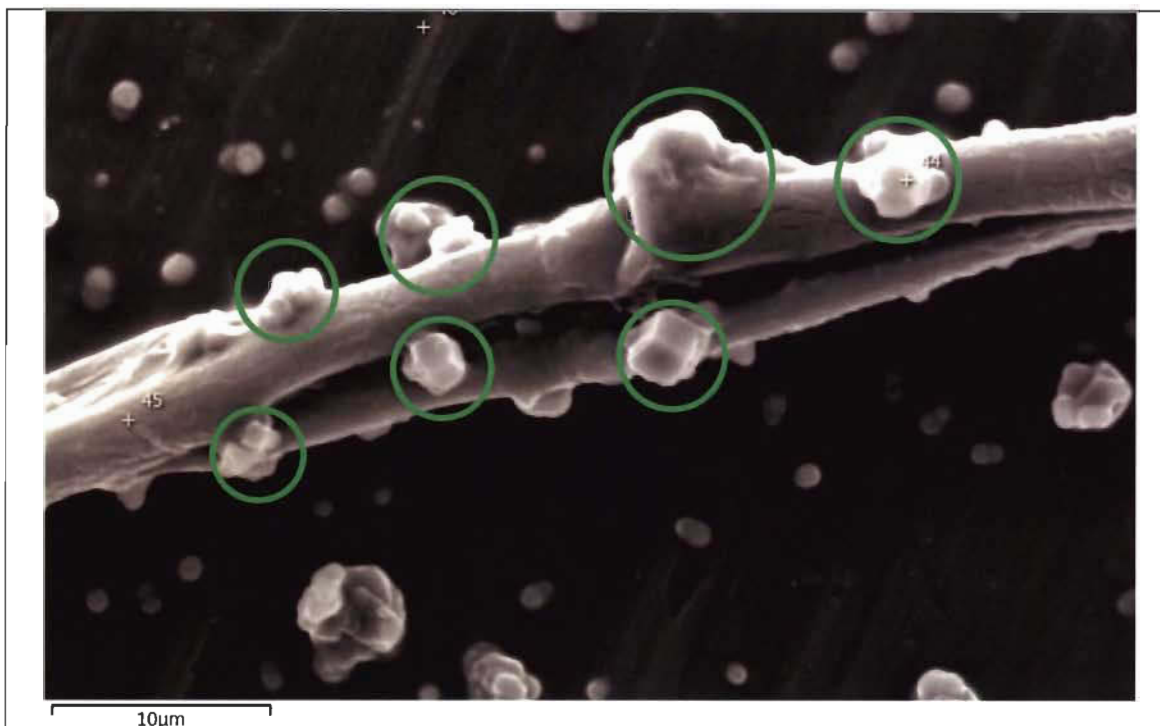


**Figure 4.28** SEM picture of L-CMC 0 with fibril (2500X)



**Figure 4.29** SEM picture of L-CMC 1 with fibril (5000X)

The green circles in Figure 4.28 and Figure 4.29 present the particle zone which has been proved to be calcium carbonate. As it can be seen on L-CMC 0 and L-CMC 1 pictures, there are calcium carbonate crystals adsorbed on the surface of fibrils. As mentioned in 4.3.5: the CMC + CaCO<sub>3</sub> complexes may exist with CMC addition. Therefore the adsorption of CMC + CaCO<sub>3</sub> complexes on fibrils is most likely to occur.

#### 4.3.7 Discussion on the interaction mechanism of CMC and MNFC

Although our proposed mechanism and complex formation is new, the CMC + CaCO<sub>3</sub> complexes inferred from anionic charge quantity measurement, the SEM observation, and elemental analysis have some equivalent in the literature. Figure 4.30 exhibits the formation of calcium alginate from sodium alginate and calcium. Sodium alginate is a natural polysaccharide product extracted from brown seaweed that grows in cold water regions. In presence of calcium, sodium alginate forms the gel of calcium alginate without heating [52-54].

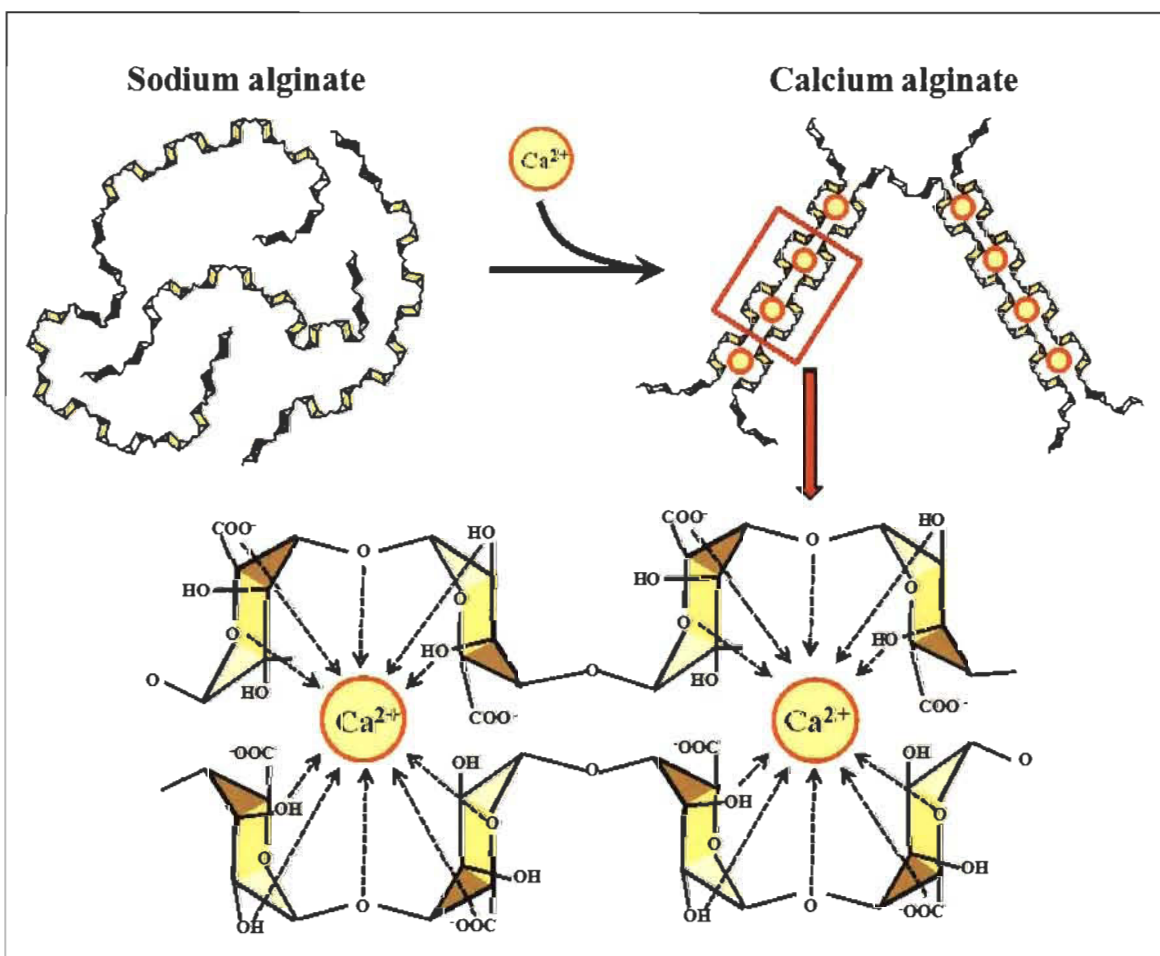


**Figure 4.30 Formation of calcium alginate from sodium alginate [53]**

The structure of CMC used is shown in Figure 4.31. It is a cellulose derivative with sodium carboxy-methyl groups (-CH<sub>2</sub>-COONa) bound to some of the hydroxyl groups of the gluco-pyranose monomers. Similar to sodium alginate, CMC is also a polysaccharide product and present sodium carboxy-methyl groups. Therefore, with the presence of CaCO<sub>3</sub>, CMC and CaCO<sub>3</sub> probably form such a complex.

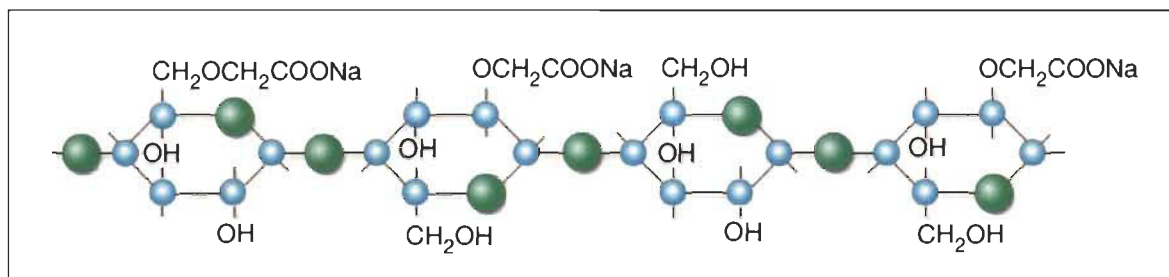


**Figure 4.31 Structure of sodium carboxy-methyl cellulose**

There must exist some interaction among CMC, fibrils and CaCO<sub>3</sub>. In Table 4.11 the interaction and mechanisms deduced from our experiments are schematically represented. The blue particles represent CaCO<sub>3</sub> crystals; red thin line stands for CMC molecules, and black line for fibrils.

**Table 4.11 Interaction between fibrils and CMC+CaCO<sub>3</sub> complexes**

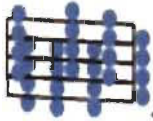
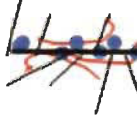
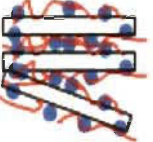
	L-CMC 0	L-CMC 1	L-CMC 2	L-CMC 4	L-CMC 6	L-CMC 8
CaCO <sub>3</sub>						
Fibril						
Zeta potential						
Anionic charge						

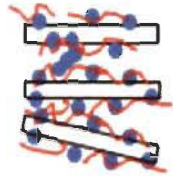
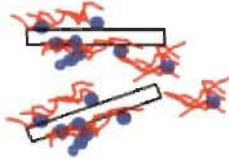
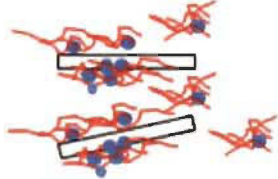
Without CMC,  $\text{CaCO}_3$  adsorbs on the surface of fibrils; the addition of CMC forms the CMC +  $\text{CaCO}_3$  complexes which adsorb on fibrils for L-CMC 1 and L-CMC 2. More CMC addition from 4-8% ends up in two effects. On the one hand, it makes the complexes bigger, the big complexes left the fibrils and become free in the supernatant because of their dimension, on the other hand, it leads to some CMC alone and free in the suspension, and this occurs after saturation of complexes formation.

The adsorption of CMC +  $\text{CaCO}_3$  complexes at low CMC addition is consistent with the zeta potential results. However, as the anionic charge quantity increases linearly with the CMC concentration, it is supposed that the CMC adsorbed on the fibrils account for a small proportion of the total CMC addition.

Combining the information gathered and here proposed from the interactions between CMC and L-MNFC with the influences of CMC on the formation of fibrils agglomerations and on fiber morphology, Table 4.12 summarizes and outlines schematically the dispersion effects of CMC on L-MNFC.

Table 4.12 Dispersion effects of CMC on L-MNFC

	Fibrils agglomeration ↓	Diameter ↓ ↑
L-CMC 0		
L-CMC 1		
L-CMC 2		

L-CMC 4		
L-CMC 6		
L-CMC 8		

For L-CMC 0, there are fibrils agglomerations in the suspension with some  $\text{CaCO}_3$  crystals adsorbing on the surface of fibrils. Once CMC is added, the CMC +  $\text{CaCO}_3$  complexes are formed. At low CMC concentration (1-2%), the complexes are small and adsorb on the fibrils; the adsorbed CMC contribute to the fibrils separation and decrease the fibrils diameter resulting in a good MNFC dispersion. When the addition of CMC is increased, it has effect to expand the complex dimension which further contributes to keeping the fibrils separated from each other, hence eliminating the fibrils agglomerations. At high CMC concentration (4-8%), the complexes become too large to be adsorbed on the surface of fibrils, fewer complexes stay on the fibrils so that the fibrils rejoin together and measured diameter increases.

To have a global overview in the suspension of L-MNFC, Figure 4.32 presents the distribution of fibrils, CMC molecules, and  $\text{CaCO}_3$  in L-CMC 0, 2 and 8 suspensions.

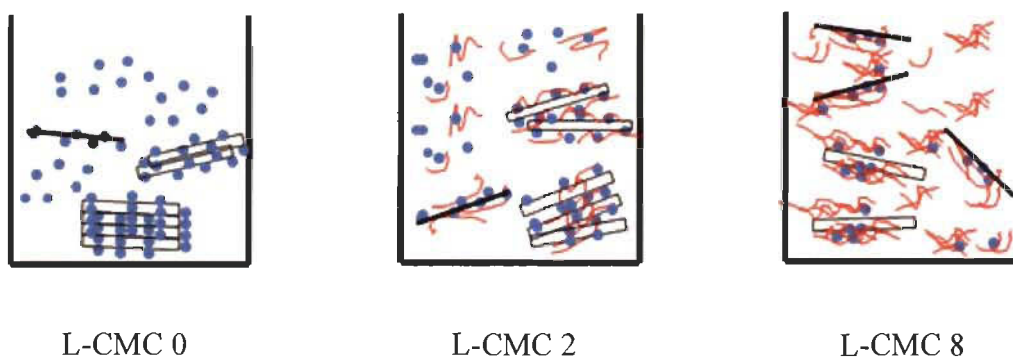


**Figure 4.32 Fibrils, CMC molecules, and CaCO<sub>3</sub> in the suspensions of L-CMC 0, L-CMC 1 and L-CMC 8**

Without CMC addition, CaCO<sub>3</sub> crystals either adsorb on the fibrils surface or are free in the suspension. With CMC addition, the CMC molecules bind with CaCO<sub>3</sub> crystals to form the CMC + CaCO<sub>3</sub> complexes which are adsorbed on fibrils or free in the suspensions. When the complexes grow larger with the augmented CMC concentration, the complexes gradually leave the fibrils and become free in the suspension. Another explanation comes from the free calcium ions presence in the initial L-MNFC suspension which is due to the slight dissociation of the calcium carbonate crystals. From the literature, we may infer that these ions induce the adsorption of CMC on cellulose. According to the dispersion behaviour, the adsorption takes place in the low CMC level (up to 2%) leading to the increase of the absolute ZP and so the reduction in the fibril diameter mean. At CMC concentrations above 2%, the free calcium ions are already “saturated” so the CMC will bind to the calcium ions in the calcium carbonate crystal surface, forming the complexes CMC + CaCO<sub>3</sub> that probably act as bridges to reduce aggregates/flocs formation.

Increasing the CMC concentration from 0 to 8%, both the complexes adsorbed on fibrils surface and free in the suspensions form “bridges” to prevent the fibrils agglomeration formation. However, only the CMC adsorbed on the fibrils surface helps to decrease the fibril diameter and the lowest fibril diameter is found when CMC addition is at about 2%.

It demonstrates that CMC really contributes positively to the dispersion of MNFC suspensions. But the optimal CMC concentrations for the diminution of the fibrils agglomeration and the minimum fibril diameter are somehow different. For application, both effects need to be considered: elimination of the fibrils agglomeration and reduction of the fibril diameter, *i.e.* obtaining the best fibrils separation/dispersion to achieve the best performance of MNFC as a coating agent. From our work, with Omya International AG MNFC, we may affirm that the optimal concentration of CMC is around 4-6% because these CMC addition levels combine the targeted decrease in fibrils agglomeration and provide an acceptable fibril diameter (although not necessarily the lowest one (synonym of optimum dispersion)).

To apply this newly developed knowledge and know-how, the process ability of MNFC in curtain coating has been evaluated through a short/preliminary study of the runnability of the Hydra-Sizer™ and the performance of MNFC suspensions in the Hydra-Sizer™. As L-MNFC is considered to have more market potential (among others for processing cost reasons, and the potential to develop/manufacture a larger variety of potential packaging products) than H-MNFC (produced at a higher cost and targeting more the high quality end of products), the application trials have only been performed for the L-MNFC grade.

#### **4.4 L-MNFC + CMC process ability in offline Hydra-Sizer™ trials**

The application of MNFC as coating agent in curtain coating is achieved by the Hydra-Sizer™ from GL&V. The objective of this section is first to investigate the Hydra-Sizer™ operation and then to applied a part of the know-how develop for the MNFC dispersion in the actual process. First, the runnability of the Hydra-Sizer™ is tested (with water only) then the performance of MNFC in the Hydra-Sizer™ is evaluated

#### 4.4.1 Runnability of the Hydra-Sizer™

Runnability of the Hydra-Sizer™ is critical for an efficient, controlled application of MNFC suspensions in curtain coating. It is then of interest to explore the uniformity and the effects of solutions with different viscosity on the operation of the Hydra-Sizer™.

##### 4.4.1.1 Water flow

To be used as a base line, the runnability is first evaluated with water flow uniformity along the outlet of Hydra-Sizer™. It should also be noted that the Hydra-Sizer™ we are using in these trials is a pilot scale equipment provided by GL&V that can be fitted on Innofibre (collegial technology transfer centre, partner to UQTR CRML) pilot paper machine.

Presented in Table 4.13, 4 tests with different recirculation rates have been carried out (recirculation enable to adjust the flow rate inside the HS). Recirculation 0 means that the recirculation valve is completely closed; test #2 and test #3 represent the valve open to around 1/3 and 2/3, respectively; Recirculation 1 achieves the maximum recirculation rate.

**Table 4.13 Water flow tests in off-line Hydra-Sizer™ trials**

Test # 1	Recirculation 0	Test # 3	Recirculation 2/3
Test # 2	Recirculation 1/3	Test # 4	Recirculation 1

For each test, the mass flow of the three positions (in reference to Figure 3.8) along the outlet is measured to evaluate the flow uniformity. In addition, the nozzle gap of the three positions is accurately measured. Figure 4.33 shows the mass flow and the nozzle gap.

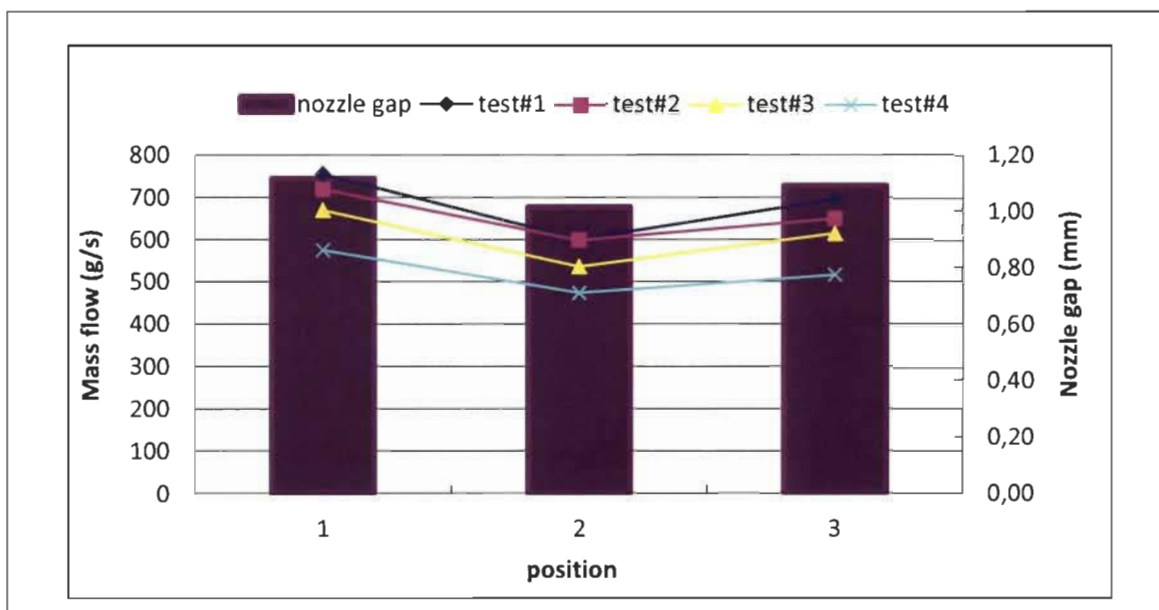


**Figure 4.33 Mass flow of water with different recirculation rates and the nozzle gap at different positions**

Shown in Figure 4.33, the nozzle gap in position 2 is a little smaller than the other positions, which results in the inferior mass flow found for position 2. The increased recirculation leads to the reduction of mass flow for each position, but uniformity does not change with recirculation settings. The curtain uniformity may be improved by adjusting precisely the nozzle gap: the defect is most probably related to the equipment (the only available) we had at our disposal for these experiments.

#### 4.4.1.2 Water + rheological modifier (CMC)

As the final goal is to explore the dispersion of MNFC in Hydra-Sizer™, the influence of the rheology of MNFC on the operation of Hydra-Sizer™ is a pre-requisite to be analyzed. In this case, CMC is used as a rheological modifier to research the effect of viscosity change on Hydra-Sizer™ runnability.

CMC solutions with different concentrations are operated in the off-line Hydra-Sizer™. Figure 4.34 presents the viscosity of each solution and the global mass flow during operation.

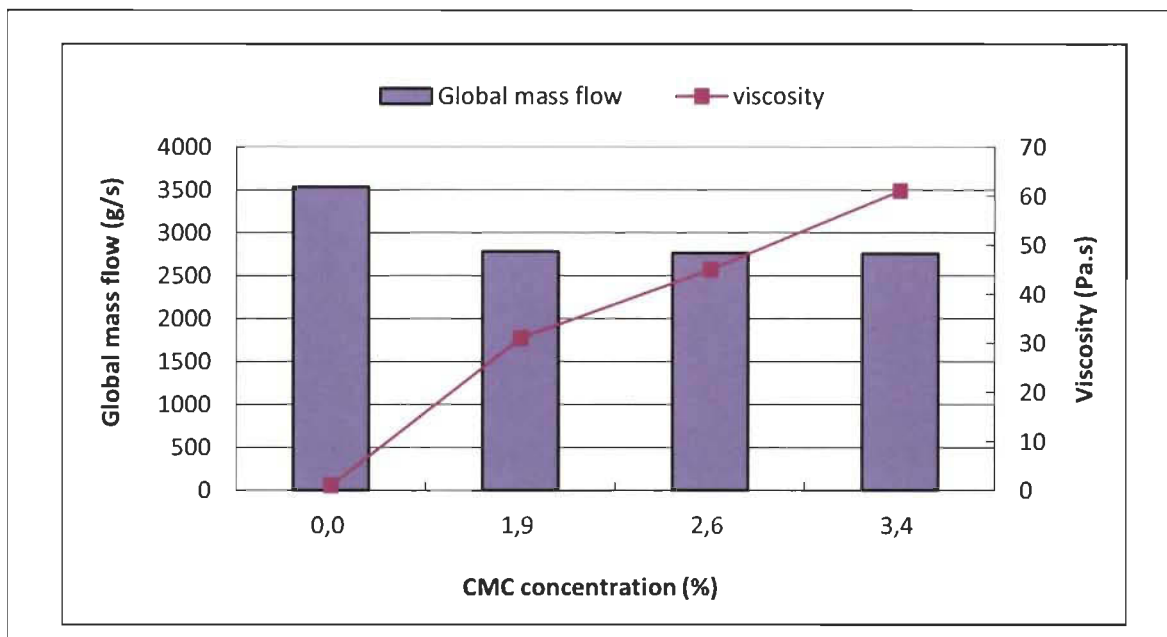


**Figure 4.34 Global mass flow and viscosity of CMC**

As seen in Figure 4.34, while increasing the concentration of CMC, and so the viscosity, the global mass flow decreases slightly but stay constant of the three CMC concentrations tested. Using a positive displacement pump, it is found that the viscosity has little influence on the global mass flow: a point of practical interest as one would then be able to focus on the best dispersion level of MNFC.

#### 4.4.2 MNFC performance in off-line Hydra-Sizer™ trials

The nozzle gap has been adjusted to 1.02 mm to improve the uniformity of outflow and two suspensions: L-MNFC 0.5% and L-MNFC 0.5% + CMC 6% are applied for the off-line trials at flow rates corresponding to 50 and 70 L/min. These trials aim to verify the performance of L-MNFC in the Hydra-Sizer™ (before actual paper machine pilot test trials) including the stability of the curtain and the uniformity of the outflow.

##### 4.4.2.1 L-MNFC 0.5%

Figure 4.35 shows the curtain of L-MNFC 0.5% at the flow rate of 50 L/min and 70L/min. For L-MNFC 0.5%, both curtains remained stable for several tens of seconds. The curtain at 70 L/min exhibits some degradation in the low part, but one should note that real in online operation, the Hydra-Sizer™ will be installed a mere 6 cm or less

above the formation section of paper machine, hence the degradation occurring well below this 6 cm limit is not critical.

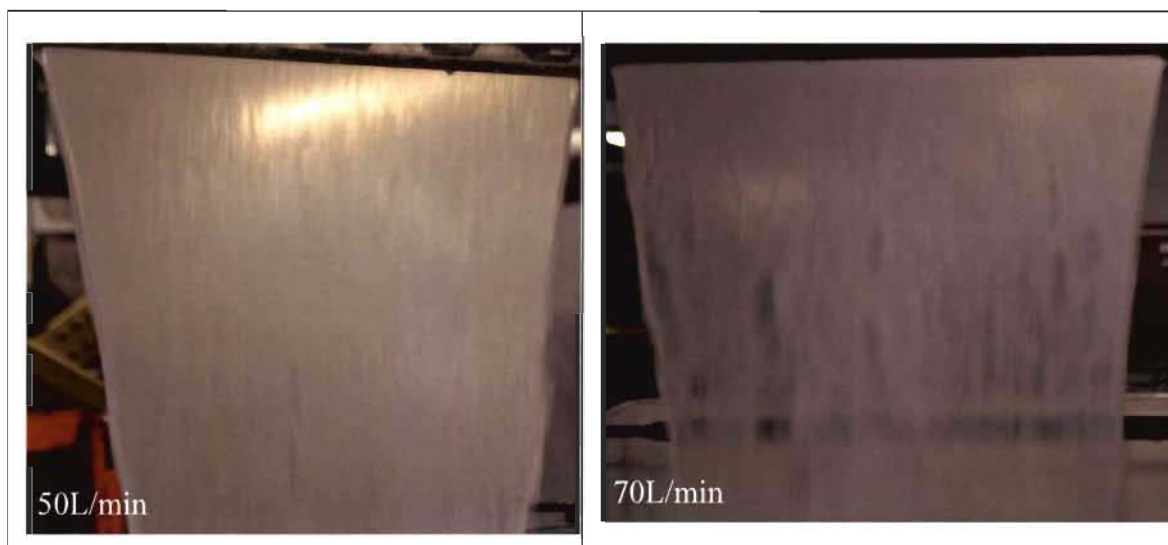


**Figure 4.35** Flow curtains of L-MNFC 0.5% at the flow rate of 50L/min (left) and 70L/min (right)

At the flow rates of 50 L/min and 70L/min, the mass flow of the three positions along the outlet of Hydra-Sizer™ are measured and presented in Figure 4.36.

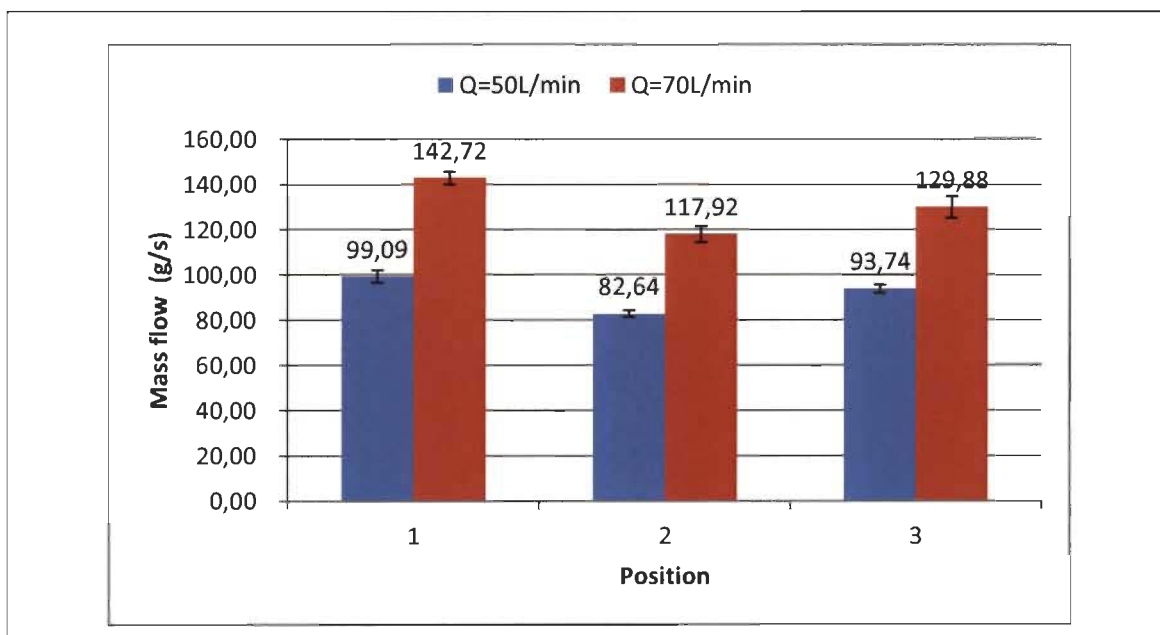


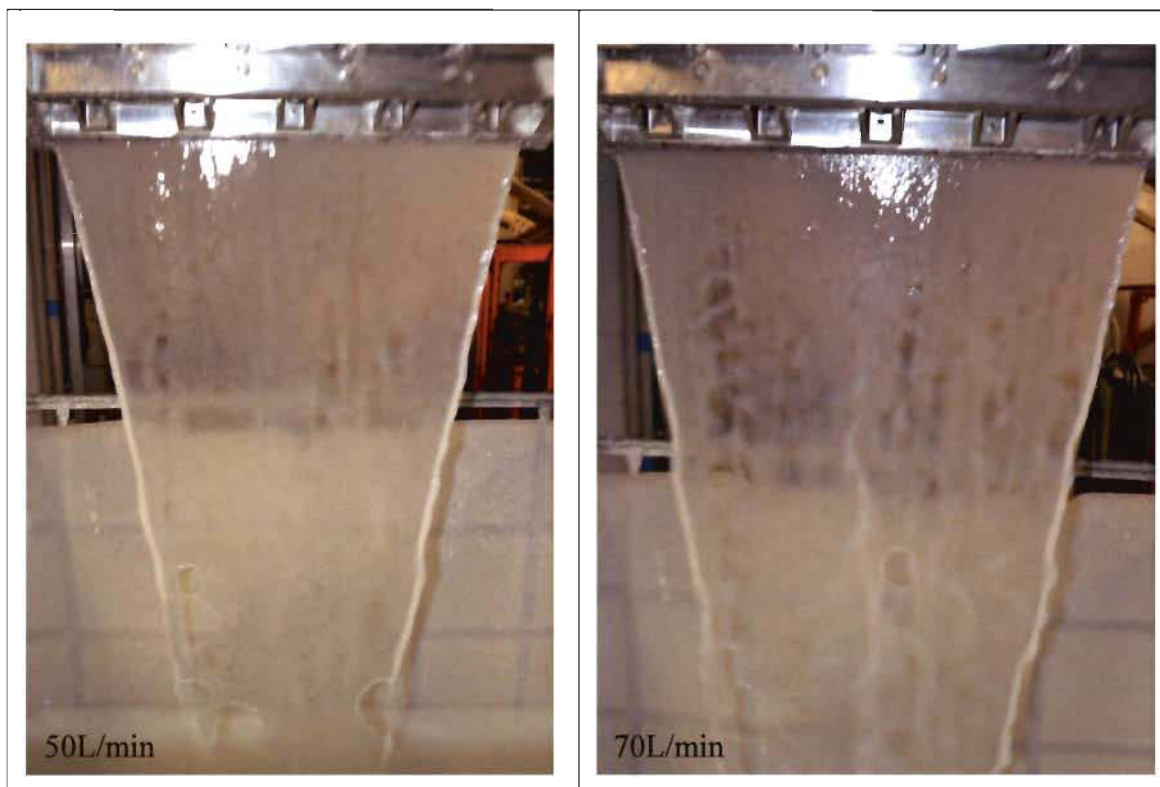
**Figure 4.36** Mass flow of L-MNFC 0.5% along the outlet of Hydra-Sizer™

As Figure 4.36 shows, for 50 L/min and 70 L/min, the mass flows at positions 1 and 3 are almost the same, while position 2 is slightly lower. Comparing to the runnability test of water in Figure 4.33, the uniformity of L-MNFC suspension is better to ensure an even curtain along the outlet of Hydra-Sizer<sup>TM</sup>. It illustrates that the adjustments of nozzle gap before the offline tests of L-MNFC suspensions was effective. When the flow rate is increased from 50 to 70 L/min, the mass flow of each position augment proportionally.

#### **4.4.2.2 L-MNFC 0.5% + CMC 6%**

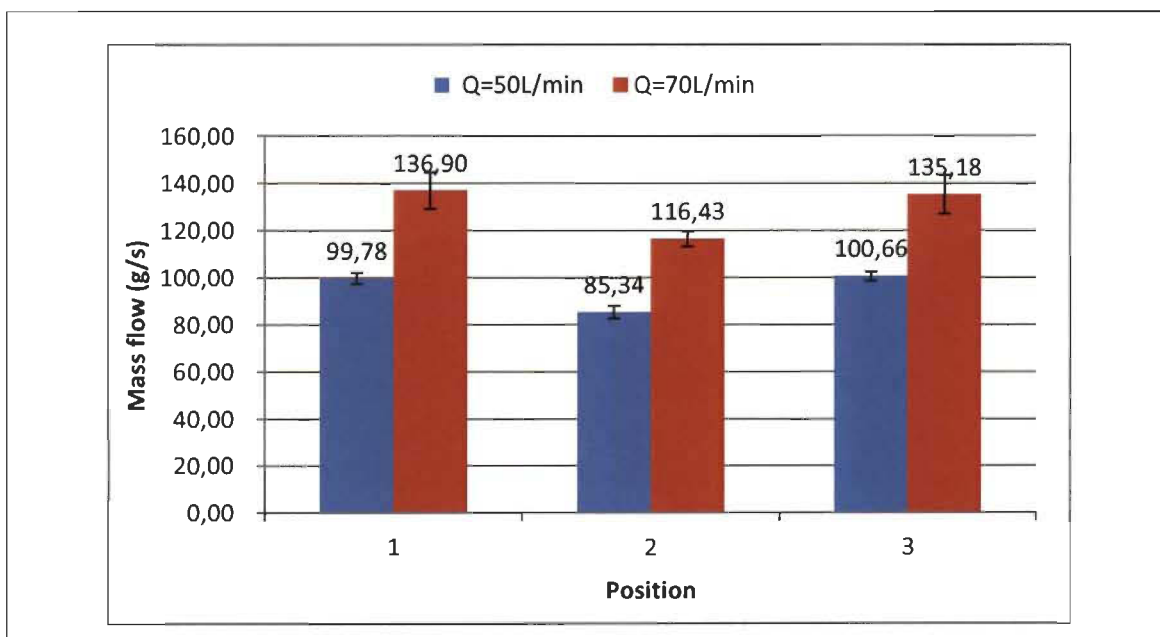
As found previously concerning CMC dispersion effects on MNFC, the CMC addition at 4-6% is supposed to provide optimum dispersion effects. Therefore suspension L-MNFC 0.5% + CMC 6% is used to conduct a trial to evaluate the performance of L-MNFC suspensions with CMC in curtain coating.

Figure 4.37 presents the curtain of L-MNFC 0.5% + CMC 6% at 50 L/min and 70 L/min. At the different flow rates, the curtain still remains stable for several tens of seconds and the flocs that might have formed in the Hydra-Sizer<sup>TM</sup> are quickly evacuated by the flow. For the time being, in lack of better evaluation than eye observation, the curtain stability of L-MNFC 0.5% + CMC 6% appears almost the same as L-MNFC 0.5%: no difference can be observed with the naked eye.



**Figure 4.37** Flow curtain of L-MNFC 0.5% + CMC 6% at the flow rate of 50 L/min (left) and 70 L/min (right)

To evaluate the uniformity of outflow, the mass flow of the three positions along the outlet of Hydra-Sizer™ is presented in Figure 4.38.



**Figure 4.38 Mass flow of L-MNFC 0.5% + CMC 6% along the outlet of Hydra-Sizer™**

As for L-MNFC 0.5%, the mass flows of position 1 and 3 remain at the same level and the position 2 is a little lower (mechanical constraint). Increasing the flow rate from 50 to 70 L/min, as expected, the mass flow of each position increases proportionally.

**4.4.3 Discussion on the MNFC+CMC process ability in the Hydra-Sizer™**

As observed, in Hydra-Sizer™ both L-MNFC 0.5% and L-MNFC 0.5% + CMC 6% present stable curtains with satisfactory outflow uniformity, which makes the application of MNFC in curtain coating feasible (and commercially available). Comparing the two suspensions, no difference of curtain performance between L-MNFC 0.5% and L-MNFC 0.5% + CMC 6% is detected with the naked eye. We may conclude that the improved dispersion level of L-MNFC suspension would need more accurate flow quality analysis (like a precise image analysis of the curtain for instance). It also means that the optimal CMC concentration needed be confirmed by the improved mechanical and barrier properties of paper coated with MNFC through online trials on the paper machine. It should finally be noted that effective paper machine trials with MNFC, and MNFC with CMC have been achieved (and more pilot scale trials still need to be performed) on Innofibre pilot paper machine but these are not part of present Master's thesis work.

## Chapter 5 Conclusions

For the application of MNFC as structuring layer in TMP sheet, the dispersion of MNFC has to be optimum and micro-nano fibrils well developed and separated to provide the best mechanical and barrier properties and to ensure a good performance in coating process. Our master's work focus has been developing some fundamental understanding of the improvement of MNFC dispersion by adding CMC and the final performance of MNFC suspension in curtain coating process.

First we have found that the improvement of MNFC dispersions by adding low levels of CMC is possible. CMC helps to disperse MNFC by decreasing fibrils agglomeration number and size and decreasing the mean fibril diameter. However the two optimum CMC concentrations are different: 8% CMC addition makes the MNFC suspensions homogenous by eliminating the fibrils agglomeration while the minimum mean fibril diameter is found at about 2%. The different optimum in CMC concentrations is due to the difference interaction mechanisms between CMC and MNFC.

It appears that CMC may not solely interact with fibril directly. It adsorbs on fibril surface through the formation of CMC + CaCO<sub>3</sub> complexes. At low CMC concentration (0-2%), the CMC molecules that are adsorbed on fibrils surface promote the fibrillation thus decreasing the fibril diameter. Increasing the CMC concentration from 4 to 8%, the added CMC molecules enlarge the CMC + CaCO<sub>3</sub> complexes' dimension, which makes the free complexes act as bridges between the fibrils and eliminate fibrils agglomeration. Thus at highest CMC concentration (8%), the MNFC suspension presents and homogenous flow (rheological) behaviour without further reduction in the fibril diameters.

Considering the fibrils agglomeration and fibril diameters, the optimum CMC addition for MNFC dispersion is found to be around 4-6% because of the elimination of fibrils agglomeration and the acceptable fibril diameter at that concentration (although lowest fibril diameter, *i.e.* best dispersion is at around 2-4%).

The application of MNFC suspension in curtain coating process conducted by Hydra-Sizer™ is practicable. In Hydra-Sizer™, MNFC suspension presents good curtain stability and uniformity. The addition of CMC has not revealed any difference in the measured outflow. This makes the application of MNFC+CMC as coating agent in curtain coating achievable.

The main achievement of present Master's thesis is the proposal of a “complex” (in the sense that many factors and parameters need to be considered simultaneously) mechanism to explain the interaction between CMC – CaCO<sub>3</sub> and micro-nano fibrils in MNFC suspensions. The proposed mechanisms explain both the rheological behaviour of the suspensions and the level of dispersion obtained with various levels of CMC additions.

### **Future work**

For the fulfillment of the MNFC application in papermaking industry, several research areas are proposed below to help the understanding of MNFC suspensions.

- Additional fundamental research work is required to firm up and confirm the proposed theory and mechanisms of MNFC dispersion.
- Pilot scale trials needs to be achieve to manufacture papers integrating MNFC with different concentrations of CMC in order to evaluate and understand and optimise the impact of MNFC dispersion on mechanical and barrier properties.
- As original approach was to develop “structured papers” through curtain coating on a paper machine, further trials are needed to explore the appropriate positioning of the Hydra-Sizer™ on the wet-end of the paper machine as to modify the MNFC surface layer integration in the thickness of the paper.
- Perform above trials with different fibrillated grades of MNFC (only two grades were evaluated in present work) as to extend the potential of packaging products that may be developed though the z-structuring approach proposed by Professor Patrice J. Mangin.

## List of presentations and posters

### Presentation

1. Fabrice Roussière, Xiaoman Xu, Martin Dubé, Pierre Carreau, Joachim Schoelkopf, Patrick A.C. Gane, and Patrice J. Mangin, "*Dispersion of Micro-Nano-Fibrillated-Cellulose (MNFC) by Carboxy Methyl Cellulose (CMC) and its characterization*", 2014 TAPPI International Conference on Nanotechnology for Renewable Materials, 23-26 June 2014, Vancouver, British Columbia, Canada.

### Posters

2. Xiaoman Xu, Gilles Lenfant, Fabrice Roussière, Martin Dubé, Weawkamol Leelapornpisit, Pierre Carreau, and Patrice J. Mangin, "*Measuring the Dispersion of Micro-Nano-Fibrillated-Cellulose (MNFC) with Carboxy Methyl Cellulose (CMC)*", 2014 PaperWeek Canada, 3-6 Feb 2014, Montréal, Québec, Canada.
3. Xiaoman Xu, Abdeladim Tibouda, Mohamed Ali Charfeddine, Daniel Matte, Fabrice Roussière, and Patrice J. Mangin, "*Inclusion of Micro-Nano-Fibrillated-Cellulose (MNFC) in papermaking with a Hydra-Sizer<sup>TM</sup>: the HS study - Part 2*", 1<sup>st</sup> FIBER Network Conference, 13-16 May 2013, Cornwall, Ontario, Canada.
4. Xiaoman Xu, Abdeladim Tibouda, Mohamed Ali Charfeddine, Daniel Matte, Fabrice Roussière, and Patrice J. Mangin, "*Inclusion of Micro-Nano-Fibrillated-Cellulose (MNFC) in papermaking with a Hydra-Sizer<sup>TM</sup>: the HS study - Part 1*", 2013 PaperWeek Canada, 4-7 Feb 2014, Montréal, Québec, Canada.

## References

1. MINNES, G." Pulp and Paper Industry - The Canadian Encyclopedia". 2013; Available from: <http://www.thecanadianencyclopedia.com/articles/pulp-and-paper-industry>.
2. Harinath, E., L.T. Biegler, and G.A. Dumont, *Control and optimization strategies for thermo-mechanical pulping processes: Nonlinear model predictive control*. Journal of Process Control, **21**(4):519-528 (2011)
3. Lavoine, N., et al., *Microfibrillated cellulose—Its barrier properties and applications in cellulosic materials: A review*. Carbohydrate polymers, **90**(2):735-764 (2012)
4. Welcome to ArboraNano". 2009; Available from: <http://www.arboranano.ca/>.
5. Ioelovich, M., *Cellulose as a nanostructured polymer: A short review*. BioResources, **3**(4):1403-1418 (2008)
6. Habibi, Y., L.A. Lucia, and O.J. Rojas, *Cellulose nanocrystals: chemistry, self-assembly, and applications*. Chemical reviews, **110**(6):3479 (2010)
7. Siró, I. and D. Plackett, *Microfibrillated cellulose and new nanocomposite materials: A review*. Cellulose, **17**(3):459-494 (2010)
8. Azizi Samir, M.A.S., F. Alloin, and A. Dufresne, *Review of recent research into cellulosic whiskers, their properties and their application in nanocomposite field*. Biomacromolecules, **6**(2):612-626 (2005)
9. Nutrition resources". Chemistry review 2014 [cited 2014 08 jui]; Available from: <http://nutrition.jbpub.com/resources/chemistryreview9.cfm>.
10. Nakagaito, A. and H. Yano, *The effect of morphological changes from pulp fiber towards nano-scale fibrillated cellulose on the mechanical properties of high-strength plant fiber based composites*. Applied Physics A, **78**(4):547-552 (2004)
11. Ridgway, C.J. and P.A. Gane, *Constructing NFC-pigment composite surface treatment for enhanced paper stiffness and surface properties*. Cellulose, **19**(2):547-560 (2012)
12. Vartiainen, J., et al., *Health and environmental safety aspects of friction grinding and spray drying of microfibrillated cellulose*. Cellulose, **18**(3):775-786 (2011)
13. Syverud, K. and P. Stenius, *Strength and barrier properties of MFC films*. Cellulose, **16**(1):75-85 (2009)

14. Taniguchi, T. and K. Okamura, *New films produced from microfibrillated natural fibres*. *Polymer International*, **47**(3):291-294 (1998)
15. Henriksson, M. and L.A. Berglund, *Structure and properties of cellulose nanocomposite films containing melamine formaldehyde*. *Journal of applied polymer science*, **106**(4):2817-2824 (2007)
16. Dufresne, A., J.Y. Cavallé, and M.R. Vignon, *Mechanical behavior of sheets prepared from sugar beet cellulose microfibrils*. *Journal of applied polymer science*, **64**(6):1185-1194 (1997)
17. Isogai, A., T. Saito, and H. Fukuzumi, *TEMPO-oxidized cellulose nanofibers*. *Nanoscale*, **3**(1):71-85 (2011)
18. Plackett, D., et al., *Physical properties and morphology of films prepared from microfibrillated cellulose and microfibrillated cellulose in combination with amylopectin*. *Journal of applied polymer science*, **117**(6):3601-3609 (2010)
19. Svagan, A.J., M.S. Hedenqvist, and L. Berglund, *Reduced water vapour sorption in cellulose nanocomposites with starch matrix*. *Composites science and technology*, **69**(3):500-506 (2009)
20. Hult, E.-L., M. Iotti, and M. Lenes, *Efficient approach to high barrier packaging using microfibrillar cellulose and shellac*. *Cellulose*, **17**(3):575-586 (2010)
21. Aulin, C., M. Gällstedt, and T. Lindström, *Oxygen and oil barrier properties of microfibrillated cellulose films and coatings*. *Cellulose*, **17**(3):559-574 (2010)
22. Herrick, F.W., et al., *Microfibrillated cellulose: morphology and accessibility*. 1983. Medium: X; Size: Pages: 797-813.
23. Pääkko, M., et al., *Enzymatic hydrolysis combined with mechanical shearing and high-pressure homogenization for nanoscale cellulose fibrils and strong gels*. *Biomacromolecules*, **8**(6):1934-1941 (2007)
24. Iotti, M., et al., *Rheological Studies of Microfibrillar Cellulose Water Dispersions*. *Journal of Polymers and the Environment*, **19**(1):137-145 (2011)
25. Wikipedia." Zeta potential". 2013 20 May 2013 at 10:40; Available from: [http://en.wikipedia.org/wiki/Zeta\\_potential](http://en.wikipedia.org/wiki/Zeta_potential).
26. Öhman, L.-O., et al., *Adsorption of aluminum (III) on cellulosic fibres in neutral to alkaline solutions: Influence of charge and size of the particles formed*. *Journal of pulp and paper science*, **23**(10):J467-J474 (1997)
27. Zaucha, M., Z. Adamczyk, and J. Barbasz, *Zeta potential of particle bilayers on mica: A streaming potential study*. *Journal of Colloid and Interface Science*, **360**(1):195-203 (2011)

28. Schneider, C., et al., *Experimental study of electrostatically stabilized colloidal particles: Colloidal stability and charge reversal*. Journal of Colloid and Interface Science, **358**(1):62-67 (2011)
29. Olszewska, A., et al., *The behaviour of cationic NanoFibrillar Cellulose in aqueous media*. Cellulose, **18**(5):1213-1226 (2011)
30. Gardner, D.J., et al., *Adhesion and surface issues in cellulose and nanocellulose*. Journal of Adhesion Science and Technology, **22**(5-6):545-567 (2008)
31. Zimmermann, T., N. Bordeanu, and E. Strub, *Properties of nanofibrillated cellulose from different raw materials and its reinforcement potential*. Carbohydrate Polymers, **79**(4):1086-1093 (2010)
32. Myllytie, P., et al., *Effect of polymers on aggregation of cellulose fibrils and its implication on strength development in wet paper web*. Nord Pulp Pap Res J, **24**:124-133 (2009)
33. Liimatainen, H., et al., *Influence of adsorbed and dissolved carboxymethyl cellulose on fibre suspension dispersing, dewaterability, and fines retention*. BioResources, **4**(1):321-340 (2009)
34. Ahola, S., et al., *Effect of polymer adsorption on cellulose nanofibril water binding capacity and aggregation*. BioResources, **3**(4):1315-1328 (2008)
35. Food ingredients - Hawkins Watts New Zealand - Products - Hydrocolloids > MCC - Microcrystalline Cellulose". Available from: [http://www.hawkinswatts.com/prod\\_stabs9.htm](http://www.hawkinswatts.com/prod_stabs9.htm).
36. Vesterinen, A.H., et al., *The effect of water - soluble polymers on rheology of microfibrillar cellulose suspension and dynamic mechanical properties of paper sheet*. Journal of applied polymer science, **116**(5):2990-2997 (2010)
37. Wagberg, L., *Polyelectrolyte adsorption onto cellulose fibres-A review*. Nordic Pulp and Paper Research Journal, **15**(5):586-597 (2000)
38. Decent, S., *A simplified model of the onset of air entrainment in curtain coating at small Capillary number*. Chemical engineering research and design, **86**(3):311-323 (2008)
39. Bohnenkamp, B., M. Tietz, and M. Trefz. *New development results of curtain coating for various paper grades*. 2005. Toronto, ON.
40. Martinez, P., *Etude expérimentale et simulation d'écoulements de fluides modèles et de dispersions pigmentaires dans une coucheuse rideau*. 2011, Université de Grenoble.

41. Foulger, M., et al., *New technology to apply starch and other additives*. Pulp & Paper Canada, **100**(2):24-25 (1999)
42. Ascanio, G., P. Carreau, and P. Tanguy, *High-speed roll coating with complex rheology fluids*. Experiments in fluids, **40**(1):1-14 (2006)
43. Kelco, C." CP Kelco – The World Leader in Carboxymethylcellulose (CMC) Production". Available from: [http://www.bisi.cz/cmsres.axd/get/cms\\$7CVwRhc3USVqgzxkKF96gI\\$2BChNrXcTq\\$2BOUz0Xj7EmggLIJILTc\\$2BnjT05VW4kCumkdM](http://www.bisi.cz/cmsres.axd/get/cms$7CVwRhc3USVqgzxkKF96gI$2BChNrXcTq$2BOUz0Xj7EmggLIJILTc$2BnjT05VW4kCumkdM).
44. GmbH, B.M." Operation manual PCD 03/ PCD 03 PH Particle Charge Detector". 2003 [cited 2013; Available from: [http://www.inven.nl/documenten/PCD03\\_handleiding.pdf](http://www.inven.nl/documenten/PCD03_handleiding.pdf).
45. Wikipedia." Scanning electron microscope". 2014; Available from: [http://en.wikipedia.org/wiki/Scanning\\_electron\\_microscope](http://en.wikipedia.org/wiki/Scanning_electron_microscope).
46. AB, R.I., *USER'S MANUAL STRESSTECH Rheometer (REOLOGICA Instruments AB)*.
47. Box plot explanation". 2014; Available from: <http://www2.ecology.su.se/dbhjf/2011gif/explanation.htm>.
48. Jacobasch, H.-J., G. Bauböck, and J. Schurz, *Problems and results of zeta-potential measurements on fibers*. Colloid and Polymer Science, **263**(1):3-24 (1985)
49. Liu, Z., et al., *Quartz crystal microbalance with dissipation monitoring and surface plasmon resonance studies of carboxymethyl cellulose adsorption onto regenerated cellulose surfaces*. Langmuir, **27**(14):8718-8728 (2011)
50. Lee, S.-Y., et al., *Nanocellulose reinforced PVA composite films: effects of acid treatment and filler loading*. Fibers and Polymers, **10**(1):77-82 (2009)
51. Hussain, A., *Adsorption of Polyvinyl Alcohol on Nano-Cellulose Fibers*. (2010)
52. Sugiura, S., et al., *Size control of calcium alginate beads containing living cells using micro-nozzle array*. Biomaterials, **26**(16):3327-3331 (2005)
53. Kashima, K. and M. Imai, *Advanced Membrane Material from Marine Biological Polymer and Sensitive Molecular-Size Recognition for Promising Separation Technology*. (2012)
54. Blandino, A., M. Macias, and D. Cantero, *Formation of calcium alginate gel capsules: Influence of sodium alginate and CaCl<sub>2</sub> concentration on gelation kinetics*. Journal of bioscience and bioengineering, **88**(6):686-689 (1999)